UNIVERSITY OF CALIFORNIA,
IRVINE

Molecular mechanisms of *LMNA* gene mutation in dilated cardiomyopathy with conduction defects

DISSERTATION

Submitted in partial satisfaction of the requirements
for the degree of

DOCTOR OF PHILOSOPHY

in Biological Chemistry

by

Halida Putri Widyastuti

Dissertation Committee:
Associate Professor Michael V. Zaragoza, Chair
Professor Kyoko Yokomori
Professor Peter Donovan
Associate Professor Anna Grosberg
Assistant Professor Timothy L. Downing

2020

DEDICATION

For Mom and Dad, the lighthouse shining in the darkness

For Zakiy. Here's looking at you, kid

For my grandparents, Mbah Wiryo Sunarjo and Mbah Painem,
Mbah Kyai Abdul Fattah Al-Manshur and Mbah Daiyyatul Khairat
I wish I knew you when I was young. I hope I have made you proud

TABLE OF CONTENTS

LIST OF FIGURES

LIST OF TABLES

ACKNOWLEDGMENTS

I would like to express my deep gratitude and appreciation to my thesis advisor Dr. Mike Zaragoza, who bravely took a chance on me to be his first (but hopefully **not** last) graduate student in his newly established lab, back when I started my graduate studies in 2016. Mike's guidance and tutelage was immensely crucial during the four years I spent in his lab. Mike encouraged me to pursue whatever avenue of research that best suit my interests and allowing me to work independently as a scientist. Without his unwavering support and his confidence in my scientific aptitudes and capabilities, this dissertation would not have been completed.

I would also like to thank my thesis committee members Drs. Anya Grosberg, Kyoko Yokomori, Peter Donovan and Tim Downing. Their feedback and advice on my thesis proposals and dissertation have been invaluable. They have also been instrumental in helping me obtain (or strive to obtain) fellowships and grants through their generosity in writing countless recommendation letters. Thank you for everything.

I would also like to thank my Bioinformatics collaborator and *guru* and my co-author Dr. Trina Norden-Krichmar, for teaching me everything I know about Bioinformatics. Without Trina's help in educating me in the basics of programming I would not have been able to do any of the Bioinformatics analysis that make up the vast majority of this work.

Additionally, I would like to thank Dr. Mehrsa Mehrabi for showing me the ins and outs of cardiomyocyte differentiation; my former lab mate Cecilia Nguyen for being an invaluable sounding board for all of my ridiculous hypothesis and theories, saving me from spending hours and probably days on futile experiments.

I want to thank my friends and emotional support systems Chang, Betty, Joann and Rob. Without them, these arduous years of graduate school would have been unbearable. I am grateful to have found friendships that last a lifetime. One can hardly find a better and cooler group of people to be friends with.

Finally, I would like to thank my families, both in Indonesia and Boston, for their unwavering support, encouragement, understanding and unconditional love. In particular, I would like to thank my Mom and Dad (Dr. Puji Winarni, MA and Professor Dr. Muhammad A.S. Hikam, MA), my *raison d'etre*, for always encouraging me to pursue my dreams, even if it meant letting go of their only daughter at the tender age of fifteen. Thank you, Mom, for all of the sacrifices you've made for my sake and your prayers for me. Thank you for paving the way and showing me how to be a strong, independent woman. Thank you, Dad, for instilling the dogged determination and disciplined work ethics needed see through this ambitious scholastic endeavor, even if it's "all Greek to you." I would also like to thank all of my uncles, aunts, cousins, nieces and nephews. I hope I have made you all proud.

Thank you to my *namborus*, Namboru Renta and Heidi Hutabarat, for raising me from adolescence until now and for Namboru Renta in particular for being a role model and inspiring me to pursue a career in the life sciences realm. To my "siblings" Indah and Bimo, I'm grateful to have grown up with you.

Ultimately, I would like to thank my fiancé, Fadhli Zakiy, whose unconditional love, affection, patience and acceptance has been my fuel since the day we met. You're a diamond in the rough, and thank you for being my shoulder to cry on, for always encouraging me to get up and try again whenever my experiments fail, for helping me with my Bioinformatics homework, for being my unending source of happiness and laughter and being my best friend. I can't imagine what my life would be like without you.

CURRICULUM VITAE

Halida Putri Widyastuti

Education

2016-2020 **Doctor of Philosophy** in Biological Chemistry
Department of Biological Chemistry, School of Medicine
University of California, Irvine, Irvine, CA
Thesis advisor: Michael V. Zaragoza, M.D., Ph.D.

2014-2016 **Master of Science** in Biotechnology with Stem Cell Emphasis
Department of Molecular Biology and Biochemistry
University of California, Irvine, Irvine, CA

2008-2012 **Bachelor of Science** in Chemical Engineering
Department of Chemical Engineering
Pennsylvania State University, University Park, PA

Research Experience

2016-2020 **Graduate student**
Department of Biological Chemistry, School of Medicine, UC Irvine, CA
Advisor: Michael V. Zaragoza, M.D., Ph.D.
- *Molecular mechanisms of LMNA gene mutation in dilated cardiomyopathy with conduction defects*

2015-2016 **Graduate student**
Department of Developmental and Cell Biology, UC Irvine, CA
Advisor: Maksim V. Plikus, Ph.D.
- *Molecular mechanisms and signaling pathways responsible for delayed anagen phase in Leptin deficient mice*

2013-2014 **Research assistant**
Stem Cell and Cancer Institute, Jakarta, Indonesia
Advisor: Indra Bachtiar, Ph.D.
-*Isolation and characterization of Mesenchymal stem cells (MSCs) from Wharton's Jelly of the umbilical cord*

Publications

1. **Widyastuti, H.P.,** Norden-Krichmar, T.M., Grosberg, A., Zaragoza, M.V. Gene expression profiling of fibroblasts in a family with *LMNA*-related cardiomyopathy reveals molecular pathways implicated in disease pathogenesis. *BMC Med Genet* **21**, 152 (2020).
2. Zaragoza, M.V.; Nguyen, C.H.H.; **Widyastuti, H.P.;** McCarthy, L.A.; Grosberg, A. Dupuytren's and Ledderhose Diseases in a Family with *LMNA*-Related Cardiomyopathy and a Novel Variant in the *ASTE1* Gene. *Cells* 2017, 6, 40.

3. Widowati, W; Wijaya, L; Murti, H; **Widyastuti, H**; Agustina, D; Laksmitawati, D.R; Fauziah, N; Sumitro, S.B; Widodo, M.A; Bachtiar, I. Conditioned medium from normoxia (WJMSCs-norCM) and hypoxia-treated WJMSCs (WJMSCs-hypoCM) in inhibiting cancer cell proliferation. Biomarkers and Genomic Medicine 2015, 7, 8.

Abstracts

1. Morival, Julien. L, **Widyastuti, Halida. P**. Targeted epigenetic tools for the control of variability in cardiac differentiation of patient-derived iPSCs. In: UCI Center for Complex Biological Systems (CCBS) Annual Retreat; 2020 May 20; Irvine, CA: CCBS; 2020.
2. **Widyastuti, Halida. P**, Mehrabi, Mehrsa. scRNA-seq studies on novel *LMNA*-associated cardiomyopathy iPSC disease model revealed in-vitro cellular heterogeneity and dysregulation of early gene expression. In: Multiscale Cell Fate Annual Symposium; 2019 October 28-29; Irvine, CA: CMCF; 2019.
3. **Widyastuti, Halida. P**, Mehrabi, Mehrsa. Patient-specific iPSC disease modeling reveals tissue-specific molecular mechanisms of *LMNA*-associated cardiac disease. In: American Society of Human Genetics; 2018 October 16-20; San Diego, CA: ASHG; 2018.
4. **Widyastuti, Halida. P,** Tu, Christina. H. Induced pluripotent stem cell disease modeling of *LMNA*-associated cardiomyopathy reveals perturbations in embryoid body formation. In: International Society for Stem Cell Research (ISSCR) Annual Meeting; 2017 June 14-17; Boston, MA: ISSCR; 2017.

Honors and Awards

2019 Predoctoral Fellowship, American Heart Association
2019 Graduate student research award, Center for Complex Biological Systems, UC Irvine
2014 Scholarship recipient, Indonesian Endowment Fund for Education, Ministry of Finance, Republic of Indonesia.

Teaching Experience

2019 Teaching assistant. DNA to Organisms (undergraduate course). UC Irvine
2016 Teaching assistant. Developmental Biology Lab (undergraduate course). UC Irvine.
2016 Teaching assistant. Microbiology Lab (undergraduate course). UC Irvine.
2015 Teaching assistant. Molecular Biology Lab (undergraduate course). UC Irvine.
2015 Teaching assistant. AIDS Fundamentals (undergraduate course). UC Irvine.

ABSTRACT OF THE DISSERTATION

Molecular mechanisms of *LMNA* gene mutations in Dilated Cardiomyopathy with conduction defects

By

Halida Putri Widyastuti

Doctor of Philosophy in Biological Chemistry

University of California, Irvine, 2020

Associate Professor Michael V. Zaragoza, Chair

Lamin A/C are intermediate filament proteins that construct the nuclear lamina of a cell encoded by the *LMNA* gene. Lamin A/C has been implicated in processes such as chromatin localization and cell differentiation. Consequently, mutations in *LMNA* have detrimental effect in cell functions which results in diseases collectively termed as laminopathies. Some diseases that are caused by defective Lamin A/C include cardiac diseases, which are the focus of this project. Whole exome sequencing on dilated cardiomyopathy patients identified a novel splice site mutation in intron 1 of *LMNA* (*LMNA* c.357-2A>G), which is predicted to result in exon skipping and subsequently Lamin A/C haploinsufficiency. This project aims to elucidate the molecular mechanism contributing to the pathology of cardiac diseases. Approaches include developing a disease model by differentiating patient-specific iPSCs to cardiomyocytes to recapitulate the disease *in-vitro*. Using the cardiomyocytes generated, RNA and protein studies were conducted to elucidate on the molecular mechanism of the splice-site *LMNA* mutation. Our results showed that there was monoallelic expression of wild type *LMNA* allele in patient fibroblasts and cardiomyocytes.

Whereas, Lamin A/C protein expression remained equal between patient and control fibroblasts, we found significant reduction in Lamin A/C protein level in patient cardiomyocytes underscoring the tissue-specificity of laminopathies. Further studies using single cell RNA-sequencing (scRNA-seq) followed by pathway analysis revealed that there was delayed activation of crucial cardiogenic genes due to the inhibition of the BMP signaling pathway, combined with the activation of PTEN signaling pathway that prevented beta-catenin nuclear accumulation leading to suppression of Wnt signaling pathway activity. Furthermore, we managed to link Lamin A/C haploinsufficiency to the activation of signaling pathways associated with apoptosis and accumulation of DNA damage. Taken together, our studies highlighted the utility of iPSC-based disease modeling to study molecular mechanisms of diseases and identified possible signaling pathways that affected cardiomyocyte differentiation and contributed to the pathology of Lamin-associated cardiac diseases.

CHAPTER 1

INTRODUCTION

1.1. Lamin A/C

Lamin A/C is an intermediate filament protein that constructs the nuclear lamina of a cell encoded by the gene *LMNA*. Lamins are one of the six types of intermediate filament (IF) proteins ubiquitous in metazoans. Lamins are classified as type V IF with specialized functions and localization in the nuclei and nuclear envelope of animal cells. As a result of alternative splicing of the *LMNA* mRNA, two distinct protein products, Lamin A and Lamin C proteins (Lamin A/C), originated from a single gene. Lamin A is translated from twelve exons of the *LMNA* gene, while Lamin C comprises only 10 exons of the *LMNA* gene (Figure I.1). While Lamin C was translated as the full-length, mature and functional form, Lamin A was produced as a precursor protein, prelamin A, that needed to undergo further post-translational modification. Since Lamin A and Lamin C are generated from the same gene, there is a high degree of sequence homology between these two proteins, with several exceptions. First, Lamin C contains six unique amino acids in its C-terminus, not found in prelamin A. Next, when compared to prelamin A, Lamin C is devoid of approximately 98 amino acid residues that are present in the C-terminus of prelamin A prior to maturation to Lamin A. Finally, prelamin A, the precursor to Lamin A, contains a CaaX tail common among all lamin isoforms but absent in Lamin C. The presence of the CaaX tail is crucial for prelamin A to be able to undergo post-translational modification which consisted of farnesylation of the CaaX box to produce mature Lamin A protein [1].

At the protein level, Lamin A is a 74 kDa protein, while Lamin C is smaller in size, at 62 kDa [2]. Structurally, Lamin A and Lamin C contain alpha helical rod domains in the head region and an Ig fold in the tail region. The tail region also contained a nuclear localization signal to ensure translocation of nascent proteins from the cytoplasm back to

the nucleus. Lamins are capable of forming extensive polymer networks through intricate assembly of Lamin monomers. Both Lamin A and Lamin C are able to form dimers through their respective alpha helical domains. These dimers then form higher order structures when multiple Lamin A and Lamin C dimers associate to form Lamin polymers. After Lamin polymers are formed, multiple polymers then associate in an anti-parallel manner to form protofilaments. Finally, protofilaments associate to form an intermediate filament meshwork located in the inner nuclear membrane of the nucleus [3].

Lamin A/C expression is developmentally regulated. In undifferentiated cells such as germ cells or embryonic stem cells, Lamin A/C expression are low. Yet, as cells start to differentiate Lamin A/C levels started to increase until its expression are ubiquitous in the nuclei of terminally differentiated cells. On the other hand, the expression of other nuclear lamina proteins Lamin B1 and Lamin B2 are not under such strict developmental regulation as they can be detected in undifferentiated and differentiated cells [4-6].

Canonically, nuclear lamina proteins have been documented to provide structural support to the nuclear envelope and play a crucial role in maintaining nuclear shape and stability [7]. Cells that are deficient in Lamin A/C have been shown to have abnormal nuclear morphology, with nuclear blebbing being the most prominent phenotype [8, 9]. Additionally, nuclear lamins, more specifically Lamin A, are also distributed throughout the nucleoplasm leading to new insight on the protein's functions [10]. New studies have also shown that Lamin A/C plays an important role in regulating gene expression by sequestering transcription factors [11].

Recently, Lamin A/C have also been implicated in processes such as nuclear chromatin localization and organization [12-16], DNA replication [17-19] and cell

differentiation [20-23]. In addition, Lamin A/C has been shown to regulate cell proliferation [24-26]. It has also been shown that *LMNA* mutation activates the MAPK signaling pathway which in turn causes aberrant expression of target genes implicated in cell differentiation and proliferation [27, 28]. The presence of Lamin-associated domains (LADs) and its association with gene repression indicate that Lamin A/C plays a role in modulating gene expression. Recently, an epigenetic study interrogating the LAD size in *LMNA* mutant and control myoblasts showed that mutant myoblasts have diminished LAD size and aberrant expression of *SOX2* that hinders differentiation [29]. This study suggested that the one of the underlying causes of laminopathies is changes in the epigenome (Figure I.2). These studies uncovered the diverse role and functionality of Lamin A/C, in addition to its most known role as a structural protein. Unsurprisingly, when mutations occur in the *LMNA* gene they caused severe damage to the cell's health and functionality. These detrimental effects then compounded and manifested *in-vivo* as diseases collectively termed as laminopathies.

1.2. Laminopathies

Mutations in the *LMNA* gene have long been documented to give rise to a group of diseases termed laminopathies, due to these diseases being brought about by mutation in the nuclear lamina. Laminopathies manifest most notably in mesoderm derived tissues such as skeletal muscles, adipose tissue and cardiac muscles. Some diseases that are classified as laminopathies are dilated cardiomyopathy [30-33], Charcot-Marie-Tooth disorder [34], partial lipodystrophy [35-37], muscular dystrophy [38, 39] and Hutchinson-Gilford progeria syndrome (HGPS), also known as progeria, a progressive genetic disorder

that causes rapid aging in affected individuals [40-43]. The molecular mechanisms that give rise to different phenotypes, despite similarities in genotype, are still unidentified. In addition, the complex and poorly characterized pathology of *LMNA*-associated cardiac diseases make them challenging to treat. In addition to the varying number of phenotypic manifestations, laminopathies have a wide range of molecular mechanisms that have been identified so far to contribute to the disease. Certain laminopathies that manifested as dilated cardiomyopathy involved the downregulation of Wnt/β-catenin signaling pathway [44], while other Lamin-associated dilated cardiomyopathy involved the aberrant activation of the MAPK pathway [27, 28, 45, 46]and the mTOR pathway [47, 48]. These differences in molecular mechanisms contributed to the vast complexity of laminopathies where the same phenotypes are caused by different molecular mechanisms, and also add to the complexity of treatment prescription since the same pathologies arise from different signaling pathways *in-vitro*.

Many patients suffering from laminopathies are asymptomatic, which leads to late diagnosis and a high number of patients dying from sudden death syndrome. Current treatments are focused on ameliorating symptoms by prescribing medications or pacemaker to regulate heartbeat in arrhythmia patients. Yet, these approaches do nothing to address the root cause of the disease which is the *LMNA* mutation. For that reason, there is a great need to understand the underlying mechanism of Lamin-associated cardiac diseases. My goal is to identify key pathways and protein targets to potentially develop a more efficient and reliable method to treat cardiomyopathies.

There are two prevailing hypotheses in the field as to how *LMNA* mutations give rise to laminopathies: the mechanical defect hypothesis and the gene expression dysregulation

hypothesis. In the first case, *LMNA* mutation is predicted to lead to vulnerable nuclear structure which makes *LMNA* deficient cells more vulnerable to physiological and mechanical stresses and more prone to apoptosis [49, 50]. These vulnerabilities can be observed through the prevalence of abnormal nuclei shapes, most notably nuclear membrane blebbing. The second hypothesis posits that *LMNA*, through its ability to interact with various transcription factors in the nucleus as well as its ability to organize LADs to repress certain gene expression, plays a major role in regulating gene expression, and when *LMNA* mutations disrupt its expression, these gene expression regulation processes are affected and potentially give rise to laminopathies [29, 51]. Various *in-vitro* studies on the wide array of *LMNA* mutations have shown that both of these phenomena occur in *LMNA* deficient cells, underscoring the fact that *LMNA* mutations affect different cellular processes and highlights the importance of having a functional nuclear lamina in maintaining proper nuclear structure and gene expression regulation to sustain viable and functional cells.

1.3. Study Objective

The main focus of this dissertation is to determine the underlying molecular mechanisms of Lamin A/C mutations and how the genotype manifests as cardiac diseases. Previous studies have approached this question by performing *in-vitro* studies on somatic cells obtained from affected individuals and non-affected individuals. Approaches to elucidate molecular mechanisms of mutations have conventionally been molecular and protein expression studies, followed by any intervention to ameliorate any pathologies associated with the mutation. In this age of bioinformatics, genome-wide transcriptomic

and proteomic profiling is now also widely used to further elucidate on how mutations affect normal gene and protein expression and how these changes would relate to the phenotypes seen in the affected individuals.

The Zaragoza lab has previously identified two *LMNA* mutations in two large multi-generational families afflicted with dilated cardiomyopathy. Using whole exome sequencing on fibroblasts collected from affected individuals and unaffected family members, two distinct and novel *LMNA* mutations are identified: *LMNA* missense mutation (*LMNA* c.736 C>T) and *LMNA* splice-site mutation (*LMNA* c.357-2A>G) (Figure I.3A). Once the pathogenic mutations were discovered, we aimed to elucidate their molecular mechanisms by studying the *LMNA* expression in fibroblasts of affected individuals, compared to unaffected individuals. Our lab previously published findings regarding the molecular expression studies aimed to determine the molecular mechanisms of *LMNA* splice-site mutation (*LMNA* c.357-2A>G) [52]. Here, we describe the monoallelic expression of *LMNA* mRNA in *LMNA* mutant fibroblast. We also postulated that the absent mutant *LMNA* transcript was eliminated by nonsense mediated decay in fibroblasts, and that we will observe the presence of mutant *LMNA* transcript in the cardiomyocytes of affected individuals. Additionally, we offered two hypotheses on how the *LMNA* splice-site mutation will manifest *in-vitro*: 1) Lamin A/C haploinsufficiency or 2) the Dominant Negative effect (Figure I.3B). In the Lamin A/C haploinsufficency hypothesis, we predicted that the *LMNA* splice-site mutation caused monoallelic expression of *LMNA* mRNA, which eventually lead to a reduction in the amount of Lamin A/C protein that disrupt normal cellular processes. On the other hand, the Dominant Negative effect hypothesis predicted that both wild-type and mutant *LMNA* alleles are expressed in the cardiomyocytes of affected individuals.

However, since the mutant *LMNA* allele contained a premature truncation codon (PTC), the protein product from the mutant *LMNA* allele would be a truncated Lamin A/C protein. In the Dominant Negative effect hypothesis, we predict a reduction of full-length Lamin A/C protein in addition to the presence of a truncated Lamin A/C protein. To determine which of these predicted mechanisms occur *in-vitro*, it is necessary to perform subsequent molecular and protein expression studies in a cell type that most represent the affected cell type *in-vivo*.

The discovery that somatic cells can be reverted to their undifferentiated state, generating induced pluripotent stem cells (iPSC) using four defined transcription factors broadens the use of stem cells as a tool for disease modeling [53, 54]. Our lab used the Yamanaka factors (*Oct4, Sox2, Klf4* and *c-Myc*) to reprogram patient fibroblasts, and several clones have been established for further characterization and study. Similarly, other groups have also established *LMNA*-associated iPSC disease models, as previously reported [55-58]. By performing molecular and protein studies on patient and control specific iPSC-derived cardiomyocytes, we will be able to elucidate the effects of *LMNA* splice site mutation in cardiac tissues and investigate changes in gene and protein expression.

In chapters 2 and 3, I seek to determine molecular mechanisms of *LMNA* missense mutation (*LMNA* c.736 C>T) and *LMNA* splice-site mutation (*LMNA* c.357-2A>G). This is accomplished by evaluating *LMNA* gene expression levels between patients and control fibroblasts. In the process, I would also evaluate whether the use of fibroblasts as a platform for disease modeling studies is the best choice. Next, bulk RNA sequencing (RNA-seq) on patient and control fibroblasts was performed to test the hypothesis that splice-site mutation in the *LMNA* gene is associated with altered expression of genes that played a

significant role in the nuclear lamina structure and function. By deep RNA-seq of patient and control fibroblasts, I evaluated expression of Lamins A and C, tested for aberrant splicing of *LMNA* transcripts, and altered ratio of *LMNA* transcript variants. I also sought to determine whether there are any compensatory mechanisms by Lamin B1 and/or Lamin B2 in response to the mutation that might account for the otherwise normal appearance of affected individuals at the time of their births. Finally, I performed pathway analysis on significantly differentially expressed genes to elucidate on signaling pathways involved in the pathogenesis of laminopathy.

In Chapter 4, I focused on generating patient-specific induced pluripotent stem cells (iPSCs) and iPSC-derived cardiomyocytes (iPSC-CMs) to establish a disease model platform to study Lamin-associated cardiac diseases and to perform comprehensive study on how the Lamin A/C splice site mutation give rise to dilated cardiomyopathy. The *LMNA* mutation is predicted to result in an out of frame exon deletion resulting in Lamin A/C haploinsufficiency, thereby disrupting cellular functions and processes such as cell differentiation and gene expression. By using this disease modeling system, I aim to assess whether the novel Lamin A/C splice site mutation affected stem cell pluripotency, chromosomal stability, cell differentiation process and Lamin A/C expression in iPSC-CMs. With the advent of single cell RNA-sequencing (scRNA-seq) technology, it is now possible to conduct transcriptomic profiling at a single cell resolution, providing new insight on various biological processes such as cellular differentiation trajectory and cellular heterogeneity and how it impacts gene expression [59, 60]. Using scRNA-seq, several groups have uncovered novel information on diseases such as cystic fibrosis, glioblastoma and breast cancer, providing new insights and understanding on how to treat these

diseases [61-63]. Here, I utilized scRNA-seq to further explicate how the novel *LMNA* splice-site mutation affect the cardiac differentiation process by performing a time-course differentiation experiment on one control and one patient iPSC-CMs. My study expanded on previous time-course cardiomyocyte differentiation studies conducted on non-diseased iPSC-CMs [64, 65]. Together, these studies will provide new insight to the cell-specific effects of Lamin A/C haploinsufficiency.

Ultimately, our studies aim to discover novel target genes or pathways that can be utilized for the development of new therapeutics to treat inheritable cardiac diseases. In this dissertation, I will detail the studies conducted to test the hypothesis that Lamin A/C haploinsufficiency causes altered differentiation capabilities and expression of genes that play a significant role in the nuclear and lamina structure and function in affected individuals.

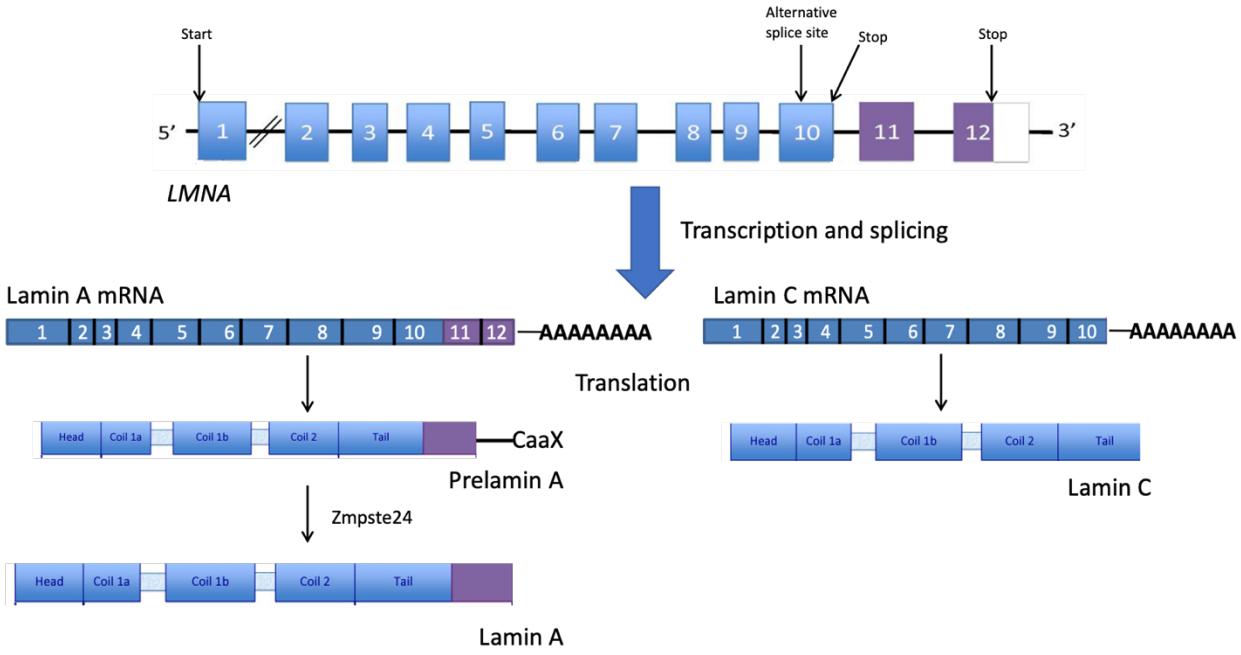

Figure I.1: Lamin A/C processing schematic. The *LMNA* gene contains an alternative splice site at exon 10, which when transcribed enables the production of both Lamin A (12 exons) and Lamin C (10 exons) mRNAs. While Lamin C mRNA is readily translated to produce mature Lamin C protein, Lamin A mRNA is translated to the Lamin A precursor protein Prelamin A which undergoes further posttranslational modification involving the protease Zmpste24 to produce functional Lamin A protein.

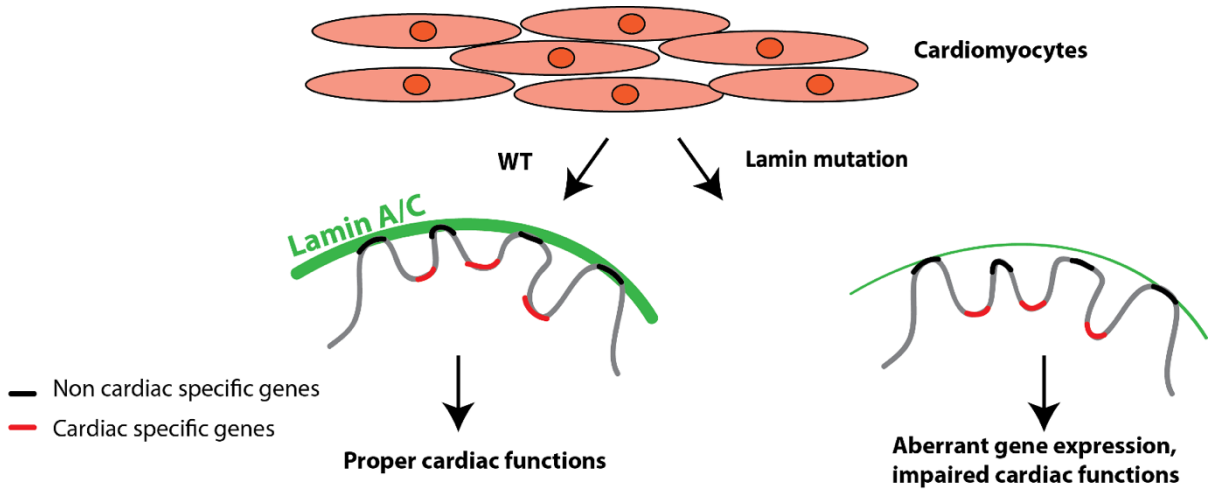

Figure I.2: Mutations in the *LMNA* gene give rise to laminopathies through a wide array of molecular mechanisms. *LMNA* mutation has been shown to give rise to laminopathies through deregulation of various cellular processes, such as the reduction in Lamin-associated domain (LAD) size as shown here. Lamin mutations might reduce the amount of Lamin A/C proteins available to form LADs, or deform the nuclear structure leading to less available space to form LADs which ultimately lead to laminopathies.

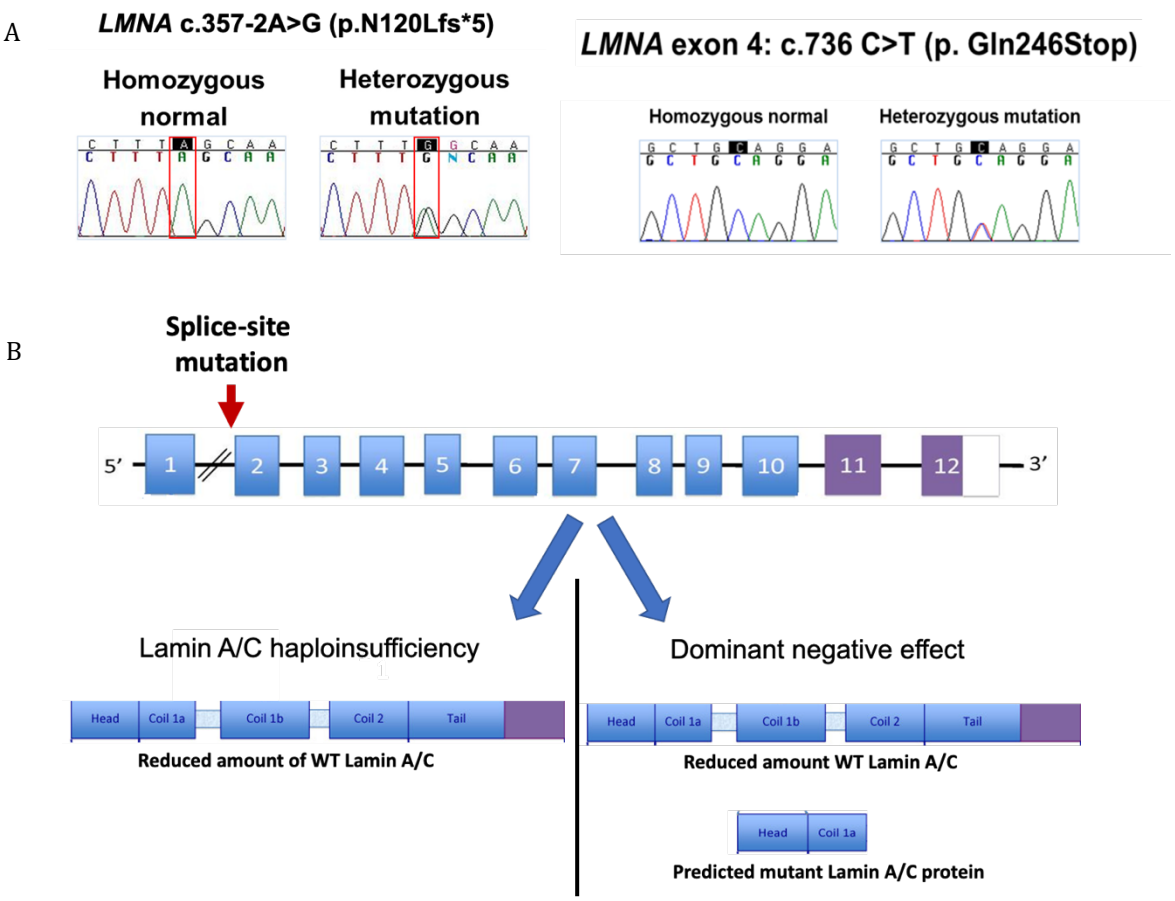

Figure I.3: *LMNA* mutations featured in this study, and the predicted molecular mechanism of Lamin A/C splice site-mutation. (A) We previously identified two *LMNA* mutations in two large families affected by cardiac diseases: *LMNA* splice site mutation at intron 1 (*LMNA* c.357-2A > G) predicted to result in exon skipping and frameshifting and *LMNA* missense mutation at exon 4 (*LMNA* c.736 C>T) predicted to result in premature stop codon. (B) The predicted molecular mechanisms of *LMNA* splice site mutation. Two possible mechanisms are outlined here. The goal of this dissertation is to ascertain which of these mechanisms occur *in-vitro*.

1.4. References

1. Davies, B.S., et al., *The posttranslational processing of prelamin A and disease.* Annu Rev Genomics Hum Genet, 2009. **10**: p. 153-74.
2. Burke, B. and C.L. Stewart, *Life at the edge: the nuclear envelope and human disease.* Nat Rev Mol Cell Biol, 2002. **3**(8): p. 575-85.
3. Dittmer, T.A. and T. Misteli, *The lamin protein family.* Genome Biol, 2011. **12**(5): p. 222.
4. Broers, J.L., et al., *A- and B-type lamins are differentially expressed in normal human tissues.* Histochem Cell Biol, 1997. **107**(6): p. 505-17.
5. Lin, F. and H.J. Worman, *Expression of nuclear lamins in human tissues and cancer cell lines and transcription from the promoters of the lamin A/C and B1 genes.* Exp Cell Res, 1997. **236**(2): p. 378-84.
6. Tilli, C.M., et al., *Lamin expression in normal human skin, actinic keratosis, squamous cell carcinoma and basal cell carcinoma.* Br J Dermatol, 2003. **148**(1): p. 102-9.
7. Fong, L.G., et al., *Prelamin A and lamin A appear to be dispensable in the nuclear lamina.* J Clin Invest, 2006. **116**(3): p. 743-52.
8. Sullivan, T., et al., *Loss of A-type lamin expression compromises nuclear envelope integrity leading to muscular dystrophy.* J Cell Biol, 1999. **147**(5): p. 913-20.
9. Lammerding, J., et al., *Lamin A/C deficiency causes defective nuclear mechanics and mechanotransduction.* J Clin Invest, 2004. **113**(3): p. 370-8.
10. Lutz, R.J., et al., *Nucleoplasmic localization of prelamin A: implications for prenylation-dependent lamin A assembly into the nuclear lamina.* Proc Natl Acad Sci U S A, 1992. **89**(7): p. 3000-4.
11. Mariappan, I. and V.K. Parnaik, *Sequestration of pRb by cyclin D3 causes intranuclear reorganization of lamin A/C during muscle cell differentiation.* Mol Biol Cell, 2005. **16**(4): p. 1948-60.
12. Glass, C.A., et al., *The alpha-helical rod domain of human lamins A and C contains a chromatin binding site.* EMBO J, 1993. **12**(11): p. 4413-24.
13. Galiova, G., et al., *Chromatin changes induced by lamin A/C deficiency and the histone deacetylase inhibitor trichostatin A.* Eur J Cell Biol, 2008. **87**(5): p. 291-303.
14. Lund, E., et al., *Lamin A/C-promoter interactions specify chromatin state-dependent transcription outcomes.* Genome Res, 2013. **23**(10): p. 1580-9.
15. McCord, R.P., et al., *Correlated alterations in genome organization, histone methylation, and DNA-lamin A/C interactions in Hutchinson-Gilford progeria syndrome.* Genome Res, 2013. **23**(2): p. 260-9.
16. Solovei, I., et al., *LBR and lamin A/C sequentially tether peripheral heterochromatin and inversely regulate differentiation.* Cell, 2013. **152**(3): p. 584-98.
17. Spann, T.P., et al., *Disruption of nuclear lamin organization alters the distribution of replication factors and inhibits DNA synthesis.* J Cell Biol, 1997. **136**(6): p. 1201-12.
18. Kennedy, B.K., et al., *Nuclear organization of DNA replication in primary mammalian cells.* Genes Dev, 2000. **14**(22): p. 2855-68.
19. Singh, M., et al., *Lamin A/C depletion enhances DNA damage-induced stalled replication fork arrest.* Mol Cell Biol, 2013. **33**(6): p. 1210-22.
20. Constantinescu, D., et al., *Lamin A/C expression is a marker of mouse and human embryonic stem cell differentiation.* Stem Cells, 2006. **24**(1): p. 177-85.
21. Frock, R.L., et al., *Lamin A/C and emerin are critical for skeletal muscle satellite cell differentiation.* Genes Dev, 2006. **20**(4): p. 486-500.
22. Melcer, S., et al., *Histone modifications and lamin A regulate chromatin protein dynamics in early embryonic stem cell differentiation.* Nat Commun, 2012. **3**: p. 910.
23. Bermeo, S., et al., *Lamin A/C Acts as an Essential Factor in Mesenchymal Stem Cell Differentiation Through the Regulation of the Dynamics of the Wnt/beta-Catenin Pathway.* J Cell Biochem, 2015. **116**(10): p. 2344-53.
24. Naetar, N. and R. Foisner, *Lamin complexes in the nuclear interior control progenitor cell proliferation and tissue homeostasis.* Cell Cycle, 2009. **8**(10): p. 1488-93.
25. Moiseeva, O., et al., *Retinoblastoma-independent regulation of cell proliferation and senescence by the p53-p21 axis in lamin A /C-depleted cells.* Aging Cell, 2011. **10**(5): p. 789-97.

26. Pongsakul, N., et al., *Lamin A/C in renal tubular cells is important for tissue repair, cell proliferation, and calcium oxalate crystal adhesion, and is associated with potential crystal receptors.* FASEB J, 2016. **30**(10): p. 3368-3377.
27. Muchir, A., et al., *Activation of MAPK in hearts of EMD null mice: similarities between mouse models of X-linked and autosomal dominant Emery Dreifuss muscular dystrophy.* Hum Mol Genet, 2007. **16**(15): p. 1884-95.
28. Muchir, A., et al., *Abnormal p38alpha mitogen-activated protein kinase signaling in dilated cardiomyopathy caused by lamin A/C gene mutation.* Hum Mol Genet, 2012. **21**(19): p. 4325-33.
29. Perovanovic, J., et al., *Laminopathies disrupt epigenomic developmental programs and cell fate.* Sci Transl Med, 2016. **8**(335): p. 335ra58.
30. Fatkin, D., et al., *Missense mutations in the rod domain of the lamin A/C gene as causes of dilated cardiomyopathy and conduction-system disease.* N Engl J Med, 1999. **341**(23): p. 1715-24.
31. Muchir, A., et al., *Identification of mutations in the gene encoding lamins A/C in autosomal dominant limb girdle muscular dystrophy with atrioventricular conduction disturbances (LGMD1B).* Hum Mol Genet, 2000. **9**(9): p. 1453-9.
32. Charniot, J.C., et al., *Functional consequences of an LMNA mutation associated with a new cardiac and non-cardiac phenotype.* Hum Mutat, 2003. **21**(5): p. 473-81.
33. Salvarani, N., et al., *The K219T-Lamin mutation induces conduction defects through epigenetic inhibition of SCN5A in human cardiac laminopathy.* Nat Commun, 2019. **10**(1): p. 2267.
34. De Sandre-Giovannoli, A., et al., *Homozygous defects in LMNA, encoding lamin A/C nuclear-envelope proteins, cause autosomal recessive axonal neuropathy in human (Charcot-Marie-Tooth disorder type 2) and mouse.* Am J Hum Genet, 2002. **70**(3): p. 726-36.
35. Garg, A., R.M. Peshock, and J.L. Fleckenstein, *Adipose tissue distribution pattern in patients with familial partial lipodystrophy (Dunnigan variety).* J Clin Endocrinol Metab, 1999. **84**(1): p. 170-4.
36. Shackleton, S., et al., *LMNA, encoding lamin A/C, is mutated in partial lipodystrophy.* Nat Genet, 2000. **24**(2): p. 153-6.
37. Ostlund, C., et al., *Properties of lamin A mutants found in Emery-Dreifuss muscular dystrophy, cardiomyopathy and Dunnigan-type partial lipodystrophy.* J Cell Sci, 2001. **114**(Pt 24): p. 4435-45.
38. Bonne, G., et al., *Mutations in the gene encoding lamin A/C cause autosomal dominant Emery-Dreifuss muscular dystrophy.* Nat Genet, 1999. **21**(3): p. 285-8.
39. Walter, M.C., et al., *Deletion of the LMNA initiator codon leading to a neurogenic variant of autosomal dominant Emery-Dreifuss muscular dystrophy.* Neuromuscul Disord, 2005. **15**(1): p. 40-4.
40. DeBusk, F.L., *The Hutchinson-Gilford progeria syndrome. Report of 4 cases and review of the literature.* J Pediatr, 1972. **80**(4): p. 697-724.
41. De Sandre-Giovannoli, A., et al., *Lamin a truncation in Hutchinson-Gilford progeria.* Science, 2003. **300**(5628): p. 2055.
42. Eriksson, M., et al., *Recurrent de novo point mutations in lamin A cause Hutchinson-Gilford progeria syndrome.* Nature, 2003. **423**(6937): p. 293-8.
43. Cao, H. and R.A. Hegele, *LMNA is mutated in Hutchinson-Gilford progeria (MIM 176670) but not in Wiedemann-Rautenstrauch progeroid syndrome (MIM 264090).* J Hum Genet, 2003. **48**(5): p. 271-274.
44. Le Dour, C., et al., *Decreased WNT/beta-catenin signalling contributes to the pathogenesis of dilated cardiomyopathy caused by mutations in the lamin a/C gene.* Hum Mol Genet, 2017. **26**(2): p. 333-343.
45. Muchir, A., et al., *Activation of MAPK pathways links LMNA mutations to cardiomyopathy in Emery-Dreifuss muscular dystrophy.* J Clin Invest, 2007. **117**(5): p. 1282-93.
46. Muchir, A., et al., *Inhibition of extracellular signal-regulated kinase 1/2 signaling has beneficial effects on skeletal muscle in a mouse model of Emery-Dreifuss muscular dystrophy caused by lamin A/C gene mutation.* Skelet Muscle, 2013. **3**(1): p. 17.
47. Ramos, F.J., et al., *Rapamycin reverses elevated mTORC1 signaling in lamin A/C-deficient mice, rescues cardiac and skeletal muscle function, and extends survival.* Sci Transl Med, 2012. **4**(144): p. 144ra103.
48. Liao, C.Y., et al., *Rapamycin Reverses Metabolic Deficits in Lamin A/C-Deficient Mice.* Cell Rep, 2016. **17**(10): p. 2542-2552.
49. Broers, J.L., et al., *Both lamin A and lamin C mutations cause lamina instability as well as loss of internal nuclear lamin organization.* Exp Cell Res, 2005. **304**(2): p. 582-92.
50. Jaalouk, D.E. and J. Lammerding, *Mechanotransduction gone awry.* Nat Rev Mol Cell Biol, 2009. **10**(1): p. 63-73.

51. Brayson, D. and C.M. Shanahan, *Current insights into LMNA cardiomyopathies: Existing models and missing LINCs.* Nucleus, 2017. **8**(1): p. 17-33.
52. Zaragoza, M.V., et al., *Exome Sequencing Identifies a Novel LMNA Splice-Site Mutation and Multigenic Heterozygosity of Potential Modifiers in a Family with Sick Sinus Syndrome, Dilated Cardiomyopathy, and Sudden Cardiac Death.* PLoS One, 2016. **11**(5): p. e0155421.
53. Takahashi, K., et al., *Induction of pluripotent stem cells from adult human fibroblasts by defined factors.* Cell, 2007. **131**(5): p. 861-72.
54. Takahashi, K., et al., *Human induced pluripotent stem cells on autologous feeders.* PLoS One, 2009. **4**(12): p. e8067.
55. Siu, C.W., et al., *Modeling of lamin A/C mutation premature cardiac aging using patient-specific induced pluripotent stem cells.* Aging (Albany NY), 2012. **4**(11): p. 803-822.
56. Lee, Y.K., et al., *Modeling Treatment Response for Lamin A/C Related Dilated Cardiomyopathy in Human Induced Pluripotent Stem Cells.* J Am Heart Assoc, 2017. **6**(8).
57. Lee, J., et al., *Activation of PDGF pathway links LMNA mutation to dilated cardiomyopathy.* Nature, 2019. **572**(7769): p. 335-340.
58. Perepelina, K., et al., *Generation of two iPSC lines (FAMRCi007-A and FAMRCi007-B) from patient with Emery-Dreifuss muscular dystrophy and heart rhythm abnormalities carrying genetic variant LMNA p.Arg249Gln.* Stem Cell Res, 2020. **47**: p. 101895.
59. Liu, Z., et al., *Single-cell transcriptomics reconstructs fate conversion from fibroblast to cardiomyocyte.* Nature, 2017. **551**(7678): p. 100-104.
60. Wang, W., et al., *Exploring the changing landscape of cell-to-cell variation after CTCF knockdown via single cell RNA-seq.* BMC Genomics, 2019. **20**(1): p. 1015.
61. Patel, A.P., et al., *Single-cell RNA-seq highlights intratumoral heterogeneity in primary glioblastoma.* Science, 2014. **344**(6190): p. 1396-401.
62. Plasschaert, L.W., et al., *A single-cell atlas of the airway epithelium reveals the CFTR-rich pulmonary ionocyte.* Nature, 2018. **560**(7718): p. 377-381.
63. Nguyen, Q.H., et al., *Single-cell RNA-seq of human induced pluripotent stem cells reveals cellular heterogeneity and cell state transitions between subpopulations.* Genome Res, 2018. **28**(7): p. 1053-1066.
64. Friedman, C.E., et al., *Single-Cell Transcriptomic Analysis of Cardiac Differentiation from Human PSCs Reveals HOPX-Dependent Cardiomyocyte Maturation.* Cell Stem Cell, 2018. **23**(4): p. 586-598 e8.
65. Churko, J.M., et al., *Defining human cardiac transcription factor hierarchies using integrated single-cell heterogeneity analysis.* Nat Commun, 2018. **9**(1): p. 4906.

CHAPTER 2

Dupuytren's and Ledderhose Diseases in a Family with *LMNA*-Related Cardiomyopathy and a Novel Variant in the *ASTE1* Gene

This work was previously published Zaragoza MV, Nguyen CHH, Widyastuti HP, McCarthy LA, Grosberg A. Dupuytren's and Ledderhose Diseases in a Family with *LMNA*-Related Cardiomyopathy and a Novel Variant in the *ASTE1* Gene. *Cells*. 2017;6(4):40. Published 2017 Nov 1. doi:10.3390/cells6040040

In this work, I performed *LMNA* transcript quantification, analyzed the results, wrote the results and parts of the Discussions, specifically those concerning the molecular mechanism of the mutation.

2.1. Introduction

Dupuytren's disease (DD) or palmar fibromatosis is characterized by abnormal proliferation of fibroblasts in the palmar fascia and leads to progressive and disabling contractures of the fingers [1]. Initially, a palmar nodule is observed which is followed by cord formation as the disease progresses. Disease pathogenesis is complex and involves activation of fibroblasts to myofibroblasts, production of several profibrotic cytokines including transforming growth factor beta 1 (TGF-beta1), transforming growth factor alpha (TGF-alpha) and epidermal growth factor (EGF), dysregulation of signaling pathways including mitogen-activated protein kinase (MAPK), Akt, and Wnt/beta-catenin signaling pathways, and increased extracellular matrix proteins including collagen I and III [2]. Treatment includes surgical excision but there is a high risk of relapse [3]. Ledderhose disease (LD) or palmar fibromatosis is a rarer disease that affects the plantar fascia as nodules and cords formed along the tendons of the foot which can lead to painful walking or standing with disease progression [4-6].

Family studies have shown that there is a genetic component with manifestation of the diseases. About 40% of those affected with DD have an affected relative and a family history of the disease is correlated with increased number of affected fingers and increased frequency of extrapalmar involvement [7]. Although inheritance is heterogeneous, DD is most often transmitted in an autosomal dominant fashion with variable penetrance; a similar hereditary pattern may be possible for LD since it is considered the plantar counterpart of Dupuytren's disease [8-10]. Given the low prevalence of the disease [5], the genetics of LD has not yet been fully characterized and the genetic mechanism of both diseases remains largely unknown.

The *LMNA* gene encodes for Lamin A/C, intermediate filament proteins that serve as structural components crucial in maintaining cell nucleus integrity [11,12]. Due to its adjacency to the nuclear inner membrane and proximity to the genome, Lamin A/C has also been implicated in key nuclear functions including cell differentiation, regulation of gene expression through chromatin localization and remodeling, and activation or repression of signaling pathways [12-17]. Over 400 *LMNA* mutations have been reported in patients with phenotypes known collectively as laminopathies including premature aging syndromes (Hutchinson-Gilford Progeria Syndrome and atypical Werner syndrome), skeletal muscle myopathies (Emery-Dreifuss Muscular Dystrophy and Limb-Girdle Muscular Dystrophy), and cardiac diseases (dilated cardiomyopathy and cardiac conduction defects) [11,18]. While musculoskeletal features have been frequently noted in *LMNA*-associated diseases, DD has been reported only once in a patient with *LMNA*-associated atypical Werner syndrome [19]. Comorbidity of DD and Limb-Girdle Muscular Dystrophy has been reported in another patient; however, the three most common *LMNA* mutations were not detected in the patient [20].

Here, we report a unique family with cardiac disease due to a previously reported nonsense mutation in the Lamin A/C gene (*LMNA* c.736 C>T (p. Gln246Stop)) and variable features of DD and LD. After fibroblast RNA studies revealed a mechanism consistent with *LMNA* haploinsufficiency, we used whole exome sequencing, bioinformatics analysis, and family studies to identify a novel, heterozygous missense variant in the Asteroid Homolog 1 gene (*ASTE1* c.230T>C, p.Val77Ala) as a candidate susceptibility variant in fibromatosis for patients with *LMNA* haploinsufficiency and a potential genetic factor in the etiology of DD and LD.

2.2. Materials and Methods

2.2.1. Study family

Pedigree and consent: A family (Figure II.1) with English, Scottish, Irish, German, and Native American ancestry was studied. All subjects gave their informed consent for inclusion before they participated in the study. The study was conducted in accordance with the Declaration of Helsinki, and the protocol was approved by the University of California institutional review board (#2011-8030). Pedigree, completed questionnaire on health history, medical records, and samples (saliva and/or skin biopsies) were obtained for each individual. Additional signed consent was obtained prior to manuscript submission. One family member (Patient 3) was removed from the pedigree after consent to publish was declined.

Clinical features: Each individual was classified by clinical status as affected, unaffected, or unknown for heart disease, DD, and LD (Figure II.1). Classification for heart disease was as described previously [21]. For DD, individuals were classified as affected if they displayed physical signs of fibromatosis in their hands including dimpling, tethering, or puckering of palmar skin, flexion contracture with limited extension of the fingers, subcutaneous palmar nodules or cords [3]. For LD, individuals were classified as affected with foot involvement including plantar nodules, cords, or limited toe movement [5,6]. Risk factors associated with DD were also evaluated including smoking, alcohol abuse, and diabetes [3]. For deceased individuals, family history and review of available medical records were used to determine the status of cardiac disease, DD, and LD.

Proband: The proband (IV-2, Figure II.1) is a 58-year-old female who was healthy until age 45 when she had syncope and an irregular heartbeat. Holter studies showed

periods of sinus arrest. She was diagnosed with Sick Sinus Syndrome and a dual chamber pacemaker was placed. She had a normal echocardiogram [Ejection Fraction (EF) = 50% (normal >45%), Interventricular Septal (IVS) thickness = 11 mm (normal 7-12 mm), Left Ventricular Posterior Wall (PW) thickness, LVPW = 8 mm (normal 7-12 mm), Left Ventricular End Diastolic Diameter (LVEDD) = 53 mm (normal 35mm-55mm), Fractional Shortening (FS) = 25% (normal >25%)]. At age 55, she developed worsening fatigue and dyspnea on exertion and was found to have atrial fibrillation, non-sustained ventricular tachycardia, and high degree atrioventricular block. Echocardiogram showed reduced systolic function (EF = 33%, LVEDD = 52 mm). Due to these findings plus her family history, clinical genetic testing for dilated cardiomyopathy (DCM) was performed and the results showed a heterozygous nonsense mutation in *LMNA* exon 4 (c.736 C>T, p.Gln246Stop). The pacemaker was replaced with biventricular implantable cardioverter defibrillator (ICD). At her current age, she was doing well with no shortness of breath, palpitations, or syncope and no ICD shocks. Her medications include carvedilol, losartan, and warfarin, and her most recent echocardiogram showed mild-moderately impaired LV systolic function with normal LV size and wall thickness [EF = 40-45%, IVS = 10 mm, LVPW = 7 mm, LVEDD = 50 mm, FS = 28%].

At age 50, she noticed early signs of DD. She developed right hand stiffness after driving her car for extended periods and noted skin dimpling on her right palm (Figure II.2). At age 55, she developed two plantar nodules (less than 1cm in diameter), one each at the central medial region of her right and left soles consistent with LD (Figure II.2). At her present age of 58, she denied hand or foot pain. She has no cord formation, contractures, or knuckle pads of her hands. She has full extension of her fingers and toes with no limitations

in function. She noted limited alcohol use (1 glass of wine/week) and no tobacco use. She had a normal birth and development with no signs or symptoms of neuromuscular disease.

Affected family members: There are at least 12 family members affected with cardiac disease, DD, and/or LD (Figure II.1): five living (one maternal aunt (III-4), one sister (IV-3), and one maternal first cousin (IV-4) and seven deceased individuals (I-2, II-2, II-5, II-7, II-8, III-2, III-5). Clinical features for one affected living family member with cardiac disease and DD (Patient 3) were removed after additional consent to publish was declined. The maternal grandfather (II-7) had an irregular heart beat diagnosed in his 40s, pacemaker implantation at age 64, heart failure at age 66, and cardiac arrest at age 68. With sudden death of two siblings (II-2, II-5) and his mother (I-2) all in their 50s, *LMNA*-related cardiac disease was likely introduced into the family by the maternal grandfather (II-7). DD was likely introduced into the family by the maternal grandmother (II-8), the only individual with known DD without cardiac disease. The main clinical features are provided in Table S1, Supplementary Material.

2.2.2. Molecular studies

Sanger sequencing for LMNA exon 4: DNA sequencing and analysis of *LMNA* exon 4 were done first using saliva DNA as described [21]. The presence (+) or absence (-) of the *LMNA* nonsense mutation (c.736 C>T, p.Gln246Stop) was tested for seven individuals: five affected with cardiac disease (III-4, proband: IV-2, IV-3, IV-4, and Patient 3) and two unaffected (IV-1 and IV-5) family members.

LMNA RNA and DNA studies in fibroblast: To evaluate the molecular mechanism of the *LMNA* mutation, primary cultures were established using skin biopsies obtained from six

individuals, four affected (patients: P1 (IV-4), P2 (IV-3), P3, and P4 (III-4)) and two unaffected (controls: C1 (IV-5) and C2 (IV-1)) family members. Fibroblasts were not available for the proband (IV-2). In addition, skin fibroblast from a healthy individual (CC-251, Lonza Group Ltd, Basel, Switzerland) was used as an unrelated control. Total RNA and genomic DNA extractions, qualitative RNA analysis using targeted PCR amplifications of cDNA, Sanger sequencing, and PCR primers used to evaluate for exonic variants in *LMNA* were conducted as described [21]. Real time quantitative PCR (RT-qPCR) was also performed on cDNA from P1 (IV-4) and P2 (IV-3) and their gender-age matched controls, C1 (IV-5) and C2 (IV-1), respectively. P3 and P4 (III-4) were not included in the RT-qPCR studies due to absence of matched controls from the family. Pre-designed KiCqStart™ Primers (Sigma-Aldrich, Saint Louis, MO) for Lamin A, Lamin C, and Beta macroglobulin (*B2M*) transcripts and the ViiA7 Real Time PCR system (Applied Biosystems, Carlsbad, CA) were used to amplify the cDNA samples in triplicate. Ct values were analyzed using the comparative Ct method to obtain relative gene expression (RGE) for Lamin A and C. Student's t-test was used to determine statistical significance, with $P< 0.05$ considered as statistically significant.

Exome sequencing, bioinformatics analysis, and variant filtering: For four family members, genomic DNA isolated from skin fibroblast was sent to DNA Link USA, Inc. (San Diego, CA) for whole exome sequencing (WES). These studies included three affected individuals with cardiac disease, DD and/or LD (III-4, IV-3, and Patient 3) and one unaffected individual without cardiac disease, DD and LD (IV-1). The proband (IV-2) was not included in the exome sequencing studies since fibroblast were not available. The WES studies used

enrichment by Agilent SureSelect XT Human All Exon V5 library and paired-end sequencing by Illumina HiSeq2500 at 100X coverage. The CLC bio Biomedical Genomics Workbench v3.5 (Qiagen, Valencia, CA) was used to align the data to the human genome reference (hg38). The Identify and Annotate Variants (WES-HD) workflow and variant analysis tools for splicing effects were utilized to identify DNA variants. The lists of variants for each of the four family members were filtered in a step-wise approach to identify potential mutations and modifiers similar to the approach as described [21,22]. Candidate variants were identified as potentially deleterious single nucleotide variants (SNV) and insertion-deletion variants (indels) that were shared among the three affected family members (III-4, IV-3, and Patient 3) and not shared with the one individual unaffected at age 60 years old (IV-1). Using the ExAC human genome database [23] the candidates were ranked by allele frequency to identify rare variants (allele frequency <1%) as high-priority candidates.

Family studies: To validate the exome sequencing results and to further evaluate the high-priority candidate variants as potential genetic factors in DD and LD, family studies of five individuals using saliva or fibroblast DNA were conducted by Sanger sequencing to determine co-segregation of each candidate variant and phenotype. These studies included four affected individuals with cardiac disease, DD and/or LD (III-4, proband: IV-2, IV-3, and Patient 3) and one unaffected individual without cardiac disease, DD and LD (IV-1). Due to questionable phenotype and age-related penetrance for DD and LD, exome sequencing and family studies were not done for two family members, a 49-year-old female (IV-4) heterozygous for the *LMNA* mutation with no hand signs of DD and questionable foot findings for LD and a 47-year-old female (IV-5) without the *LMNA* mutation and no signs of DD or LD. Primer sequences and PCR conditions are available by request.

2.3. Results

2.3.1. LMNA DNA and RNA studies

First, DNA sequencing of *LMNA* exon 4 was conducted for seven family members (Figure II.1 and Figure II.3). All five individuals (III-4, proband: IV-2, IV-3, IV-4, and Patient 3) affected with cardiac disease were heterozygous for *LMNA* nonsense mutation (NM_170707.3: c.736 C>T, p.Gln246Stop). The mutation is predicted to result in a stop codon at amino acid 246 and premature truncation of the Lamin A/C protein. The mutation was absent in both unaffected individuals (IV-1 and IV-5).

Next, to evaluate the molecular mechanism of the *LMNA* mutation, RNA and DNA studies were done on mutant (patient) and normal (control) skin fibroblasts derived from four affected and two unaffected family members, respectively. The qualitative and sequence analyses comparing *LMNA* mRNA in fibroblast showed only the expected sequences and no differences in cDNA fragment length consistent with normal mRNA splicing (Figure II.4a). To determine which *LMNA* allele was expressed, two heterozygous exonic variants, rs538089 (NM_170707.3:c.861T>C, Ala287Ala) located in exon 5 and rs505058 (NM_170707.3: c.1338T>C, Asp446Asp) in exon 7, detected in our fibroblast DNA sequencing for all 12 exons were examined in cDNA. Comparison of *LMNA* sequences from cDNA and genomic DNA showed that both C and T alleles for each variant (rs538089 and rs505058) were detected in all control fibroblasts (Figure II.4b). In contrast, only the C alleles for each variant (rs538089 and rs505058) and the normal C allele at the mutation site in exon 4 were detected in all patient fibroblasts (Figure II.4b). These findings were consistent with the normal C allele in exon 4 being in cis with both C alleles in exons 5 and 7 and supported monoallelic expression of the normal *LMNA* allele (Figure II.4b). In

addition, these results confirmed the presence of only the single heterozygous *LMNA* mutation for patient fibroblasts and the absence of *LMNA* mutations in the control fibroblasts. To confirm Lamin A/C haploinsufficiency in patients, RT-qPCR was performed on patients and controls fibroblasts. Relative gene expression (RGE) quantification showed a reduction of Lamin A and Lamin C transcripts in patient fibroblasts compared to control fibroblasts (Figure II.4c). For Lamin A, RGE was 0.067 ± 0.012 in patient fibroblast and 0.112 ± 0.009 in control fibroblast, a 1.6 fold reduction of gene expression. For Lamin C, RGE was 0.526 ± 0.033 in patient fibroblast and 0.624 ± 0.038 in control fibroblast, a 1.2 fold reduction.

Results of the WES studies from four family members : III-4, IV-3, and Patient 3 (affected) and IV-1 (unaffected) are provided in Figure II.5 and Table II.S2, Supplementary Material. On average per sample, exome sequencing resulted in 8.1 gigabases of data (90.4% > Quality Score (Q30)) from 107.2 million reads. Bioinformatics analysis showed 99.4% of the reads mapped to hg38 for each sample and on average per sample, 81X mean depth of coverage of the target bases with 85.8% having mean coverage of at least 30X. Variant calling analysis identified on average, 20,416 total high-quality, unique variants with 12,874 heterozygous variants per sample. Of these heterozygous variants, an average of 6,488 variants were predicted to result in non-synonymous amino acids changes with 1,734 of these variants located at highly-conserved sites (phastCons score >0.90). Exome data is available from the NCBI Sequence Read Archive under NCBI BioProject " Human Exome Sequencing in *LMNA* Cardiomyopathy, " (Accession: PRJNA320422, ID: 320422).

To identify candidate variants in DD and LD, the four lists of heterozygous, non-synonymous, highly-conserved variants were compared between the three affected family

members (III-4, IV-3, and Patient 3) and one unaffected family member (IV-1) (Figure II.5). Among the three affected family members, 275 variants were shared. Of these, 98 variants were identified as candidates and 177 variants were excluded when compared to the list of variants found in the one unaffected family member (Figure II.5).

To identify high-priority candidates for further evaluation, the 98 candidates were ranked by allele frequency (Table II.S3, Supplementary Material). Seven novel or rare variants were identified including the expected *LMNA* mutation c.736C>T (p.Gln246Stop), three novel SNVs: *ASTE1* c.230T>C (p.Val77Ala), *FZD2* c.535A>C (p.Thr179Pro), and *FSD1* c.608G>A (p.Arg203Gln), two known SNVs: *OR51A7* c.763A>G (p.Ile255Val), and *SYPL2* c.272A>T (p.Tyr91Phe), and one known indel *USF3* c.4416_4418delGCA (p.Gln1478del). The *USF3* variant was not further evaluated because it is an in-frame deletion of one codon and the clinical significance of the variant is likely benign (ClinVar variant # 218482).

The remaining five high-priority candidates were further evaluated by Sanger sequencing in family studies using one additional affected family member (proband: IV-2) (Table II.1). Only two of the five high-priority candidates were validated, shared by all four affected individuals (III-4, proband: IV-2, IV-3, and Patient 3), and unshared with the one unaffected individual (IV-1). These two variants included a novel missense variant (NM_001288950: c.230T>C, p.Val77Ala) in the Asteroid Homolog 1 gene (*ASTE1*), and a rare known missense variant (NM_001004749: c.763A>G, p.Ile255Val) in the Olfactory Receptor Family 51 Subfamily A Member 7 gene (*OR51A7*). These results also excluded three of the five high-priority candidates: *FSD1* c.608G>A (p.Arg203Gln), *FZD2* c.535A>C (p.Thr179Pro), and *SYPL2* c.272A>T (p.Tyr91Phe). The *FSD1* variant was excluded because it was not found in the proband (IV-2) (Table 1). The *FZD2* and *SYPL2* variants were

excluded because of the lack of validation by Sanger sequencing. Review of the WES data found the discrepancies consistent with a false-negative result for *SYPL2* variant in the unaffected individual (IV-1) and false-positive results for *FZD2* variant in the affected individuals (III-4, IV-3, and P3).

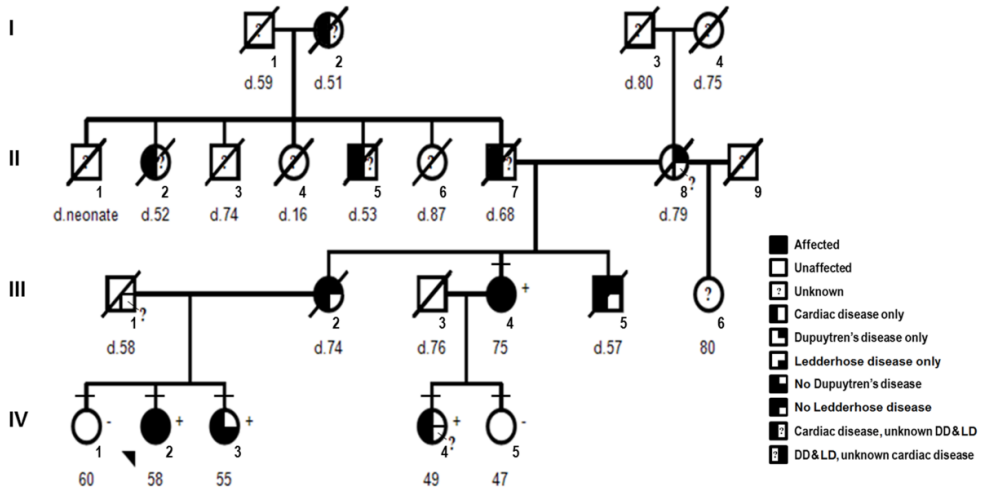

Figure II.1. Pedigree: *LMNA*-related cardiac disease, Dupuytren's disease, and Ledderhose disease. Squares denote males and circles females with current age below. Short horizontal lines mark individuals consented in the study. Diagonal lines indicate deceased individuals with age of death (d). The proband (IV-2) is designated with an arrow. Complete-filled symbols indicate cardiac disease (cardiomyopathy, arrhythmia, or sudden death), Dupuytren's disease, and Ledderhose disease. Left half-filled indicate only cardiac disease and right half-filled symbols indicate only Dupuytren's disease (upper right) or only Ledderhose disease (lower right). Individuals with unknown or unconfirmed clinical status are noted with a question mark. The presence (+) or absence (-) of the *LMNA* c.736 C>T (p.Gln246Stop) is provided. One additional family member (Patient 3) was removed after consent to publish was declined.

Figure II.2. Dupuytren's and Ledderhose disease. Photographs: [top panel] right hand, left hand, and left foot of the aunt (III-4), [bottom panel, left-middle] right hand and feet of the proband (IV-2) and [bottom panel, right] left foot of the sister (IV-3) with skin tethering/puckering or dimpling (white arrows), cord formation (yellow arrows), and central medial plantar nodules (black arrows). An image from one additional family member (Patient 3) was removed after consent to publish was declined.

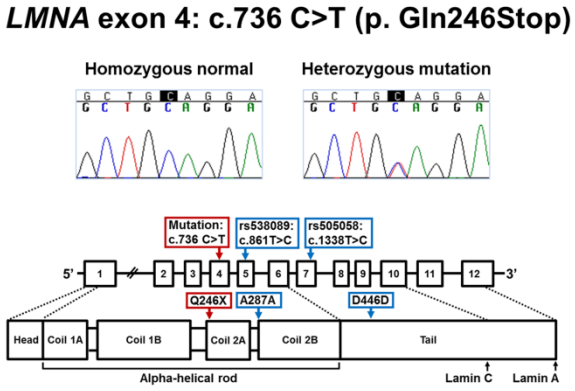

Figure II.3. *LMNA* c.736C>T (p.Gln246Stop). Top panel shows the Sanger sequencing chromatograms: normal allele for unaffected individuals and heterozygous mutation for affected individuals. Bottom panel depicts the location of the nonsense mutation and two expressed polymorphisms rs538089 (c.861T>C, Ala287Ala) and rs505058 (c.1338T>C, Asp446Asp) in the mRNA and Lamin A/C protein.

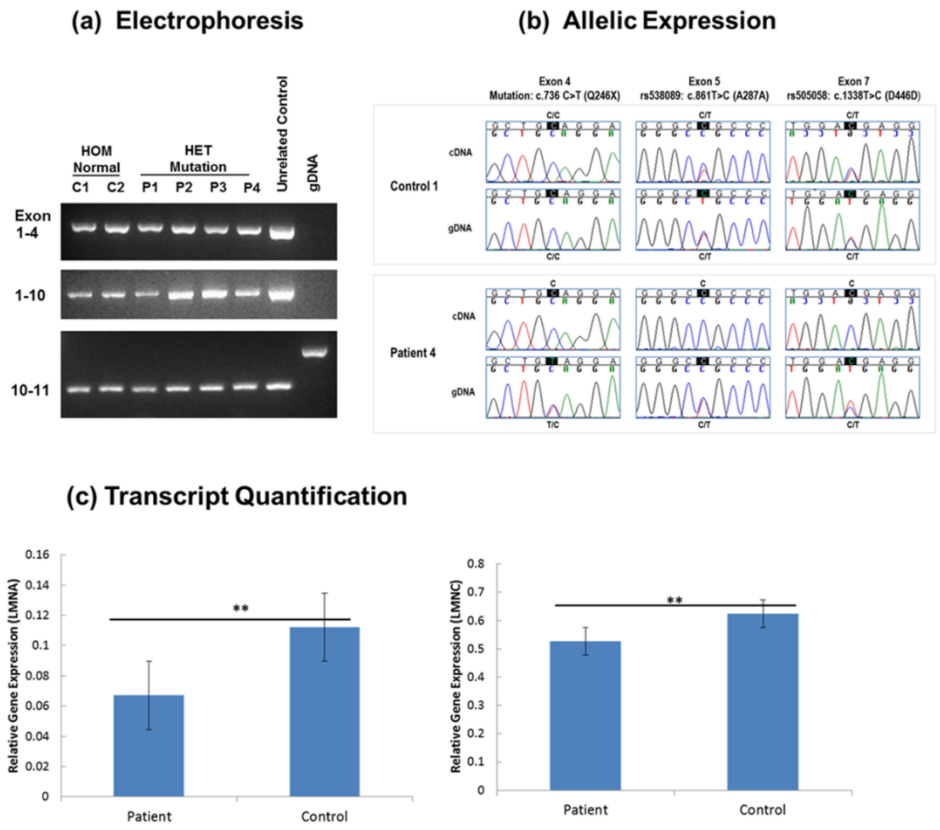

Figure II.4. Expression analysis of *LMNA* in patient and control fibroblasts. (**A**) Electrophoresis: cDNA fragment analysis of *LMNA* mRNA (Exon 1-4, Exon 1-10, and Exon 10-11) for fibroblasts from two unaffected family members: C1 (IV-5) and C2 (IV-1) (HOM Normal: lanes 1-2), four patients: P1 (IV-4), P2 (IV-3), P3, and P4 (III-4) (HET Mutation: lanes 3-6), and an unrelated control (lane 7). Genomic DNA served as a negative control (lane 8). Only the expected products were observed with cDNA amplification (lanes 1-7): 898 bp for Exon 1-4, 1886 bp for Exon 1-10, and 297 bp for Exon 10-11. No products were observed with gDNA amplification (lane 8) for Exon 1-4 and Exon 1-10. For Exon 10-11, the expected 1041 bp product was observed with gDNA (lane 8) and was absent with cDNA amplification (lanes 1-7). (**B**) Allelic Expression: Sanger sequencing chromatograms from genomic DNA and cDNA for control C1 (IV-5) and patient P4 (III-4). For control fibroblasts, biallelic expression (C/T) in the cDNA and heterozygosity for C/T in the genomic DNA is shown at variants rs538089 in exon 5 and rs505058 in exon 7. In contrast, detection of only the normal C allele at the mutation site in exon 4 and single C alleles at rs538089 and rs505058 demonstrates monoallelic expression for patient fibroblasts. (**C**) Lamin A/C transcript quantification: RT-qPCR results from patient and control cDNA measuring the relative transcript level of Lamin A and Lamin C. Results shown are the mean transcript levels of patient: P1 (IV-4), P2 (IV-3) and control: C1 (IV-5) and C2 (IV-1). For both Lamin A and C, there is a significant reduction of transcribed mRNA in patient fibroblasts compared to control fibroblasts ($N = 6$, $P < 0.05$).

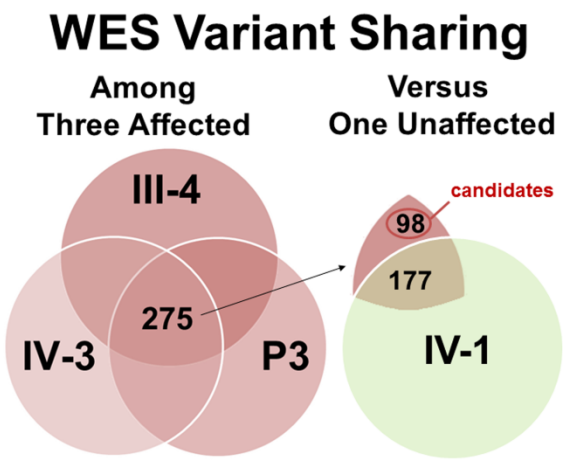

Figure II.5. Whole Exome Sequencing Studies and Variant Sharing of Four Family Members to Identify Candidate Variants in DD and LD. Diagram provided to represent the total number of potentially deleterious variants found in the three affected individuals: 1,677 variants for III-4, 1,681 variants for IV-3, and 1,815 variants for Patient 3 (red circles) and the one unaffected individual: 1,761 variants for IV-1 (green circle). For the affected individuals, the central overlapping region represents the shared variants (n=275). When compared to the variants of the unaffected individual, 177 shared variants (overlapping region) were excluded and 98 unshared variants (non-overlapping region) were identified as candidates in DD and LD.

Table II.1. Family studies of the high-priority variants to identify genetic factors in DD and LD[a].

		DNA	Protein		ExAC	Family Studies: Genotype[e]				
Gene[b]	Position (hg38)	Variant	Change	dbSNP[c]	Frequency[d]	III-4	IV-2	IV-3	P3	IV-1
ASTE1	Chr3:131025077	c.230T>C	p.Val77Ala	novel	No data	-/+	-/+	-/+	-/+	-/-
FZD2	Chr17:44558223	c.535A>C	p.Thr179Pro	novel	No data	-/-	-/-	-/-	-/-	-/-
FSD1	Chr19:4311959	c.608G>A	p.Arg203Gln	novel	No data	-/+	-/-	-/+	-/+	-/-
LMNA	Chr1:156134901	c.736C>T	p.Gln246Ter	rs267607587	No data	-/+	-/+	-/+	-/+	-/-
OR51A7	Chr11:4908132	c.763A>G	p.Ile255Val	rs144609747	0.0040	-/+	-/+	-/+	-/+	-/-
SYPL2	Chr1:109476793	c.272A>T	p.Tyr91Phe	rs79613472	0.0086	-/+	-/+	-/+	-/+	-/+

[a]Variants shared by all four affected individuals (III-4, IV-2, IV-3, P3) and unshared with the one unaffected individual (IV-1) are highlighted in blue (n=3).

[b]Hyperlinked to GeneCards database (www.genecards.org)

[c]Hyperlinked to dbSNP (www.ncbi.nlm.nih.gov/projects/SNP)

[d]Hyperlinked to ExAC database (http://exac.broadinstitute.org)

[e]Genotypes: -/+, heterozygous for variant allele; +/+ homozygous for variant allele; -/- homozygous for non-variant allele.

2.4. Discussion

2.4.1. Molecular mechanism of LMNA c.736 C>T (p.Gln246Stop)

We report *LMNA* c.736 C>T (p.Gln246Stop), a previously described nonsense mutation as the primary mutation in a family with typical *LMNA*-related cardiac disease that includes DCM, cardiac conduction defects, and sudden death [24-26]. To investigate the molecular mechanism by which *LMNA* c.736 C>T (p.Gln246Stop) may lead to disease, we conducted RNA studies on patient and control fibroblasts. These results were consistent with haploinsufficiency due to monoallelic expression of the normal *LMNA* allele in mutant fibroblasts and elimination of aberrant mRNAs transcribed from the mutated allele by nonsense-mediated mRNA decay (NMD). These results in fibroblasts concur with a previous study using gene and protein expression in blood and myocardial samples [27]. Lamin A/C haploinsufficiency may lead to cardiac disease in our family as the result of nuclear dysfunction such as abnormal cell differentiation, altered gene expression, and dysregulation of cell signaling [13-17]. Defects in Lamin A/C have been shown specifically to dysregulate the TGF beta 1, MAPK, mTOR, and Wnt/ beta-catenin signaling pathways [15-17,28,29]. *LMNA* mutation in a mouse model was associated with increased MAPK activity in response to stress that resulted in aberrant expression of target genes and with decreased Wnt/beta-catenin activity that supports the involvement of both signaling in the pathogenesis for lamin-cardiomyopathy [15,17]. The role of Lamin A/C haploinsufficiency in cell differentiation has been suggested in studies of mouse embryonic stem cells that showed the levels of Lamin A/C were important in lineage-specific differentiation [30].

2.4.2. Dupuytren's and Ledderhose disease as primary features of laminopathies?

We also report the novel occurrence of DD and LD in *LMNA* c.736 C>T (p.Gln246Stop) DCM patients. Our studies found that four (III-4, IV-2, IV-3, and Patient 3) of

five family members heterozygous for the mutation had DD and/or LD along with typical *LMNA*-related cardiac disease. Severe DD that required surgery was noted for two deceased family members (III-2 and III-5) who were obligate carriers for the mutation. The co-occurrence of DD and a *LMNA* mutation has been previously reported in a patient with atypical Werner syndrome, a 31-year-old male with mild DD and a heterozygous missense mutation, *LMNA* c.898 G>A (p.Asp300Asn) [19]. These findings suggest that both palmar and plantar fibromatosis could be a part of the primary laminopathy phenotype, extra-cardiac features with clinical variability.

However, we argue that the presence of DD and LD in our family may be instead due to additional genetic factors and not primarily due to the *LMNA* mutation. First, our pedigree analysis indicated while the *LMNA*-related cardiac disease was introduced into the family by the maternal grandfather (II-7), DD was introduced by the proband's maternal grandmother (II-8), the only DD-affected individual with no cardiac disease. Furthermore, patients previously reported to carry the same nonsense mutation as our family or other premature truncation mutations with mechanisms consistent with Lamin A/C haploinsufficiency, did not have DD or LD [21,24,25,27]. *LMNA* c.736 C>T (p.Gln246Stop) has been previously described in two families with DCM and atrioventricular block that includes an Italian proband [24] and a Polish 40-year-old male proband with a family history of heart failure [25]; however, extra-cardiac features were not reported. These observations suggest that DD is not exclusive to laminopathy patients and additional genetics factors in family members heterozygous for the *LMNA* mutation may increase the susceptibility to develop DD along with the primary laminopathy phenotype of cardiac disease.

2.4.3. Identification of a candidate susceptibility variant for DD and LD in the ASTE1 gene

To identify potential genetics factors in the etiology DD and LD, we performed WES on three family members heterozygous for the *LMNA* mutation and affected with cardiac disease, DD, and/or LD (III-4, IV-3, and Patient 3) and one unaffected family member without the *LMNA* mutation and unaffected with cardiac disease, DD, and LD (IV-1). Bioinformatics analysis and variant filtering was used to identify 98 total candidate variants and five high-priority variants based on allele frequencies (Table S3). Family studies by Sanger sequencing were performed to validate the WES results and to further evaluate the high-priority candidate using a fourth affected family member with cardiac disease, DD, and LD (proband: IV-2) (Table 1). In addition to the *LMNA* mutation c.736C>T (p.Gln246Stop), only two variants co-segregated with the fibromatosis phenotype: a novel missense variant in the Asteroid Homolog 1 gene (*ASTE1* NM_001288950: c.230T>C, p.Val77Ala) and a rare known missense variant in the Olfactory Receptor Family 51 Subfamily A Member 7 gene *OR51A7* NM_001004749: c.763A>G, p.Ile255Val).

Our results provides initial evidence for *ASTE1* c.230T>C (p.Val77Ala) as a candidate susceptibility variant for DD and LD and a potential role for the *ASTE1* gene in the etiology of fibromatosis. The *ASTE1* gene is located at chromosome 3q22.1 and encodes for the protein Asteroid Homolog 1 (Uniprot entry: ASTE1_HUMAN, accession no. Q2TB18) [31,32]. Although there is limited information available, the *ASTE1* gene is expressed in skin tissue and the ASTE1 protein has 679 amino acids with a possible role in EGFR signaling by sequence similarity to the *asteroid* gene in *Drosophila* [31,33]. The *ASTE1* c.230T>C (p.Val77Ala) variant is located in the Xeroderma Pigmentosum complementation group G (XPG) N-terminal domain (AA 1-96) and PIN domain-like (AA 1-207) of the ASTE1

protein with inferred functions of nuclease activity and in DNA repair [34]. No primary disease-associated mutations have been reported for *ASTE1* [31,35]; however, secondary mutations in *ASTE1* were detected in colorectal cancers with microsatellite instability [36]. Thus, functional effects of *ASTE1* c.230T>C (p.Val77Ala) relevant to DD and LD are possible and warrant further investigation. No support was found for the *OR51A7* variant or human olfactory receptor gene family after review of the literature and databases [31,37].

With the possible role of *ASTE1* in EGFR signaling [33], the complex pathway with significant roles in cell-cell communication, cell fate, and proliferation [38], our findings raise the possibility that *ASTE1* c.230T>C (p.Val77Ala) may result in susceptibility to palmar and plantar fibromatosis in our family. EGFR signaling has been implicated in the pathogenesis of fibromatosis in previous studies of diseased tissues from patients with DD [2,39-41]. Co-expression of EGFR protein and TGF-alpha has been found in proliferating myofibroblasts in palmar fibromatosis nodules of DD patients [39]. A synergistic effect of EGF and TGF-beta1 on fibroblast proliferation in patients with DD compared to normal fibroblast was found [40]. In addition, as an indicator of receptor activation, a higher ratio of surface to intracellular EGFR in palmar fascia was found during the progression of disease in DD patients [41].

2.5. Conclusions

In summary, we report the novel co-occurrence of palmar and plantar fibromatosis and *LMNA*-related cardiac disease in a family with a previously described nonsense mutation, *LMNA* c.736 C>T (p.Gln246Stop). *LMNA* expression studies in fibroblasts support haploinsufficiency as the primary molecular mechanism due to monoallelic expression of

the normal *LMNA* allele. To identify additional genetic factors that may contribute to the pathogenesis of fibromatosis in the setting of Lamin A/C haploinsufficiency, we used exome sequencing and family studies to identify *ASTE1* c.230T>C (p.Val77Ala) as a candidate susceptibility variant for DD and LD and a possible role for the *ASTE1* gene in the etiology of fibromatosis. Since Lamin A/C haploinsufficiency may disrupt biological processes also important in the etiology of fibromatosis including cell differentiation, gene expression, and signaling pathways, additional defects in these processes due to *ASTE1* c.230T>C (p.Val77Ala) may lead to susceptibility for fibrotic disease in *LMNA* heterozygotes.

We may only speculate about the relevance of *ASTE1* c.230T>C (p.Val77Ala) at this time. Since all four family members affected with fibromatosis were double heterozygotes for the *LMNA* mutation c.736C>T (p.Gln246Stop) and *ASTE1* c.230T>C (p.Val77Ala), it is possible that both Lamin A/C haploinsufficiency and an ASTE1 defect are required for disease. Alternatively, *ASTE1* c.230T>C (p.Val77Ala) may act as an independent susceptibility variant. Thus, future research studies include functional analysis of our patient fibroblast cells for altered cell signaling (e.g., EGFR and MAPK pathways) associated with increased cell proliferation, profibrotic gene expression, and ECM production. Ultimately, disease modeling utilizing induced pluripotent stem cells (iPSC) derived from our patient fibroblast cells may be used to investigate the effects of *LMNA* and *ASTE1* defects in lineage-specific cell proliferation and differentiation to mesodermal derivatives such as myofibroblast. Elucidation of the precise molecular pathogenesis of fibrosis in the *LMNA* mutation background may confer knowledge on the role of Lamin A/C in maintaining physiological balance for a functional organism as the basis to develop treatments for disease.

2.6. References

1. Dupuytren G (1834) Clinical Lectures on Surgery delivered by Baron Dupuytren, During the Session of 1833. The Lancet 2: 222-225.

2. Tripoli M, Cordova A, Moschella F (2016) Update on the role of molecular factors and fibroblasts in the pathogenesis of Dupuytren's disease. J Cell Commun Signal.

3. Akhavani MA, McMurtrie A, Webb M, Muir L (2015) A review of the classification of Dupuytren's disease. J Hand Surg Eur Vol 40: 155-165.

4. Ledderhose G (1894) Über Zerreisungen der Plantarfascie. Arch Klin Chir 48: 853–856.

5. Pickren JW, Smith AG, Stevenson TW, Jr., Stout AP (1951) Fibromatosis of the plantar fascia. Cancer 4: 846-856.

6. Veith NT, Tschernig T, Histing T, Madry H (2013) Plantar fibromatosis--topical review. Foot Ankle Int 34: 1742-1746.

7. Michou L, Lermusiaux JL, Teyssedou JP, Bardin T, Beaudreuil J, et al. (2012) Genetics of Dupuytren's disease. Joint Bone Spine 79: 7-12.

8. Chen KT, Van Dyne TA (1985) Familial plantar fibromatosis. J Surg Oncol 29: 240-241.

9. de Palma L, Santucci A, Gigante A, Di Giulio A, Carloni S (1999) Plantar fibromatosis: an immunohistochemical and ultrastructural study. Foot Ankle Int 20: 253-257.

10. Hu FZ, Nystrom A, Ahmed A, Palmquist M, Dopico R, et al. (2005) Mapping of an autosomal dominant gene for Dupuytren's contracture to chromosome 16q in a Swedish family. Clin Genet 68: 424-429.

11. Worman HJ (2012) Nuclear lamins and laminopathies. J Pathol 226: 316-325.

12. Dechat T, Adam SA, Taimen P, Shimi T, Goldman RD (2010) Nuclear lamins. Cold Spring Harb Perspect Biol 2: a000547.

13. Perovanovic J, Dell'Orso S, Gnochi VF, Jaiswal JK, Sartorelli V, et al. (2016) Laminopathies disrupt epigenomic developmental programs and cell fate. Sci Transl Med 8: 335ra358.

14. Guelen L, Pagie L, Brasset E, Meuleman W, Faza MB, et al. (2008) Domain organization of human chromosomes revealed by mapping of nuclear lamina interactions. Nature 453: 948-951.

15. Muchir A, Pavlidis P, Decostre V, Herron AJ, Arimura T, et al. (2007) Activation of MAPK pathways links LMNA mutations to cardiomyopathy in Emery-Dreifuss muscular dystrophy. J Clin Invest 117: 1282-1293.

16. Van Berlo JH, Voncken JW, Kubben N, Broers JL, Duisters R, et al. (2005) A-type lamins are essential for TGF-beta1 induced PP2A to dephosphorylate transcription factors. Hum Mol Genet 14: 2839-2849.

17. Le Dour C, Macquart C, Sera F, Homma S, Bonne G, et al. (2017) Decreased WNT/beta-catenin signalling contributes to the pathogenesis of dilated cardiomyopathy caused by mutations in the lamin a/C gene. Hum Mol Genet.

18. Luo YB, Mastaglia FL, Wilton SD (2014) Normal and aberrant splicing of LMNA. J Med Genet 51: 215-223.

19. Renard D, Fourcade G, Milhaud D, Bessis D, Esteves-Vieira V, et al. (2009) Novel LMNA mutation in atypical Werner syndrome presenting with ischemic disease. Stroke 40: e11-14.

20. Lace B, Inashkina I, Micule I, Vasiljeva I, Naudina MS, et al. (2013) Dupuytren's Contracture Cosegregation with Limb-Girdle Muscle Dystrophy. Case Rep Neurol Med 2013: 254950.

21. Zaragoza MV, Fung L, Jensen E, Oh F, Cung K, et al. (2016) Exome Sequencing Identifies a Novel *LMNA* Splice-Site Mutation and Multigenic Heterozygosity of Potential Modifiers in a Family with Sick Sinus Syndrome, Dilated Cardiomyopathy, and Sudden Cardiac Death. PLoS One 11: e0155421.

22. Zaragoza MV, Hakim SA, Hoang V, Elliott AM (2017) Heart-hand syndrome IV: a second family with LMNA-related cardiomyopathy and brachydactyly. Clin Genet 91: 499-500.

23. Karczewski KJ, Weisburd B, Thomas B, Solomonson M, Ruderfer DM, et al. (2017) The ExAC browser: displaying reference data information from over 60 000 exomes. Nucleic Acids Res 45: D840-D845.

24. Pasotti M, Klersy C, Pilotto A, Marziliano N, Rapezzi C, et al. (2008) Long-term outcome and risk stratification in dilated cardiolaminopathies. J Am Coll Cardiol 52: 1250-1260.

25. Saj M, Bilinska ZT, Tarnowska A, Sioma A, Bolongo P, et al. (2013) LMNA mutations in Polish patients with dilated cardiomyopathy: prevalence, clinical characteristics, and in vitro studies. BMC Med Genet 14: 55.

26. Hershberger RE, Morales A (1993) Dilated Cardiomyopathy Overview. In: Pagon RA, Adam MP, Ardinger HH, Wallace SE, Amemiya A et al., editors. GeneReviews(R). Seattle (WA).

27. Narula N, Favalli V, Tarantino P, Grasso M, Pilotto A, et al. (2012) Quantitative expression of the mutated lamin A/C gene in patients with cardiolaminopathy. J Am Coll Cardiol 60: 1916-1920.

28. Choi JC, Muchir A, Wu W, Iwata S, Homma S, et al. (2012) Temsirolimus activates autophagy and ameliorates cardiomyopathy caused by lamin A/C gene mutation. Sci Transl Med 4: 144ra102.

29. Chatzifrangkeskou M, Le Dour C, Wu W, Morrow JP, Joseph LC, et al. (2016) ERK1/2 directly acts on CTGF/CCN2 expression to mediate myocardial fibrosis in cardiomyopathy caused by mutations in the lamin A/C gene. Hum Mol Genet 25: 2220-2233.

30. Sehgal P, Chaturvedi P, Kumaran RI, Kumar S, Parnaik VK (2013) Lamin A/C haploinsufficiency modulates the differentiation potential of mouse embryonic stem cells. PLoS One 8: e57891.

31. Stelzer G, Rosen N, Plaschkes I, Zimmerman S, Twik M, et al. (2016) The GeneCards Suite: From Gene Data Mining to Disease Genome Sequence Analyses. Curr Protoc Bioinformatics 54: 1 30 31-31 30 33.

32. UniProt-Consortium (2015) UniProt: a hub for protein information. Nucleic Acids Res 43: D204-212

33. Kotarski MA, Leonard DA, Bennett SA, Bishop CP, Wahn SD, et al. (1998) The Drosophila gene asteroid encodes a novel protein and displays dosage-sensitive interactions with Star and Egfr. Genome 41: 295-302.

34. Finn RD, Attwood TK, Babbitt PC, Bateman A, Bork P, et al. (2017) InterPro in 2017-beyond protein family and domain annotations. Nucleic Acids Res 45: D190-D199.

35. OMIM Online Mendelian Inheritance in Man. Baltimore, MD: McKusick-Nathans Institute of Genetic Medicine, Johns Hopkins University.

36. Tougeron D, Fauquembergue E, Rouquette A, Le Pessot F, Sesboue R, et al. (2009) Tumor-infiltrating lymphocytes in colorectal cancers with microsatellite instability are correlated with the number and spectrum of frameshift mutations. Mod Pathol 22: 1186-1195.

37. Malnic B, Godfrey PA, Buck LB (2004) The human olfactory receptor gene family. Proc Natl Acad Sci U S A 101: 2584-2589.

38. Yarden Y, Shilo BZ (2007) SnapShot: EGFR signaling pathway. Cell 131: 1018.

39. Magro G, Lanzafame S, Micali G (1995) Co-ordinate expression of alpha 5 beta 1 integrin and fibronectin in Dupuytren's disease. Acta Histochem 97: 229-233.

40. Kloen P, Jennings CL, Gebhardt MC, Springfield DS, Mankin HJ (1995) Transforming growth factor-beta: possible roles in Dupuytren's contracture. J Hand Surg Am 20: 101-108.

41. Augoff K, Tabola R, Kula J, Gosk J, Rutowski R (2005) Epidermal growth factor receptor (EGF-R) in Dupuytren's disease. J Hand Surg Br 30: 570-573.

CHAPTER 3

Gene expression profiling of fibroblasts in a family with *LMNA*-related cardiomyopathy reveals molecular pathways implicated in disease pathogenesis

This work was previously published Widyastuti, H.P.*, Norden-Krichmar, T.M.*, Grosberg, A. *et al.* Gene expression profiling of fibroblasts in a family with *LMNA*-related cardiomyopathy reveals molecular pathways implicated in disease pathogenesis. *BMC Med Genet* **21,** 152 (2020).

*Dr. Trina Norden-Krichmar and I contributed equally to this work.

3.1. Background

The Lamin A/C (*LMNA*) gene encodes for Lamin A and Lamin C proteins that, along with Lamin B1 and Lamin B2, form an intricate intermediate filament protein meshwork termed the nuclear lamina (NL) and play important roles in maintaining nuclear structure and stability and in fundamental nuclear functions [1,2,3]. Lamins A and C proteins are products of alternative splicing of the *LMNA* gene. Lamin A is produced from all twelve exons of the gene, while Lamin C is the product of only ten exons. In vivo, Lamin A is produced as prelamin A and undergoes extensive post-translational processing of the C-terminus to become mature Lamin A protein while Lamin C is produced as mature protein [4]. Aside from conveying structural integrity to the nucleus [5], nuclear lamina proteins associate with heterochromatin [6], modulate gene expression by sequestering transcription factors to the nuclear periphery [7], regulate cell cycle progression [8], and regulate molecular signaling such as ERK/MAPK and Wnt Beta-Catenin pathways [9,10,11]. The diverse roles of the nuclear lamina proteins underscore their importance in maintaining proper cellular function in an organism.

Despite having common functional roles, the expression patterns of Lamin A/C, Lamin B1, and Lamin B2 are different [12]. Lamin A/C expression is absent in human and mouse embryonic stem cells but increases once these cells are induced to differentiate [13]. In contrast, Lamin B1 and Lamin B2 expression are ubiquitous throughout development. Lamin B1 is highly expressed in the embryo and its expression persists throughout development [14]. Similarly, Lamin B2 is expressed early during development, and its expression remains ubiquitous during development [15]. Additionally, Lamin A/C expression levels vary among differentiated cell types. They are more highly expressed in

multinucleated cells, such as cardiomyocytes, compared to mononucleated cells, such as fibroblasts [12, 16, 17].

Although Lamin A/C is expressed in most differentiated cell types, *LMNA* mutations predominantly affect mesoderm-derived cell lineages in diseases collectively termed as laminopathies. Laminopathies range from dilated cardiomyopathy (DCM) with conduction defects [18,19,20] and different forms of muscular dystrophies, such as Emery-Dreyfus Muscular Dystrophy (EDMD) [21,22,23] and Limb Girdle Muscular Dystrophy type 1B (LGMD1B) [24], to severe disease characterized by premature aging such as Hutchinson-Gilford Progeria Syndrome [25, 26]. *LMNA*-related DCM with conduction defects is one of the most common forms of inherited dilated cardiomyopathy, second only to DCM associated with mutations in sarcomere protein genes [27, 28], with an estimated 5 to 10% of cases associated with a heterozygous *LMNA* mutation [29, 30,31]. Current hypotheses for how *LMNA* mutations give rise to diseases limited to cardiac tissues include the mechanical defect and the gene expression hypotheses [32]. The mechanical defect hypothesis proposes that *LMNA* mutation compromises the structural integrity of a cell, subsequently causing the cells to be more prone to necrosis leading to diseases [33]. The gene expression hypothesis proposes that *LMNA* mutation impairs the NL structure which leads to aberrant epigenetic modification, abnormalities in signaling transduction and ultimately affecting proper gene expression [32, 34]. As of now, it remains unclear which of these mechanisms is the main cause of *LMNA*-related cardiomyopathy.

We recently identified a novel splice-site mutation in the Lamin A/C gene, *LMNA* c.357-2A > G (p.N120Lfs*5), in a multigenerational family with DCM, heart failure, and sudden death [35]. In this study, we performed RNA sequencing (RNA-seq) to

test the hypothesis that the splice-site mutation in the *LMNA* gene is associated with altered expression of genes that played a significant role in the nuclear lamina structure and function. By deep RNA-seq of patient and control fibroblasts, we evaluated expression of Lamins A and C, tested for aberrant splicing of *LMNA* transcripts, and altered ratio of *LMNA* transcript variants. We also sought to determine any compensatory mechanism by Lamin B1 and/or Lamin B2 in response to the mutation.

We further expanded the analyses to examine the most significantly differentially expressed genes across the genome, and determine potential pathways affected by the *LMNA* mutation or other genes and pathways influencing the observed phenotype. Surprisingly, from the RNA-seq data we did not find any significant differential expression for the Lamin isoforms between the sample groups. However, we found plausible genes and pathways that may contribute to the cardiomyopathy phenotype that we observe in this family. Our study highlighted tissue specificity as a major feature of the novel heterozygous *LMNA* splice-site mutation as evidenced by the lack of changes in nuclear lamina gene expression and absence of aberrant splicing events in patient fibroblasts. The study conducted here laid the foundation for future disease modeling studies in cardiomyocytes to elucidate on the molecular mechanism of the novel *LMNA* splice-site mutation.

3.2. Materials and Methods

3.2.1 Fibroblasts collection

Nine primary fibroblast cell lines were cultured from skin biopsies (Table 1) as previously described [35]. These included cells from six family members: three affected

individuals (Patient 1–3) heterozygous for the *LMNA* splice-site mutation and three unaffected individuals (Control 1–3) who do not have the *LMNA* splice-site mutation. To serve as Unrelated Controls (U), fibroblast cells from three healthy individuals were obtained from biorepositories (U1: Lonza CC-2511; lot#: 0000352805; U2: Lonza CC-2511; lot#: 0000293971; U3: Coriell Institute ND31845). To confirm the *LMNA* genotype, genomic DNA (gDNA) was extracted from Patient, Control, and Unrelated Control fibroblasts and evaluated by Sanger sequencing of the 12 *LMNA* exons as previously described [35]. The *LMNA* genotype for each sample was also confirmed by examining the RNA-seq data.

3.2.2. RNA-seq

Total RNA from Patient, Control, and Unrelated Control fibroblasts (at passage 7) was isolated and quantified as described [35]. RNA-seq studies were conducted on total RNA (3 to 7 μg) at DNA Link USA, Inc. (San Diego, CA) using poly-A RNA enrichment and library preparation. RNA libraries were sequenced as 75 bp paired-end runs with at least 100 million reads per sample on an Illumina NextSeq 500 platform (Additional File 1: Table S1). The raw RNA-seq data (fastq) was stored and transferred using the BaseSpace Sequence Hub (Illumina, San Diego, CA).

3.2.3. Bioinformatics analysis

Quality control, alignment, and differential expression (DE)

RNA-seq data was first examined for quality using FastQC software [36]. Reads were filtered out due to low quality. Low quality bases at the 3′ and/or 5′ ends of the reads were trimmed. The reads that pass the quality filtering were aligned to the human reference genome (GRCh37/hg19) with TopHat2 alignment software [37]. The average overall read

mapping rate was 90.1% and average concordant pair alignment rate was 85.5% (Additional File 1: Table S1). DE analysis was performed with the Cufflinks software [38, 39], using upper quartile normalization between the data files. Normalized DE genes between the groups were filtered for absolute fold change ≥1.5, Fragments Per Kilobase of transcript per Million mapped reads (FPKM) ≥ 1, and that were significant at false discovery rate (FDR)-adjusted *p*-value ≤0.05. DE of isoforms was provided by cufflinks/cuffdiff2 software to distinguish between the expression of Lamin isoforms. From this list of significantly DE genes, we further filtered the list to include only DE genes that were expressed similarly between the Unrelated and Patient groups and between the Control and Patient groups. Our rationale to filter the genes using these parameters was to find genes that potentially were affected by the *LMNA* splice-site mutation. We reasoned that DE genes that were shared between Control and Unrelated groups were due to intrinsic gene expression differences and not due to the mutation. By looking only at genes that were at the intersection of Unrelated vs. Patient and Control vs. Patient groups, we narrowed down the candidate genes to those that potentially were affected by the mutation.

Visualization and pathway analysis

Heatmaps of the gene expression in FPKM values of the most highly DE genes were constructed with cummeRbund [40]. Heatmaps were clustered by rows, where each row contained the gene expression of a particular gene. Lamin isoforms were visualized in heatmaps along with any other genes of interest. To detect allelic expression of Lamin A/C transcripts, we used the Integrative Genomics Viewer (IGV) software [41] to visualize the distribution of alleles in mapped reads at rs538089 in Exon 5 and rs4641 in Exon 10 for

samples found to be heterozygous by Sanger sequencing of gDNA [35]. Finally, Ingenuity Pathway Analysis (IPA) software (Qiagen, Hilden, Germany) was used to determine the top canonical pathways and visualize the significant networks.

3.2.5. qPCR validation of RNA-seq results

Quantitative PCR (qPCR) assays were performed to validate RNA-seq results for Lamin A, Lamin C, Lamin B1, Lamin B2, and IGFBP5. cDNA was synthesized using QuantiTect Reverse Transcription Kit (Qiagen) from Unrelated, Control and Patient RNA samples. 100 ng/µl cDNA was used as the reaction template with 10 µM of pre-designed Kicqstart forward and reverse primer pairs (Sigma Aldrich, St. Louis, MO) specific to Lamin A and Lamin C, 10 µM of independently designed primer pairs for Lamin B1, Lamin B2, and IGFBP5 (Integrated DNA Technologies, San Diego, CA), and SYBR green dye along with the necessary reaction components (KAPA Biosystems, Wilmington, MA). The reaction was run in three technical replicates for each sample. Comparative Ct (ΔCt) method was used to determine relative quantitative gene expression (QGE) [42, 43]. Beta Actin (*ACTB*) was used as the housekeeping gene. Statistical analysis was performed using One-Way ANOVA followed by Tukey post hoc test to determine statistical significance between groups. *P* values less than 0.05 were considered statistically significant. Primer sequences used for validation are provided in Additional File 1: Table S2.

3.2.6. Lamin A/C protein level validation

Patient, Control and Unrelated Control fibroblasts were grown to confluency, harvested using TrypLE Select 1X (Thermo Fisher Scientific, Waltham, MA), and lysed using cold RIPA buffer supplemented with protease inhibitors cocktail (Sigma-Aldrich, Saint Louis, MO). Protein concentration was quantified using Pierce™ BCA Protein Assay Kit

(Thermo Fisher Scientific). 50 µg of total protein lysate along with protein ladder were run on a Bolt™ 4–12% Bis-Tris Plus Gels (Thermo Fisher Scientific) under denaturing conditions followed by wet transfer. Target protein was detected using a primary antibody for Lamin A/C (sc-376248, Santa Cruz Biotechnology, Dallas, TX), at 4 °C overnight followed by incubation with secondary antibody conjugated to HRP (1:5000, Abcam, Cambridge, UK) for one hour at room temperature. Beta Actin was used as loading control. Protein visualization was conducted using iBright FL1000 Imaging System and relative quantification of protein bands was performed using ImageJ [44].

3.3. Results

3.3.1. Expression variability in samples within and between groups

In this study, we used whole transcriptome DE analysis to investigate the genes and pathways related to *LMNA*-related cardiomyopathy. Differences between the gene expression in the pooled sample groups (Unrelated, Control, Patient) were observed by plotting the top DE genes (Fig. III.1, left panel). By plotting gene expression by replicate, we observed variation within each sample group (Fig. III.1, right panel) and found that Patient and Control groups were more similar to each other, compared to samples in the Unrelated Control group. The heatmaps show the heterogeneity between the samples, where the overall trend was that gene expression pattern of the Patient group was more similar to that of the Control group.

3.3.2. Unaltered nuclear lamina-associated gene and protein expression in patient fibroblasts

Because we hypothesized that the expression of the *LMNA* isoforms may be influenced by the *LMNA* mutation in the patient samples, we examined the expression of the *LMNA* isoforms individually (Fig. III.2). As seen in the heatmap and RNA-seq data (Fig. III.2a, Supplementary Data: Table III.S3), although the patients have the *LMNA* mutation we did not see significant DE between the sample groups for the *LMNA* isoforms. Next, we investigated whether the predicted exon skipping and aberrant splicing occurred in patient samples by examining the aligned sequences across the *LMNA* transcript. Here, we observed sequence alignment that corresponds to the presence of exon 2 of *LMNA* transcript and similar read coverage across all of the *LMNA* exons for each patient sample (Supplementary Data: Figure III.S1). Therefore, our data is consistent with the lack of exon skipping and aberrant splicing in mutant fibroblasts. We confirmed the RNA-seq data for the nuclear lamina associated genes using qPCR and found no statistically significant differences in Lamin A and Lamin C (Fig. III.2b) as well as Lamin B1 and Lamin B2 expression between all sample groups (Supplementary Data: Figure III.S2). Validation by Western Blot showed that the amount of Lamin A/C proteins did not vary significantly between the Patient and the two control groups (Fig.III.2c). In mutant fibroblasts, we also used RNA-seq to confirm that *LMNA* expression was predominately from the wild type allele [35] (Fig. III.3).

3.3.3. ERK/MAPK signaling pathway identified by DE and pathway analysis

Next, we turned our attention to other genes that were most significantly upregulated or downregulated between Patients, Controls, and Unrelated Controls. We found eight DE genes that were similarly expressed between the three groups (Fig. III.4a,

b). Among these eight DE genes were genes necessary for proper fibroblast physiological function such as Matrix Metallopeptidase 3 (*MMP3*) [45] and for epithelial-to-mesenchymal transition such as Keratin 18 (*KRT18*) [46]. In addition, we found one DE gene that was involved in the insulin-like growth factor (IGF) signaling pathway: *IGFBP5*. This gene was of particular interest due the known effects of Lamin A/C on the IGF pathway in different forms of laminopathies [47]. Previous gene expression studies by microarray have reported *IGFBP5* mRNA level to be downregulated in *Lmna* −/− mouse embryonic fibroblasts, compared to *Lmna* +/+ mouse embryonic fibroblasts [48]. We also tested the DE gene expression in the RNA-seq data by performing qPCR on the *IGFBP5* gene (Fig. III.4c). The qPCR result showed similar trend as the RNA-seq data with Patient *IGFBP5* gene expression decreased by greater than two-fold compared to Unrelated Controls. Finally, we used pathway analysis to demonstrate that these eight DE genes were connected in a gene network that included ERK/MAPK pathway genes (Fig. III.5). This finding showed the connectivity of the DE genes in a signaling network and demonstrated the possibility of this pathway being affected in fibroblasts from *LMNA*-related cardiomyopathy patients.

Table III.1. Fibroblast cell samples that were RNA sequenced (N = 9)

Abbreviation	Identification	Genotype*	Sex	Age (years) at Skin Biopsy
P1	Patient 1	+/-	F	38
P2	Patient 2	+/-	M	62
P3	Patient 3	+/-	F	70
C1	Control 1	+/+	F	49

C2	Control 2	+/+	M	69
C3	Control 3	+/+	F	68
U1[a]	Unrelated 1	+/+	F	40
U2[b]	Unrelated 2	+/+	M	51
U3[c]	Unrelated 3	+/+	F	73

*Genotypes: +/+ homozygous normal allele; +/- heterozygous LMNA splice-site mutation
[a]Unrelated: Lonza (CC-2511; lot#: 0000352805)
[b]Unrelated: Lonza (CC-2511; lot#: 0000293971)
[c]Unrelated: Coriell Institute (ND31845)

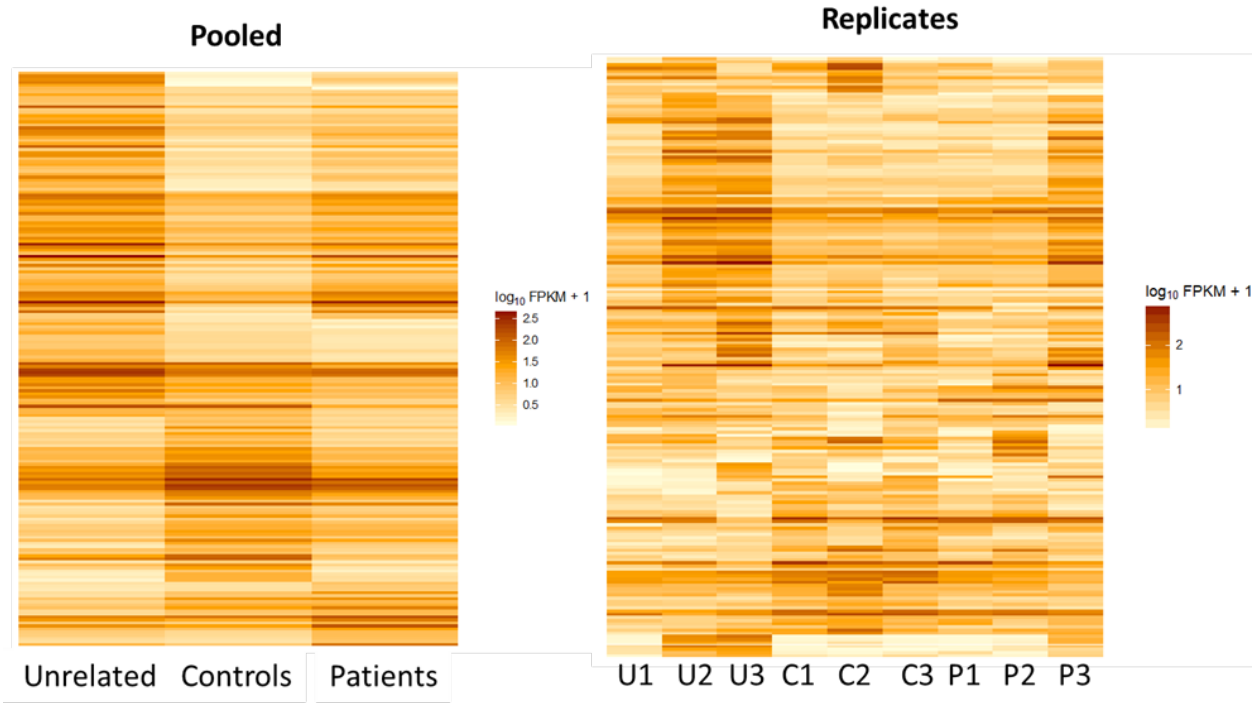

Figure III.1. Gene expression profiling of fibroblast samples by RNA-seq. Differential gene expression analysis was performed using Tophat and Cufflinks software and visualized using cummeRbund. Heatmaps of gene expression profiles are clustered by rows (genes). Heatmaps are shown as pooled samples (left panel) and replicates (right panel).

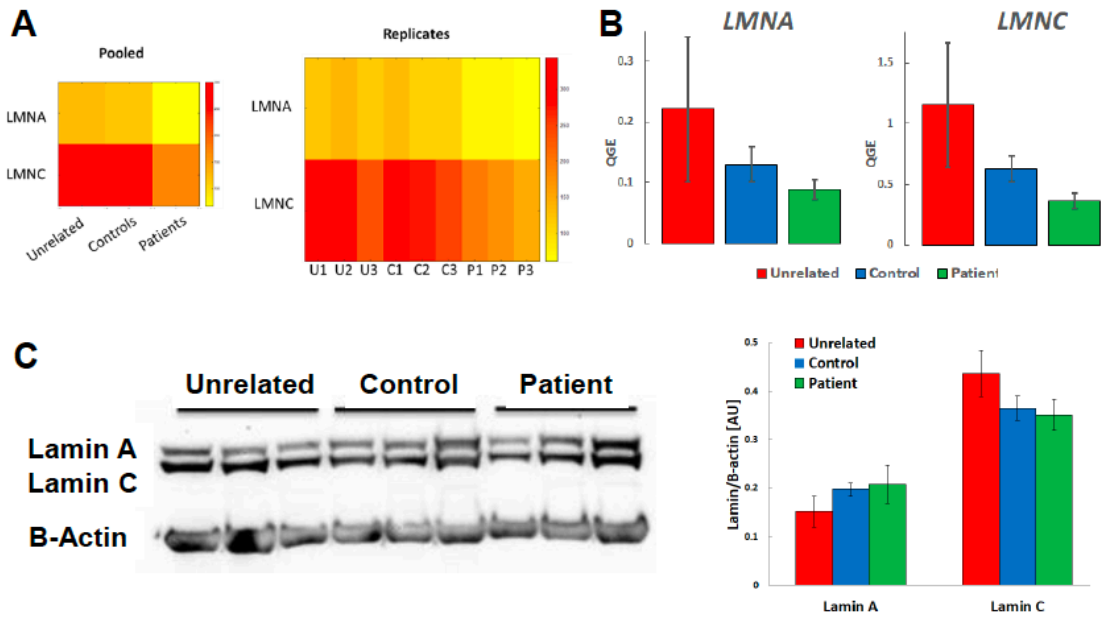

Figure III.2. Nuclear lamina-associated gene expression profiling across all samples. (**A**) Visualization of Lamin A and Lamin C expression across all samples from RNA-seq data. Lamin A and Lamin C expression obtained from RNA-seq experiments were visualized using heatmaps. Gene expression is shown pooled (left panel) and as replicates (right panel). In general, Lamin A and Lamin C expression are highest for unrelated groups and lowest for patient groups. However, there were no statistically significant differences between Lamin A and Lamin C expression across all samples (FDR adjusted p-value ≥ 0.05); (**B**) RNA-seq validation of Lamin A (LMNA) and Lamin C (LMNC) transcript levels by quantitative PCR (qPCR). qPCR was performed on cDNA generated from unrelated, control and patient fibroblasts to measure Lamin A and Lamin C transcript level. There was no statistically significant difference in Lamin A and Lamin C transcript levels across all groups, validating trends observed in RNA-seq. Statistical analysis was performed using One-way ANOVA, followed by Tukey post hoc test to determine statistical significance. (N = 9). (**C**) Western blot for Lamin A/C protein. Lamin A/C protein level was measured by immunoblotting using antibodies specific against Lamin A/C and b-Actin (upper panel). Quantification of Lamin A/C bands relative to b-Actin (lower panel). AU =

Absorbance Unit; Statistical analysis was performed using One-way ANOVA, followed by Tukey post hoc test to determine statistical significance (N = 9).

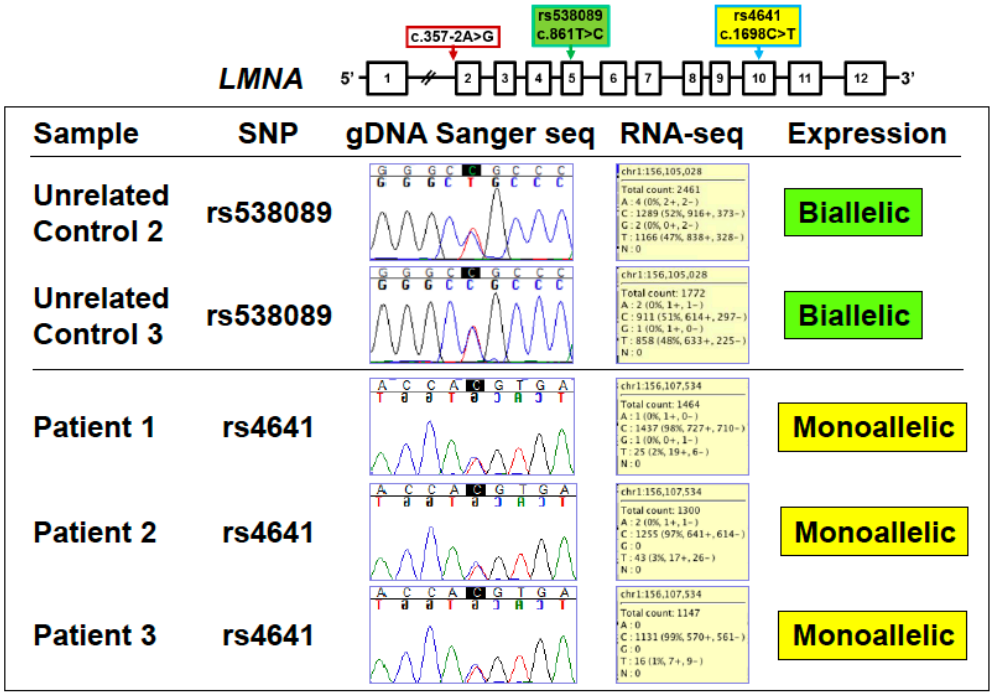

Figure III.3. *LMNA* allelic expression. Top panel depicts location of the *LMNA* splice-site mutation and two expressed single nucleotide polymorphisms (SNP), rs538089 in Exon 5 and rs4641 in Exon 10. Bottom table shows Sanger sequencing chromatograms from genomic DNA (gDNA) and distribution of allele read counts from RNA-seq. For two Unrelated Controls at rs538089, gDNA was heterozygous (C/T) with equal RNA-seq reads of C (51–52%) and T (47–48%) consistent with biallelic expression. For three Patients at rs4641, gDNA was heterozygous (C/T) with RNA-seq reads predominately of C (97–99%) consistent with monoallelic expression

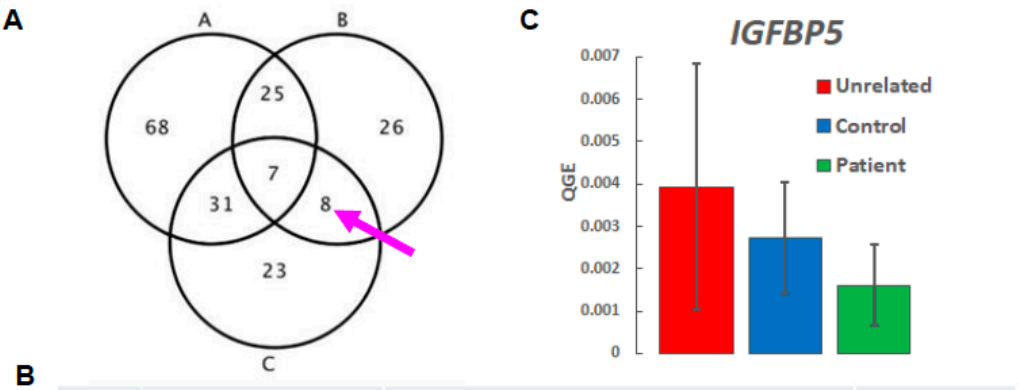

B

		RNA-seq values (FPKM)			
Gene Symbol	Gene Name	Unrelated control	Control	Patient	Expression in patient relative to controls*
FOXC2	forkhead box C2	18.70	12.71	4.36	-
IGFBP5	insulin like growth factor binding protein 5	152.32	125.74	17.71	-
KRT18	keratin 18	54.04	107.88	6.79	-
LRRC15	leucine rich repeat containing 15	38.19	25.32	135.75	+
MMP3	matrix metallopeptidase 3	12.91	5.96	69.98	+
PTN	pleiotrophin	2.09	2.38	7.50	+
STC1	stanniocalcin 1	12.87	14.86	4.51	-
TINAGL1	tubulointerstitial nephritis antigen like 1	15.33	15.21	3.90	-

Figure III.4. Eight differentially expressed genes are potentially involved in LMNA-related cardiomyopathy. (**A**) Differentially expressed genes that passed the filtering criteria were input into Ingenuity Pathway Analysis (IPA). Of these significantly differentially expressed genes for each group, there were 8 genes in the intersection between B and C, but not A, where A = Unrelated vs. Controls, B = Unrelated vs. Patients, C = Controls vs. Patients; (**B**) The gene symbols and names for the 8 genes found in the intersection between groups B and C, but not A; *Expression in patient: - : decreased, + : increased. (**C**) RNA-seq validation of Insulin Growth Factor binding protein 5 (IGFBP5) transcript levels by quantitative PCR (qPCR). qPCR was performed on cDNA generated unrelated, control and patient fibroblasts to measure IGFBP5 transcript level. There was no statistically significant difference in IGFBP5 transcript level between all groups. Statistical analysis was performed using One-way ANOVA, followed by Tukey post hoc test to determine statistical significance. (N = 9).

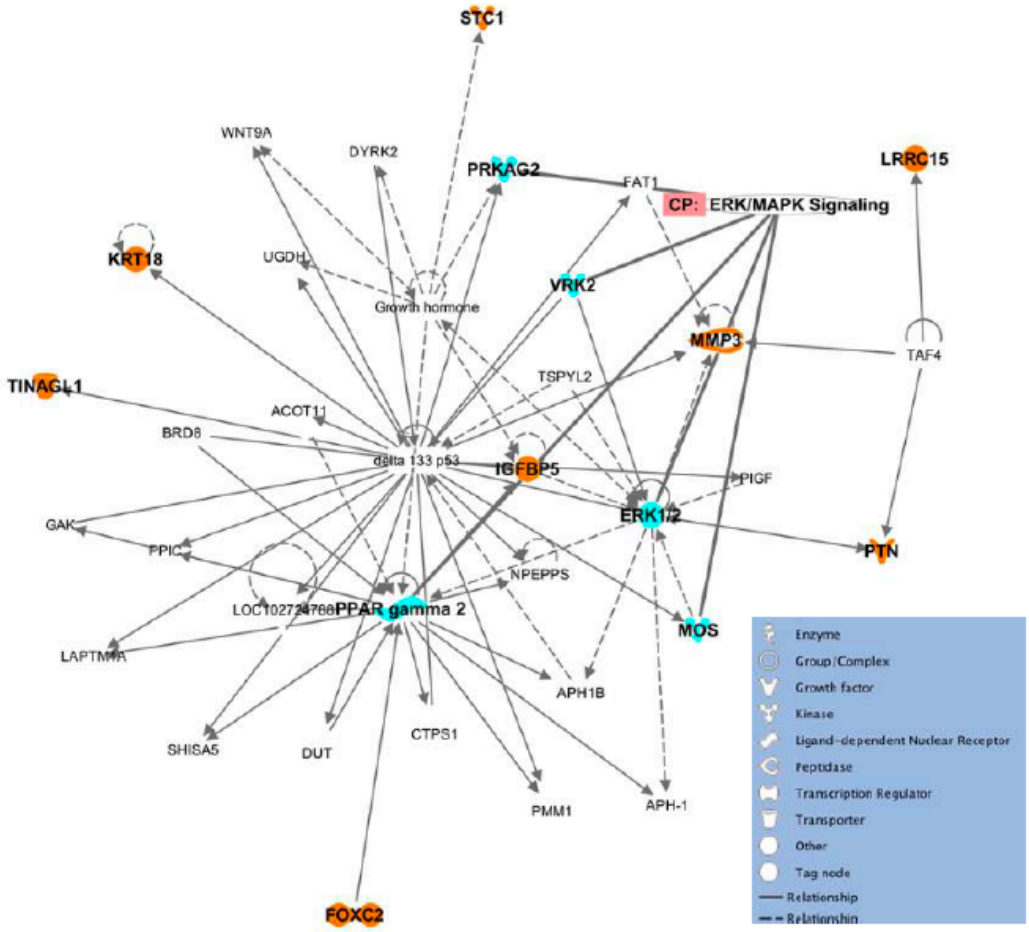

Figure III.5. Ingenuity Pathway Analysis of network of eight DE genes. The eight genes that were found by the intersection shown in Figure 3 were input into Ingenuity Pathway Analysis (IPA) to generate a network diagram with the most plausible connections to each other, and to additional genes in the IPA Knowledge Base. The eight genes of interest are highlighted in orange. A maximum of thirty-five genes are shown in the network for readability. The ERK/MAPK pathways genes found in this network are highlighted in cyan.

3.4. Discussion

3.4.1. Compensatory role of IGFBP5 in maintaining ERK/MAPK pathway homeostasis in LMNA mutant fibroblasts

Here we report gene expression profiling using RNA-seq on fibroblasts from a family bearing a pathogenic *LMNA* splice-site mutation. At present, the molecular mechanisms regulating tissue-specific manifestations of laminopathies are still

unidentified. However, multiple studies have shown that *LMNA* mutations cause nuclear envelope defects in mouse and human *LMNA* mutant fibroblasts [49,50,51] and dysregulation of molecular signaling such as ERK/MAPK and Wnt Beta-Catenin pathways in mutant cardiac tissues [9, 10]. In human cell lines, cultured cells from patients, and pluripotent stem cell disease models for *LMNA*-related diseases, upregulation of the ERK/MAPK pathway also is documented [52, 53]. Taken together, these studies suggested that laminopathies may arise from a combination of defects in the nuclear structure and the dysregulation of molecular signaling pathways in mutant cells.

Consistent with this, our gene expression profiling uncovered genes involved in signal transduction that are differentially expressed between *LMNA* mutant and normal human fibroblasts. Among eight significantly DE genes was the *IGFBP5* gene that encodes for an IGF binding protein that stabilizes IGF cytokines to promote or inhibit its signaling cascade and subsequent IGF function in cell culture [54]. Aside from its cytokine binding function, IGFBP5 protein overexpression was shown to suppress cell growth in human melanoma, osteosarcoma, and breast cancer cell lines emphasizing its function in regulating cell proliferation [55,56,57,58]. Overexpression of IGFBP5 also was shown to enhance osteogenic differentiation in mesenchymal stem cells [59]. These observations resulted in increased phosphorylation of ERK1/2 and increased activity of the MAPK pathway, and predictably IGFBP5 knock down by shRNA reduced phosphorylation of ERK1/2 and subsequently downregulated the MAPK pathway [58,59,60]. Subsequently, our pathway analysis showed that the eight DE genes, including *IGFBP5,* were connected through the ERK/MAPK pathway. Our RNA-seq data showed a significant reduction in *IGFBP5* gene expression in patient samples compared to control (7-fold reduction) and

unrelated samples (9-fold reduction). This reduction may potentially impact the signaling pathways downstream to IGFBP5 binding. IGFBP5 protein translocates to the nucleus and interacts with Early growth response-1 transcription factor in human primary lung fibroblast to induce extracellular matrix production by activating the ERK/MAPK pathway, independent of the IGF pathway [61]. Since we did not detect any significant changes in the expression of canonical IGFBP5 binding partners, such as IGF1 and IGF2, or in IGF pathway activity, this suggests that the IGF pathway maintained its normal activity in patient fibroblasts. Taken together, these observations along with findings presented in published studies suggested that IGFBP5 exerts its effect through the ERK/MAPK pathway rather than the IGF pathway.

With these findings, we hypothesize that in unaffected tissues such as *LMNA* mutant fibroblasts, the significant reduction of IGFBP5 expression may contribute to maintaining homeostasis of the ERK/MAPK signaling pathway and its downstream effects, masking the *LMNA* mutation phenotype. The postulation is supported by the observations of normal baseline ERK1/2 activity in patient fibroblasts [53]. In contrast, there is aberrant upregulation of ERK/MAPK pathway in affected tissues such as *LMNA* mutant cardiomyocytes which leads to laminopathy phenotype [10, 62]. Together, these mechanisms may provide an explanation for the absence of any significant phenotype in fibroblasts [63].

Another DE gene on the list, Forkhead Box C2 (*FOXC2*), whose overexpression induces hyperphosphorylation of ERK1/2 in cancer cells and is associated with aberrant cell proliferation [64], also has decreased mRNA expression in the affected individuals. *FOXC2* mRNA reduction by shRNA silencing has been shown to downregulate

ERK/MAPK activity [64]. The downregulation of *IGFBP5* and *FOXC2* gene expression may contribute to the compensatory mechanism that maintains the normal activity of ERK/MAPK pathway and absence of observable phenotypes in fibroblasts. While the current study was performed on an unaffected tissue, we were able to gain insight on the possible signaling pathways and molecular mechanisms involved in the tissue specificity of laminopathies and *LMNA*-related cardiomyopathy.

3.4.2. Similar expression levels of nuclear lamina-associated genes in all groups

Previously, we showed that there was monoallelic expression of *LMNA* gene in our patient fibroblasts, whereby only the wild type allele was expressed, and we predicted that the mutant allele expression was degraded by non-sense mediated mRNA decay [35]. In support of this, our RNA-seq results also showed *LMNA* expression was predominately from the wild type allele (97–99%) with no aberrantly spliced products from the mutant allele in patient fibroblasts.

We also found that there were no significant changes in *LMNA* transcript levels, ratio of Lamin A to Lamin C transcripts, or expression of other NL-genes, *LMNB1* and *LMNB2* between the Patient group and two control groups. These results are in line with our previous structural studies that found no significant difference in nuclear abnormalities and suggests that there were no compensatory mechanisms at the transcription level for the other proteins that construct the nuclear lamina [63].
Our results are in contrast to previous studies in patient fibroblasts that showed decreased Lamin A/C expression and altered ratio of Lamin A and Lamin C expression [65, 66]. Real-time PCR studies on fibroblasts from patients with a heterozygous *LMNA* mutation at the splice site of intron 5 showed reduced *LMNA* expression with the mutant *LMNA* allele

expressed at lower level compared to the normal allele [65]. In a different study, Lamin A protein expression was more diminished compared to Lamin C protein in fibroblasts from patients with Lamin-associated cardiomyopathies [66].

Numerous studies have reported that differential gene expression does not correlate directly with changes in protein expression [67,68,69,70]. Muchir et al. has previously reported that fibroblasts from EDMD, DCM and LGMD1B patients bearing heterozygous *LMNA* mutations have similar Lamin A/C protein levels compared to control fibroblasts [51]. Additional Lamin A/C protein studies in patient fibroblasts have also shown that heterozygous *LMNA* mutations do not result in significantly observable phenotypes such as nuclear abnormalities or reduced protein level [52, 71,72,73]. Here, we performed validation studies for Lamin A/C protein expression using Western Blot to resolve these discrepancies. We found that there was no significant differences in Lamin A/C protein expression in mutant fibroblasts. This contrasts the decreased or absent levels of Lamin A/C protein detected previously in patient cardiac tissues [74, 75]. Thus, our results suggest that there is upregulated expression of wild type *LMNA* allele in response to the degradation of the mutant allele or that expression of only one copy of the wild type allele is sufficient for normal levels of Lamin A/C protein to maintain normal physiological function in unaffected cell types. Other potential molecular mechanisms, such as epigenomic alterations specific to patient cardiac tissue [34, 76], tissue specific expression of Lamin proteins [17, 77], or differences in nuclear membrane proteome between tissues [78], may contribute to limit Lamin A/C haploinsufficiency to diseased cardiac tissues. Further studies comparing affected and unaffected tissues derived from the

same patient or from patient-specific disease models may provide additional insight to the molecular mechanism of this mutation.

3.4.3. Gene expression variabilities exist in samples within and between groups

We obtained in total nine dermal fibroblast samples from affected, related unaffected, and unrelated individuals to perform RNA-seq. Though we age-matched and gender-matched the patients to controls to the best of our abilities, we found significant variability between samples within groups. While age is thought to be a factor that can influence gene expression [79], recent study on cultured fibroblasts in-vitro harvested from young, middle aged and older individuals revealed no significant difference in gene expression based on age groups [80]. The similarity between the published study and ours led us to conclude that short term in-vitro culture conditions are not sufficient to induce gene expression differences that are influenced by age.

Epigenomic modifications play a role in modulating gene expression [81,82,83]. We postulate that expression differences may arise from different degrees of epigenetic modifications accumulated or inherited by the individuals studied here throughout their lifetime. Our qualitative observations indicated that variabilities intrinsic to the samples must be taken into consideration when performing gene expression analysis. At present, we believe the expression differences we observed here are due to the small sample size available for our studies. These differences must be taken into account for future gene expression profiling studies by increasing our sample sizes and technical replicates per group.

3.5. Conclusions

Using deep RNA-seq and pathway analysis, we identified eight differentially expressed genes in fibroblasts from an affected family with a novel *LMNA* splice-site mutation and heart disease. Among these eight genes, we identified *IGFBP5* as one of the candidate genes affected by *LMNA* mutation and propose a possible molecular mechanism that explains the lack of significant molecular and structural phenotype in unaffected tissues. The identification of the ERK/MAPK pathway connecting the candidate genes together supports published studies that implicate this pathway in the development of *LMNA*-related cardiomyopathy. Our results for normal Lamin A/C protein and *LMNA* gene expression from only the wild type allele in mutant fibroblasts also suggest that cardiac tissues are more sensitive to decreases in Lamin A/C protein.

We are aware of the limitations of our studies as presented here. The variation of gene expression within and between sample groups introduced confounding factors to our analysis and our use of an unaffected tissue (fibroblasts) instead of affected tissue (cardiomyocytes) result in a partial explanation of the molecular mechanisms of this particular *LMNA* splice-site mutation. Thus, our results indicate the necessity to develop a model system to study this disease in vitro. To that end, we will generate patient-specific induced pluripotent stem cells lines that will be differentiated to cardiomyocytes for molecular studies to confirm the proposed tissue-specific mechanism of disease.

3.6. References

1. Burke B, Stewart CL. The nuclear lamins: flexibility in function. Nat Rev Mol Cell Biol. 2013;14(1):13–24.
2. Dechat T, Adam SA, Taimen P, Shimi T, Goldman RD. Nuclear lamins. Cold Spring Harb Perspect Biol. 2010;2(11):a000547.
3. Prokocimer M, Davidovich M, Nissim-Rafinia M, Wiesel-Motiuk N, Bar DZ, Barkan R, et al. Nuclear lamins: key regulators of nuclear structure and activities. J Cell Mol Med. 2009;13(6):1059–85.
4. Wang Y, Ostlund C, Choi JC, Swayne TC, Gundersen GG, Worman HJ. Blocking farnesylation of the prelamin a variant in Hutchinson-Gilford progeria syndrome alters the distribution of A-type lamins. Nucleus. 2012;3(5):452–62.
5. Sullivan T, Escalante-Alcalde D, Bhatt H, Anver M, Bhat N, Nagashima K, et al. Loss of A-type Lamin expression compromises nuclear envelope integrity leading to muscular dystrophy. J Cell Biol. 1999;147(5):913–20.
6. Guelen L, Pagie L, Brasset E, Meuleman W, Faza MB, Talhout W, et al. Domain organization of human chromosomes revealed by mapping of nuclear lamina interactions. Nature. 2008;453(7197):948–51.
7. Ho CY, Lammerding J. Lamins at a glance. J Cell Sci. 2012;125(Pt 9):2087–93.
8. Johnson BR, Nitta RT, Frock RL, Mounkes L, Barbie DA, Stewart CL, et al. A-type lamins regulate retinoblastoma protein function by promoting subnuclear localization and preventing proteasomal degradation. Proc Natl Acad Sci U S A. 2004;101(26):9677–82.
9. Le Dour C, Macquart C, Sera F, Homma S, Bonne G, Morrow JP, et al. Decreased WNT/beta-catenin signalling contributes to the pathogenesis of dilated cardiomyopathy caused by mutations in the Lamin A/C gene. Hum Mol Genet. 2017;26(2):333–43.
10. Muchir A, Pavlidis P, Decostre V, Herron AJ, Arimura T, Bonne G, et al. Activation of MAPK pathways links LMNA mutations to cardiomyopathy in Emery-Dreifuss muscular dystrophy. J Clin Invest. 2007;117(5):1282–93.

11. Muchir A, Wu W, Choi JC, Iwata S, Morrow J, Homma S, et al. Abnormal p38alpha mitogen-activated protein kinase signaling in dilated cardiomyopathy caused by Lamin A/C gene mutation. Hum Mol Genet. 2012;21(19):4325–33.
12. Rober RA, Weber K, Osborn M. Differential timing of nuclear Lamin A/C expression in the various organs of the mouse embryo and the young animal: a developmental study. Development. 1989;105(2):365–78.
13. Constantinescu D, Gray HL, Sammak PJ, Schatten GP, Csoka AB. Lamin A/C expression is a marker of mouse and human embryonic stem cell differentiation. Stem Cells. 2006;24(1):177–85.
14. Vergnes L, Peterfy M, Bergo MO, Young SG, Reue K. Lamin B1 is required for mouse development and nuclear integrity. Proc Natl Acad Sci U S A. 2004;101(28):10428–33.
15. Coffinier C, Jung HJ, Nobumori C, Chang S, Tu Y, Barnes RH 2nd, et al. Deficiencies in Lamin B1 and Lamin B2 cause neurodevelopmental defects and distinct nuclear shape abnormalities in neurons. Mol Biol Cell. 2011;22(23):4683–93.
16. Stewart C, Burke B. Teratocarcinoma stem cells and early mouse embryos contain only a single major Lamin polypeptide closely resembling Lamin B. Cell. 1987;51(3):383–92.
17. Talamas JA, Capelson M. Nuclear envelope and genome interactions in cell fate. Front Genet. 2015;6:95.
18. Fatkin D, MacRae C, Sasaki T, Wolff MR, Porcu M, Frenneaux M, et al. Missense mutations in the rod domain of the Lamin A/C gene as causes of dilated cardiomyopathy and conduction-system disease. N Engl J Med. 1999;341(23):1715–24.
19. Becane HM, Bonne G, Varnous S, Muchir A, Ortega V, Hammouda EH, et al. High incidence of sudden death with conduction system and myocardial disease due to lamins a and C gene mutation. Pacing Clin Electrophysiol. 2000;23(11 Pt 1):1661–6.
20. Pan H, Richards AA, Zhu X, Joglar JA, Yin HL, Garg V. A novel mutation in Lamin A/C is associated with isolated early-onset atrial fibrillation and progressive atrioventricular block followed by cardiomyopathy and sudden cardiac death. Heart Rhythm. 2009;6(5):707–10.

21. Bonne G, Mercuri E, Muchir A, Urtizberea A, Becane HM, Recan D, et al. Clinical and molecular genetic spectrum of autosomal dominant Emery-Dreifuss muscular dystrophy due to mutations of the Lamin A/C gene. Ann Neurol. 2000;48(2):170–80.
22. Frock RL, Kudlow BA, Evans AM, Jameson SA, Hauschka SD, Kennedy BK. Lamin A/C and emerin are critical for skeletal muscle satellite cell differentiation. Genes Dev. 2006;20(4):486–500.
23. Favreau C, Delbarre E, Courvalin JC, Buendia B. Differentiation of C2C12 myoblasts expressing Lamin a mutated at a site responsible for Emery-Dreifuss muscular dystrophy is improved by inhibition of the MEK-ERK pathway and stimulation of the PI3-kinase pathway. Exp Cell Res. 2008;314(6):1392–405.
24. Muchir A, van Engelen BG, Lammens M, Mislow JM, McNally E, Schwartz K, et al. Nuclear envelope alterations in fibroblasts from LGMD1B patients carrying nonsense Y259X heterozygous or homozygous mutation in Lamin A/C gene. Exp Cell Res. 2003;291(2):352–62.
25. De Sandre-Giovannoli A, Bernard R, Cau P, Navarro C, Amiel J, Boccaccio I, et al. Lamin a truncation in Hutchinson-Gilford progeria. Science. 2003;300(5628):2055 Epub 2003/04/19.
26. Eriksson M, Brown WT, Gordon LB, Glynn MW, Singer J, Scott L, et al. Recurrent de novo point mutations in Lamin a cause Hutchinson-Gilford progeria syndrome. Nature. 2003;423(6937):293–8.
27. Herman DS, Lam L, Taylor MR, Wang L, Teekakirikul P, Christodoulou D, et al. Truncations of titin causing dilated cardiomyopathy. N Engl J Med. 2012;366(7):619–28.
28. Mestroni L, Brun F, Spezzacatene A, Sinagra G, Taylor MR. Genetic causes of
29. Taylor MR, Fain PR, Sinagra G, Robinson ML, Robertson AD, Carniel E, et al. Natural history of dilated cardiomyopathy due to Lamin A/C gene mutations. J Am Coll Cardiol. 2003;41(5):771–80.
30. Dellefave L, McNally EM. The genetics of dilated cardiomyopathy. Curr Opin Cardiol. 2010;25(3):198–204.
31. Hershberger RE, Morales A. LMNA-Related Dilated Cardiomyopathy. In: Adam MP, Ardinger HH, Pagon RA, Wallace SE, Bean LJH, Stephens K, et al., editors. GeneReviews®. Seattle (WA): University of Washington, Seattle; 1993.
32. Brayson D, Shanahan CM. Current insights into LMNA cardiomyopathies: existing models and missing LINCs. Nucleus. 2017;8(1):17–33.

33. Jaalouk DE, Lammerding J. Mechanotransduction gone awry. Nat Rev Mol Cell Biol. 2009;10(1):63–73.
34. Perovanovic J, Dell'Orso S, Gnochi VF, Jaiswal JK, Sartorelli V, Vigouroux C, et al. Laminopathies disrupt epigenomic developmental programs and cell fate. Sci Transl Med. 2016;8(335):335ra58.
35. Zaragoza MV, Fung L, Jensen E, Oh F, Cung K, McCarthy LA, et al. Exome sequencing identifies a novel *LMNA* splice-site mutation and multigenic Heterozygosity of potential modifiers in a family with sick sinus syndrome, dilated cardiomyopathy, and sudden cardiac death. PLoS One. 2016;11(5):e0155421.
36. Andrews S. FastQC: a quality control tool for high throughput sequence data. 2010. Available online: www.bioinformatics.babraham.ac.uk/projects/fastqc.
37. Kim D, Pertea G, Trapnell C, Pimentel H, Kelley R, Salzberg SL. TopHat2: accurate alignment of transcriptomes in the presence of insertions, deletions and gene fusions. Genome Biol. 2013;14(4):R36.
38. Trapnell C, Roberts A, Goff L, Pertea G, Kim D, Kelley DR, et al. Differential gene and transcript expression analysis of RNA-seq experiments with TopHat and cufflinks. Nat Protoc. 2012;7(3):562–78.
39. Trapnell C, Hendrickson DG, Sauvageau M, Goff L, Rinn JL, Pachter L. Differential analysis of gene regulation at transcript resolution with RNA-seq. Nat Biotechnol. 2013;31(1):46–53.
40. Goff L, Trapnell C, Kelley D. cummeRbund: Analysis, exploration, manipulation, and visualization of Cufflinks high-throughput sequencing data. 2019. R package version 2.28.0. Available online: bioconductor.riken.jp/packages/3.10/bioc/html/cummeRbund.html.
41. Robinson JT, Thorvaldsdóttir H, Winckler W, Guttman M, Lander ES, Getz G, et al. Integrative genomics viewer. Nat Biotechnol. 2011;29(1):24–6.
42. Livak KJ, Schmittgen TD. Analysis of relative gene expression data using real-time quantitative PCR and the 2(−Delta Delta C(T)) method. Methods. 2001;25(4):402–8.
43. Schmittgen TD, Livak KJ. Analyzing real-time PCR data by the comparative C(T) method. Nat Protoc. 2008;3(6):1101–8.

44. Schneider CA, Rasband WS, Eliceiri KW. NIH image to ImageJ: 25 years of image analysis. Nat Methods. 2012;9(7):671–5.
45. Lindner D, Zietsch C, Becher PM, Schulze K, Schultheiss HP, Tschope C, et al. Differential expression of matrix metalloproteases in human fibroblasts with different origins. Biochem Res Int. 2012;2012:875742.
46. Jung H, Kim B, Moon BI, Oh ES. Cytokeratin 18 is necessary for initiation of TGF-beta1-induced epithelial-mesenchymal transition in breast epithelial cells. Mol Cell Biochem. 2016;423(1–2):21–8.
47. Marino G, Ugalde AP, Fernandez AF, Osorio FG, Fueyo A, Freije JM, et al. Insulin-like growth factor 1 treatment extends longevity in a mouse model of human premature aging by restoring somatotroph axis function. Proc Natl Acad Sci U S A. 2010;107(37):16268–73.
48. Singh M, Hunt CR, Pandita RK, Kumar R, Yang CR, Horikoshi N, et al. Lamin A/C depletion enhances DNA damage-induced stalled replication fork arrest. Mol Cell Biol. 2013;33(6):1210–22.
49. Raharjo WH, Enarson P, Sullivan T, Stewart CL, Burke B. Nuclear envelope defects associated with LMNA mutations cause dilated cardiomyopathy and Emery-Dreifuss muscular dystrophy. J Cell Sci. 2001;114(Pt 24):4447–57.
50. Ho JC, Zhou T, Lai WH, Huang Y, Chan YC, Li X, et al. Generation of induced pluripotent stem cell lines from 3 distinct laminopathies bearing heterogeneous mutations in Lamin A/C. Aging. 2011;3(4):380–90.
51. Muchir A, Medioni J, Laluc M, Massart C, Arimura T, van der Kooi AJ, et al. Nuclear envelope alterations in fibroblasts from patients with muscular dystrophy, cardiomyopathy, and partial lipodystrophy carrying Lamin a/C gene mutations. Muscle Nerve. 2004;30(4):444–50.
52. Emerson LJ, Holt MR, Wheeler MA, Wehnert M, Parsons M, Ellis JA. Defects in cell spreading and ERK1/2 activation in fibroblasts with Lamin A/C mutations. Biochim Biophys Acta. 2009;1792(8):810–21.
53. Siu CW, Lee YK, Ho JC, Lai WH, Chan YC, Ng KM, et al. Modeling of Lamin A/C mutation premature cardiac aging using patient-specific induced pluripotent stem cells. Aging. 2012;4(11):803–22.

54. Denduluri SK, Idowu O, Wang Z, Liao Z, Yan Z, Mohammed MK, et al. Insulin-like growth factor (IGF) signaling in tumorigenesis and the development of cancer drug resistance. Genes Dis. 2015;2(1):13–25.
55. Schedlich LJ, Young TF, Firth SM, Baxter RC. Insulin-like growth factor-binding protein (IGFBP)-3 and IGFBP-5 share a common nuclear transport pathway in T47D human breast carcinoma cells. J Biol Chem. 1998;273(29):18347–52.
56. Schedlich LJ, Le Page SL, Firth SM, Briggs LJ, Jans DA, Baxter RC. Nuclear import of insulin-like growth factor-binding protein-3 and -5 is mediated by the importin beta subunit. J Biol Chem. 2000;275(31):23462–70.
57. Suh YA, Kim JH, Sung MA, Boo HJ, Yun HJ, Lee SH, et al. A novel antitumor activity of deguelin targeting the insulin-like growth factor (IGF) receptor pathway via up-regulation of IGF-binding protein-3 expression in breast cancer. Cancer Lett. 2013;332(1):102–9.
58. Wang J, Ding N, Li Y, Cheng H, Wang D, Yang Q, et al. Insulin-like growth factor binding protein 5 (IGFBP5) functions as a tumor suppressor in human melanoma cells. Oncotarget. 2015;6(24):20636–49.
59. Wang Y, Jia Z, Diao S, Lin X, Lian X, Wang L, et al. IGFBP5 enhances osteogenic differentiation potential of periodontal ligament stem cells and Wharton's jelly umbilical cord stem cells, via the JNK and MEK/Erk signalling pathways. Cell Prolif. 2016;49(5):618–27.
60. Lee DH, Kim JE, Kang YJ. Insulin like growth factor binding Protein-5 regulates excessive vascular smooth muscle cell proliferation in spontaneously hypertensive rats via ERK 1/2 phosphorylation. Korean J Physiol Pharmacol. 2013;17(2):157–62.
61. Yasuoka H, Hsu E, Ruiz XD, Steinman RA, Choi AM, Feghali-Bostwick CA. The fibrotic phenotype induced by IGFBP-5 is regulated by MAPK activation and egr-1-dependent and -independent mechanisms. Am J Pathol. 2009;175(2):605–15.
62. Muchir A, Reilly SA, Wu W, Iwata S, Homma S, Bonne G, et al. Treatment with selumetinib preserves cardiac function and improves survival in cardiomyopathy caused by mutation in the Lamin A/C gene. Cardiovasc Res. 2012;93(2):311–9.

63. Core JQ, Mehrabi M, Robinson ZR, Ochs AR, McCarthy LA, Zaragoza MV, et al. Age of heart disease presentation and dysmorphic nuclei in patients with LMNA mutations. PLoS One. 2017;12(11):e0188256.
64. Cui YM, Jiang D, Zhang SH, Wu P, Ye YP, Chen CM, et al. FOXC2 promotes colorectal cancer proliferation through inhibition of FOXO3a and activation of MAPK and AKT signaling pathways. Cancer Lett. 2014;353(1):87–94.
65. Carboni N, Floris M, Mateddu A, Porcu M, Marrosu G, Solla E, et al. Aberrant splicing in the LMNA gene caused by a novel mutation on the polypyrimidine tract of intron 5. Muscle Nerve. 2011;43(5):688–93.
66. Al-Saaidi R, Rasmussen TB, Palmfeldt J, Nissen PH, Beqqali A, Hansen J, et al. The LMNA mutation p.Arg321Ter associated with dilated cardiomyopathy leads to reduced expression and a skewed ratio of Lamin a and Lamin C proteins. Exp Cell Res. 2013;319(19):3010–9.
67. de Sousa AR, Penalva LO, Marcotte EM, Vogel C. Global signatures of protein and mRNA expression levels. Mol BioSyst. 2009;5(12):1512–26 Epub 2009/12/22.
68. Maier T, Guell M, Serrano L. Correlation of mRNA and protein in complex biological samples. FEBS Lett. 2009;583(24):3966–73.
69. Vogel C, Marcotte EM. Insights into the regulation of protein abundance from proteomic and transcriptomic analyses. Nat Rev Genet. 2012;13(4):227–32 Epub 2012/03/14.
70. Koussounadis A, Langdon SP, Um IH, Harrison DJ, Smith VA. Relationship between differentially expressed mRNA and mRNA-protein correlations in a xenograft model system. Sci Rep. 2015;5:10775.
71. Vigouroux C, Auclair M, Dubosclard E, Pouchelet M, Capeau J, Courvalin JC, et al. Nuclear envelope disorganization in fibroblasts from lipodystrophic patients with heterozygous R482Q/W mutations in the Lamin A/C gene. J Cell Sci. 2001;114(Pt 24):4459–68.
72. Caux F, Dubosclard E, Lascols O, Buendia B, Chazouilleres O, Cohen A, et al. A new clinical condition linked to a novel mutation in lamins a and C with generalized lipoatrophy, insulin-resistant diabetes, disseminated leukomelanodermic papules, liver steatosis, and cardiomyopathy. J Clin Endocrinol Metab. 2003;88(3):1006–13.

73. Favreau C, Dubosclard E, Ostlund C, Vigouroux C, Capeau J, Wehnert M, et al. Expression of Lamin a mutated in the carboxyl-terminal tail generates an aberrant nuclear phenotype similar to that observed in cells from patients with Dunnigan-type partial lipodystrophy and Emery-Dreifuss muscular dystrophy. Exp Cell Res. 2003;282(1):14–23.
74. Arbustini E, Pilotto A, Repetto A, Grasso M, Negri A, Diegoli M, et al. Autosomal dominant dilated cardiomyopathy with atrioventricular block: a Lamin A/C defect-related disease. J Am Coll Cardiol. 2002;39(6):981–90.
75. Narula N, Favalli V, Tarantino P, Grasso M, Pilotto A, Bellazzi R, et al. Quantitative expression of the mutated Lamin A/C gene in patients with cardiolaminopathy. J Am Coll Cardiol. 2012;60(19):1916–20.
76. Poleshko A, Shah PP, Gupta M, Babu A, Morley MP, Manderfield LJ, et al. Genome-nuclear Lamina interactions regulate cardiac stem cell lineage restriction. Cell. 2017;171(3):573–87 e14.
77. Dittmer TA, Misteli T. The Lamin protein family. Genome Biol. 2011;12(5):222.
78. Korfali N, Wilkie GS, Swanson SK, Srsen V, de Las HJ, Batrakou DG, et al. The nuclear envelope proteome differs notably between tissues. Nucleus. 2012;3(6):552–64.
79. Jiang Y, Mishima H, Sakai S, Liu YK, Ohyabu Y, Uemura T. Gene expression analysis of major lineage-defining factors in human bone marrow cells: effect of aging, gender, and age-related disorders. J Orthop Res. 2008;26(7):910–7.
80. Kaisers W, Boukamp P, Stark HJ, Schwender H, Tigges J, Krutmann J, et al. Age, gender and UV-exposition related effects on gene expression in in vivo aged short term cultivated human dermal fibroblasts. PLoS One. 2017;12(5):e0175657.
81. Jaenisch R, Bird A. Epigenetic regulation of gene expression: how the genome integrates intrinsic and environmental signals. Nat Genet. 2003;33(Suppl):245–54.
82. Grewal SI, Moazed D. Heterochromatin and epigenetic control of gene expression. Science. 2003;301(5634):798–802.
83. Fraga MF, Ballestar E, Paz MF, Ropero S, Setien F, Ballestar ML, et al. Epigenetic differences arise during the lifetime of monozygotic twins. Proc Natl Acad Sci U S A. 2005;102(30):106

CHAPTER 4

Patient-specific iPSC disease modeling reveals dysregulation of BMP pathway activity as part of the molecular mechanisms promoting *LMNA*-associated cardiac diseases

4.1. Introduction

Lamin A/C is an intermediate filament protein that constructs the nuclear lamina of a cell encoded by the gene *LMNA*. There are two lamin isoforms encoded by this gene: Lamin A and Lamin C as a result of alternative splicing. Canonically lamins provide structural support to the nuclear envelope; however, recent evidence shows that lamins are also distributed throughout the nucleoplasm leading to new insight on the protein's functions [1, 2]. Lamin A/C have also been implicated in processes such as nuclear chromatin localization [3], DNA replication [4] and cell differentiation [5]. It has also been shown that *LMNA* mutation impacts the regulation of numerous signaling pathways, such as BMP, Wnt, mTOR and MAPK which in turn led to aberrant expression of target genes and downstream effects implicated in cell differentiation and proliferation [6-10]. These results suggest a diverse role for Lamin A/C in addition to its main function as a structural protein.

Though Lamin A/C is ubiquitously expressed in the nuclei of all somatic cells, diseases that arise from mutations in this gene, laminopathies, the phenotypes primarily manifest in mesoderm-derived cell types. Laminopathies ranged from pathologies affecting the skeletal muscle system (limb girdle muscular dystrophy (LGMD) and Emery-Dreyfus muscular dystrophy (EDMD)), adipose tissue (lipodystrophy) and ultimately the cardiac muscle system manifesting as dilated cardiomyopathy with conduction defects, the focus of our study. There are two prevailing hypotheses in the field regarding how laminopathies manifested *in-vivo*: the mechanical defect hypothesis and the gene expression hypothesis. The mechanical defect hypothesis posited that Lamin A/C deficiency causes increased susceptibility to physiological and mechanical stresses, leading to increased apoptosis and necrosis [11-13]. On the other hand, the gene expression hypothesis proposed that because

of Lamin A/C's role in establishing lamina-associated domain (LADs) within the cell's nucleus, Lamin A/C deficiency may lead to aberrant gene expression, aberrant chromatin modifications and dysregulation of signaling pathway activities [14, 15]. Both of these hypotheses have been validated through various studies, showing that both of these processes were involved in manifestation of laminopathies.

We have previously identified, through whole exome sequencing, *LMNA* splice-site mutation (*LMNA* c.357-2A > G) in a large family in which dilated cardiomyopathy, arrythmia and sudden death syndrome are multigenerational and prevalent [16]. There is a great need to understand the underlying mechanism of cardiac diseases to identify key pathways and targets to develop a more efficient method to treat cardiomyopathies. The discovery that somatic cells can be reverted to their undifferentiated state, as induced pluripotent stem cells (iPSCs), using four defined transcription factors, known as the Yamanaka factors, broadens the use of stem cells as a tool for disease modeling [17]. Using this approach, significant findings on how Lamin A/C mutations affected gene expression and signaling pathway activities [18], cardiac functions [19, 20] and nuclear structure have been recorded [18, 21].

Since their discoveries, embryonic stem cells (ESCs) and iPSCs have emerged as indispensable tools to study cell differentiation and embryonic development, where previously such studies were limited to animal models [22-25]. More evidence recently emerged on how Lamin A/C played critical roles in cellular differentiation. In a Lamin A/C deficient mouse ESCs, the cells preferentially formed cells from the endodermal lineage when induced to differentiate [26]. In a Lamin A/C haploinsufficient skeletal muscle model, myogenesis appeared to be impaired in these myoblasts [27]. Lamin A/C have also been

shown to govern mesenchymal stem cell (MSC) lineage commitment, where Lamin A/C overexpression in MSC led to increased osteogenesis and reduced capacity of forming chondrocytes and adipocytes [28]. These results underscored the importance of Lamin A/C in cell differentiation and how disruption in Lamin A/C expression dramatically altered cell fates.

With the advent of scRNA-seq technology, it is now possible to conduct transcriptomic profiling at a single cell resolution, providing new insight on various biological processes such as identifying specific cell subtypes within a tissue sample, cellular differentiation trajectories inference and reconstruction of gene-networks. Using scRNA-seq, several groups have uncovered new information on diseases such as cystic fibrosis, glioblastoma and breast cancer, providing new insights and strategies to treat these diseases [29-31]. Previously, scRNA-seq studies have been performed in iPSC and ESC-derived cardiomyocytes [32-34], revealing important information on transcription factors that played a role in governing cardiac development and maturation *in-vitro*. While these studies offered great insight into cardiac development, these studies were performed on "normal" iPSC and ESC derived cardiomyocytes, not diseased cardiomyocytes which would provide valuable information on how genetic mutations affect cardiomyocyte differentiation and how any alterations in gene expression and signaling pathways would manifest in cardiac diseases.

To address this gap in knowledge, we used Yamanaka factors (*Oct4*, *Sox2*, *Klf4* and *c-Myc*) to reprogram patient and control fibroblasts to their corresponding iPSCs and differentiated these iPSCs to iPSC-derived cardiomyocytes (iPSC-CMs) by modulating the activity of Wnt/β-catenin signaling pathway [35, 36]. We performed molecular studies via

Sanger sequencing to determine *LMNA* allelic expression in iPSC-CMs. Additionally, Lamin A/C protein relative quantification was conducted using Western Blot to evaluate the impact of the mutation of Lamin A/C protein level. Finally, we sought to study how the splice-site Lamin A/C mutation affect cardiac differentiation process by performing single cell transcriptome profiling of iPSC-CMs generated from control and patient iPSCs cells as they progressed through cardiac differentiation process, evaluate differences in gene expression and perform pathway analysis to discover signaling pathways affected by the mutation.

Our study showed that there was no significant difference in pluripotency between iPSCs originating from fibroblasts with and without the Lamin A/C splice-site mutation. Furthermore, we successfully generated iPSC-CMs from three control iPSCs and three patient iPSCs, albeit with varying differentiation efficiencies, and differential gene expression analysis showed tissue specificity of Lamin A/C haploinsufficiency. Molecular and protein studies revealed that Lamin A/C haploinsufficiency to be the primary molecular mechanism of the Lamin A/C splice-site mutation. We also discovered disruption of mesoderm and mesendoderm gene (*TBXT, EOMES, MIXL1*) expression on the early time points of cardiac differentiation and a consistently lower expression of cardiogenic transcription factors (*NKX2-5*, *TMEM88* and *HAND1*) in patient iPSC-CMs. Finally, pathway analysis predicted the inhibition of BMP pathway, in contrast to normal cardiomyocyte differentiation process, and activation of PTEN signaling pathway in differentiating cells to play a role in retarding the cardiac differentiation process in patient iPSC-CMs. Additionally, we found signaling pathways associated with cell death, apoptosis and DNA damage predicted to be activated in the embryonic cardiomyocyte population. Ultimately, our study showed that the splice-site *LMNA* mutation resulted in Lamin A/C haploinsufficiency leading

to dysregulation of early gene expression leading to impaired cardiac differentiation and an elevated susceptibility to cell death in patient iPSC-CMs.

4.2. Materials & Methods

4.2.1. Generation and characterization of control and patient-specific iPSCs

Patient and control specific iPSC lines were generated from fibroblasts obtained from patients and their gender and age-matched biological controls. These fibroblasts were cultured to confluency and reprogrammed using CytoTune®-iPS 2.0 Sendai Reprogramming Kit (Life Technologies, Carlsbad, CA). The iPSC lines used in this study could be found in Table 1. Samples denoted as patients are individuals bearing a heterozygous splice site mutation at the *LMNA* gene (*LMNA* c.357-2A > G). These individuals presented with bradycardia, palpitation and mild cardiomyopathy, indicative of impaired cardiac function [16]. Samples designated as controls were found to have no *LMNA* mutation and were derived from family members without any signs or symptoms of cardiac disease. Donor 3, an unrelated gender matched control for P2, was used instead of Control 2 due to the low viability of Control 2 iPSC upon thawing and low differentiation efficiency.

Briefly, fibroblasts were cultured in 6-well plates at previously determined seeding densities to achieve 30-60% confluency at the start of the transduction. Next we infected the cells with Sendai virus carrying Yamanaka factors (Oct4, Sox2, Klf4, cMyc), with MOI calculated beforehand in accordance to the reprogramming protocol. Cells were incubated with the reprogramming vectors overnight until removed the following day with a fresh fibroblast growth media change. Media changes were performed every other day for 7 days

after transduction. On day 8 post-transduction, fibroblast growth media was replaced with iPSC maintenance media (mTESR1, Stem Cell Technologies). Cells were kept in mTESR1 media until iPSC colonies emerged from the fibroblasts culture and were manually picked and transferred to Matrigel-coated 12-well plates to positively select for colonies that maintain its undifferentiated state and proper stem cell morphologies. iPSC colonies were cultured in mTESR1 media for an additional 21 days until they were ready for replating to new Matrigel-coated plates for further iPSC colony expansion.

At passage 10, the iPSC clones were characterized by performing immunocytochemistry staining for pluripotent stem cell markers (Oct4, Sox2, Tra 1-60 and SSEA4). To perform immunocytochemistry, cells were seeded to 4-well chamber slides and cultured to 80% confluency. Next, the cells were fixed with 4% paraformaldehyde (4% PFA) for 15 minutes at room temperature. After a 15-minute washing process using DPBS, we permeabilized the cells using 1% saponin in DPBS for 15 minutes at room temperature. Afterwards, we incubated the cells in 3% bovine serum albumin (3% BSA) in DPBS for one hour to inhibit non-specific antibody binding. Next, we incubated the cells with primary antibodies targeting OCT4 (A24867, 1:100, Thermo Fisher Scientific), SOX2 (A24759, 1:100, Thermo Fisher Scientific), SSEA4 (A24866, 1:100, Thermo Fisher Scientific) and Tra 1-60 (A24868, 1:100, Thermo Fisher Scientific) at 4 C, overnight. The next day the cells were washed with DPBS and incubated with secondary antibodies conjugated to fluorophores at 1:250 dilution for one hour at room temperature. After a final washing step, we mount the stained cells with Fluoroshield™ with DAPI (Sigma Aldrich) before the slides were imaged using Nikon Ti inverted fluorescence microscope. A comprehensive list of antibodies used in the study can be found in the Supplementary Data: Table IV.S4.

In addition to immunocytochemistry, we also performed RT-qPCR to measure the relative expression of pluripotency genes. mRNAs were extracted from iPSCs by following the manufacturer's protocols from the RNeasy Mini kit (Qiagen, Valencia, CA) and converted to cDNA in accordance to the manufacturer's protocol included in the QuantiTect® Reverse Transcription kit (Qiagen, Valencia, CA). 100 ng/ul cDNA from C1 and P1 iPSC lines were used for each RT-qPCR run. We used the 2X KAPA SYBR FAST ROX Low Master Mix (KK4620, Roche Sequencing and Life Science, Kapa Biosystems, Wilmington, MA) to generate reaction mixture, along with 10 uM forward and reverse primers specific for *POU5F1*, *SOX2*, *KLF4* and *cMyc* (KiCqStart SYBR Green Primers, Millipore Sigma, St. Louis, MO) and PCR-grade water for a total reaction volume of 20 ul. Primer sequences are included in the Supplementary Data: Table IV.S5. The RT-qPCR cycle was run in the QuantStudio 7 Real-Time PCR system (Thermo Fisher Scientific, Carlsbad, CA) with the following cycle: 95 C for 3 minutes, 95 C for 3 seconds, 60 C for 30 seconds and 72 C for 30 seconds (40 cycles) followed by generation of melt curve. Comparative Ct (ΔCt) method was used to determine relative quantitative gene expression (QGE). N-Acetyltransferase 1 (*NAT1*) was used as the housekeeping gene [37]. Statistical analysis was performed using Student's t-test. P values less than 0.05 were considered statistically significant.

Differentiation capabilities were evaluated by inducing iPSCs to form embryoid bodies (EBs). Briefly, iPSCs were passaged as cell aggregates to 35 mm non-tissue culture treated plate to form EBs. The EBs were kept in Essential 6 (E6) media for 7 days, with media change performed on alternating days. Once some EBs began to settle on the plate surface, we transferred the remaining floating EBs to 35 mm tissue culture treated plates and kept them in culture for up to 28 days. Once the EBs have sufficiently differentiated, we

proceeded to perform immunocytochemistry staining for alpha-fetoprotein (A25530, 1:500, Thermo Fisher Scientific), β-tubulin (A25532, 1:500, Thermo Fisher Scientific) and α-smooth muscle actin (A25531, 1:100, Thermo Fisher Scientific) as described previously. Finally, karyotyping was done to ensure that there are no chromosomal abnormalities during the reprogramming process (WiCell Genetics, Madison, WI). The fully characterized patient and control iPSC lines were used for cardiac differentiation.

Table IV.1. Fibroblast cell samples that were reprogrammed and differentiated (N = 6)

Abbreviation	Identification	Genotype*	Karyotype
P1	Patient A1	+/-	46, XX
P2	Patient A2	+/-	46, XY
P3	Patient A3	+/-	46, XX
C1	Control A1	+/+	46, XX
C2	Donor 3	+/+	46, XY
C3	Control A3	+/+	46, XX

*Genotypes: +/+ homozygous normal allele; +/- heterozygous *LMNA* splice-site mutation

4.2.2. Generation and characterization of iPSC-derived cardiomyocytes (iPSC-CMs)

iPSC-derived cardiomyocytes (iPSC-CMs) were generated from all three patient iPSC lines and three age and gender matched iPSC control lines using previously described method of Wnt/β-catenin signaling modulation using small molecules (Figure IV.1) [33, 35, 36, 38].

Patient and control iPSCs were seeded to 12-well plates at the appropriate densities and cultured for ninety-six hours until they reach 90-100% confluency with mTESR1 media (Stem Cell Technologies, Vancouver, Canada). On day 0 of differentiation, the media will be

switched to cardiomyocyte differentiation medium consisting of RPMI 1640 media (Life Technologies, Carlsbad, CA) supplemented with B27 supplement without insulin (Life Technologies, Carlsbad, CA) (RPMI/B27-) and 7.5 uM CHIR99201 (Cayman Technologies) and cultured for 48 hours at 37 ^{o}C, 5% CO_2.

Forty-eight hours later, the spent differentiation medium was replaced with RPMI/B27- supplemented with 7.5 uM IWP2 (R&D Systems). After forty-eight hours, the spent differentiation medium was replenished with RPMI/B27-. On day 6 of differentiation the media was changed to RPMI 1640 media supplemented with B27 supplement with insulin (RPMI/B27+). Beating clusters could be observed starting from day 8 to 10 of differentiation and beating cells were maintained in RPMI/B27+ media from day 8 onward with media changes every other day.

4.2.3. Generation of iPSC-derived cardiomyocytes (iPSC-CMs) using Gibco ™ PSC Cardiomyocyte Differentiation Kit

C1 and P1 iPSC-CMs used on days 16 (d16) and 19 (d19) of scRNA-seq differentiation time-course study were generated using a commercially-available differentiation kit (Gibco PSC Cardiomyocyte Differentiation Kit, Thermo Fisher Scientific, Carlsbad, CA).

4.2.4. iPSC-CMs purification using lactate purification methods

To ensure purity of resulting iPSC-CMs culture, we subjected the iPSC-CMs to metabolic selection by taking advantage of the ability of cardiomyocytes to metabolize other fuel source than glucose, such as lactate. We replace the RPMI/B27+ media at day 12

of differentiation with Cardiomyocyte Enrichment media (CEM) which consists of RPMI 1640 (no glucose) supplemented with 1 M sodium lactate, Bovine albumin fraction V and ascorbic acid [39]. The purification process lasted for 6 days and 4 days for iPSC-CMs generated using Wnt activity modulation and iPSC-CMs generated using Gibco PSC Cardiomyocyte Differentiation kit, respectively. At the end of purification process, purified iPSC-CMs were used for immunocytochemistry staining (C1-3 and P1-3) and single cell RNA-sequencing at days 16 and 19 (C1 and P1).

4.2.5. iPSC-CMs harvesting for iPSC-CMs characterizations, molecular and protein studies

iPSC-CMs harvesting was conducted using STEMdiff™ Cardiomyocyte Dissociation kit (Stem Cell Technologies, Vancouver, Canada). iPSC-CMs were washed twice with 1 ml of sterile DPBS before 1 ml of pre-warmed Cardiomyocyte Dissociation medium was added to each well of a 12 well-plate. The treated wells were then incubated at 37 C for 10-12 minutes. Then 2 ml of Cardiomyocyte Support medium were added to each treated well and using a 10 ml serological pipette the cell suspension was triturated until dislodged from the well. The resulting cell suspension were then transferred to a 50 ml conical centrifuge tube containing 3 ml/well Cardiomyocyte Support media then centrifuged at 300 g for 5 minutes. After the supernatant was removed, we resuspend the cell pellet with 1-2 ml of Cardiomyocyte Support media using a 10 ml serological pipette to prevent cell shearing and minimize cell death. Using Trypan Blue exclusion method, we counted the cells then proceeded to replating or downstream characterization assays (flow cytometry and immunocytochemistry staining) and molecular, protein and scRNA-seq studies.

4.2.6. Characterization of iPSC-CMs by Troponin T quantification and immunocytochemistry staining

On day 15 of differentiation, iPSC-CMs were harvested for characterization using FACS to quantify the percentage of Troponin T+ cells. iPSC-CMs were harvested as single cells and aliquoted to individual 15 ml conical centrifuge tubes and stained with Zombie NIR™ fixable viability dye (423105, 1:10,000, BioLegend) diluted in DPBS for 30 minutes at room temperature. After washing with FACS buffer (DPBS supplemented with 3% BSA) twice, we fixed the stained cells using 4% PFA and incubated at room temperature for 15 minutes in the dark. After washing with FACS buffer twice, we permeabilize our fixed cells using 0.1% saponin in FACS buffer for 15 minutes at room temperature, protected from light. After another washing step, we stained the iPSC-CMs with Troponin T-antibody conjugated with Alexa Fluor 647 (565744, 1:200, BD Pharmingen) for 1 hour on ice. After a final washing step with FACS buffer, cells were transferred to FACS tubes with cell strainer caps. Flow cytometry analysis was performed using BD-LSR II flow cytometer (BD Biosciences) with 10,000 events recorded. Single-stained UltraComp eBeads (Thermo Fisher Scientific, Carlsbad, CA) and unstained UltraComp eBeads were used for compensation, along with fixed cells stained with Zombie NIR™ fixable viability dye (as NIR™ positive control) were used to perform compensation. FMO controls, where iPSC-CMs are only stained for one of the fluorophores tested, were also used to ensure proper gate placement. FlowJo software (FlowJo, LLC) was used to process the data. Gating strategy employed excluded debris, doublets and dead cells, so that only live cells were used in Troponin T quantification.

Immunocytochemistry was performed on iPSC-CMs post purification by seeding 10,000 iPSC-CMs to each well of a Matrigel-coated 4 well chamber slides. The cells were allowed to recover after replating for approximately one week before they were fixed and permeabilized for immunocytochemistry as described previously. We used FITC-conjugated Troponin T antibody (130-106-687, 1:200, Miltenyi Biotec Inc). The mounted slides were imaged using Olympus FV3000 confocal laser scanning microscope at 40X magnification.

4.2.7. Molecular studies on patient-specific iPSC- derived cardiomyocytes (iPSC-CMs)

Total RNA was extracted from purified iPSC-CMs using RNeasy Mini Kit (Qiagen, Valencia, CA) and cDNA synthesized using the QuantiTect® Reverse Transcription kit (Qiagen, Valencia, CA). RNA extraction and cDNA synthesis on patient and control iPSC-CMs were performed as described previously. cDNAs were amplified using primers amplifying *LMNA* exons 1-4 and 10-11 [16]. The resulting PCR products were resolved using agarose gel electrophoresis and visualized using Universal Hood II Gel Doc (Bio-Rad Laboratories, Irvine, CA) and sent for Sanger sequencing at Elim Biopharmaceuticals (Hayward, CA). Sanger sequencing results were analyzed using DNA Sequencher version 4.10.1 (Gene Codes, Ann Arbor, MI).

4.2.8. Protein studies on iPSC-CMs

Patient and control cardiomyocytes were harvested as previously described and lysed using cold RIPA buffer (Sigma Aldrich) supplemented with protease inhibitors cocktail (Sigma Aldrich). At least $5x10^6$ cardiomyocytes were resuspended with 0.5 ml

RIPA buffer and incubated for 5 minutes on ice. Afterwards, the lysate was centrifuged at 4 ^{o}C for 10 minutes, 10,000 g. The protein concentration was quantified using Pierce™ BCA protein assay kit (Thermo Fisher Scientific, Carlsbad, CA). 30 ug of total protein lysate along with protein ladder were run on a Bolt™ 4-12% Bis-Tris Plus Gels (Thermo Fisher Scientific, Carlsbad, CA) under denaturing conditions followed by wet transfer and stained with 1X TBST + 3% BSA and incubate the membrane with primary antibody N-terminus Lamin A/C antibody (sc-376248, 1:400, Santa Cruz Biotechnology) at 4 ^{o}C overnight. β-actin (PIMA515739, 1:1000, Thermo Fisher Scientific) was used as loading control. The next day, the membrane was stained with goat anti mouse IgG secondary antibody conjugated to HRP (ab205719, 1:5000, Abcam) for one hour at room temperature. The presence of Lamin A and Lamin C in each sample were detected using chemiluminescence reaction using ECL Western Blotting Substrate Kit (ab65623, Abcam). Protein visualization was performed using the ImageLab software (Bio-Rad) and relative quantification of protein bands was performed using ImageJ.

4.2.9. Single cell-RNA sequencing (scRNA-seq) on patient and control iPSC-CMs

iPSC-CMs were harvested on days 0, 2, 4, 9, 16 and 19 of differentiation to evaluate differences in gene expression during significant time points of the differentiation process. Although iPSC-CMs at days 16 and 19 were generated using a different cardiomyocyte differentiation protocol, we found that both protocols produced the same cell subpopulations with similar gene expression profiles (Supplementary Data, Figure IV.S8). Since both protocols are capable to produce the same cell types, we find it justified to use iPSC-CMs produced by the commercial kit at later time points as a continuation of iPSC-CMs

produced by Wnt signaling modulation at the earlier time points. Single cell suspensions from each time points were harvested as described previously [40] and subjected to scRNA-seq using the 10X Chromium platform [41]. Prior to performing deep sequencing, we performed multiplexed shallow single cell RNA-sequencing to determine the approximate number of cells in each library. Data analysis was conducted in collaboration with UCI Center for Complex Biological Systems. The CellRanger pipeline (version 3.0.2, 10X Genomics, Pleasanton, CA) was used to process, count and align scRNA-seq data to the GRCh38 reference genome (https://www.ncbi.nlm.nih.gov/assembly/GCF_000001405.26/).

The output gene-barcode matrix files were then used for downstream analysis which included clustering cells based on similarly expressed genes and generating a list of differentially expressed genes between the clusters or samples (FDR-adjusted p-value ≤ 0.05) using Seurat version 3.1.4 . Briefly, we performed quality control of the sequencing data by excluding cells with more than 25% mitochondrial DNA content and cells with less than 200 expressed genes (Supplementary Data, Figure IV.S7). Next, we merged respective libraries from the same time points and performed cell cycle scoring to circumvent the confounding factor of cell cycle heterogeneity in our downstream analysis.

Since we aimed to examine the differentiation processes, it was imperative that we retain actively cycling cells in the dataset as progenitor cells would be actively proliferating. To that purpose, we subtracted the difference between the S and G2M scores (CC difference). By doing so we retained actively proliferating cells in our dataset and reduce the confounding variables in the dataset. Then, we performed normalization of gene expression using sctransform by regressing out percent mitochondria and CC difference

[42]. Dimensionality reduction and cell population grouping based on similarity in gene expression were then performed as described previously [42, 43].

Next, we sought to determine differences in gene expression between C1 and P1 iPSC-CMs at each designated time points during the differentiation process. By using the FindMarkers function included in Seurat to perform differential expression testing based on the non-parametric Wilcoxon rank sum test [43], we obtained differentially expressed genes (DEGs) between samples at each time points. We also performed differential expression testing on specific cardiogenic progenitor cell subtypes identified in the datasets by taking advantage of the subset function provided by Seurat and previous knowledge on cardiac development. Finally, we performed Ingenuity Pathway Analysis (Qiagen, Valencia, CA) on a pre-filtered set of DEGs (average log fold change value $\pm$ 1.5, FDR-adjusted p-value $\leq$ 0.05) to identify signaling pathways and biological processes that were significantly overrepresented in each sample to infer which biological processes were affected by the *LMNA* mutation.

4.3. Results

4.3.1. Generation of control and patient-specific induced pluripotent stem cells (iPSCs)

iPSCs characterization studies were performed to establish that iPSCs generated from control and patient fibroblasts were pluripotent (Figure IV.2). Based on positive staining for established pluripotency markers (Oct4, Sox2, SSEA-4 and Tra 1-60) and presence of Yamanaka factors determined by RT-qPCR, the established iPSC lines are pluripotent (Figure IV.2B, IV.2C). Here, we did not observe any significant differences in the levels of pluripotency genes indicating that the novel *LMNA* splice-site mutation exerted no

effect in the reprogramming process. In addition to measuring pluripotency gene expression, we also performed embryoid body (EB)-mediated differentiation to assess the ability of each iPSC line to generate three germ layers *in-vitro* (Figure IV.2D). Additionally, karyotyping studies showed that control-derived and patient-derived iPSC lines were devoid of chromosomal aberrations (Figure IV.2E). Taken together these results showed that both patient-derived and control-derived iPSCs are pluripotent, karyotypically normal and were suitable for further disease modeling studies.

4.3.2. Generation and characterization of iPSC-derived cardiomyocytes (iPSC-CMs)

Table IV.2. iPS cell line pairs and their cardiomyocytes differentiation efficiencies (N = 6).

iPSC	Source	Genotype[a]	Sex	Age at Skin Biopsy (years)	Differentiation efficiency (% cTNT + cells)[b]
1. PATIENT-1 (P1)	Patient A1	+/-	F	38	85
2. PATIENT-2 (P2)	Patient A2	+/-	M	62	55
3. PATIENT-3 (P3)	Patient A3	+/-	F	70	18
4. CONTROL-1 (C1)	Control A1	+/+	F	49	67
5. CONTROL-2 (C2)	Donor 3	+/+	M	48	59
6. CONTROL-3 (C3)	Control A3	+/+	F	68	60

[a]Genotype: +/+ homozygous normal; +/- heterozygous *LMNA* mutation.
[b]Mean differentiation efficieny ± SD of CONTROL (62.4 ± 4.4) versus PATIENT (52.7 ± 33.6) is not significantly different ($p > 0.05$, t-test).

Using the previously described protocol, we successfully differentiated three control iPSC lines and three patient iPSC lines, albeit with varying differentiation efficiencies. We performed immunocytochemistry staining to detect the presence of Troponin T (Figure IV.3B) as well as flow cytometry to quantify the differentiation efficiencies of each lines (Figure IV.3C, Table IV.2, Supplementary Figure IV.S2).

4.3.3. Molecular and protein studies on iPSC-CMs revealed monoallelic expression of wild-type LMNA allele and Lamin A/C haploinsufficiency

Molecular studies on iPSC-CMs were conducted to assess the impact of *LMNA* mutation. Sanger sequencing of *LMNA* exons 1-4 and 10-11 was conducted on three control iPSC-CMs and three patient iPSC-CM lines to determine whether the predicted exon skipping occurred in patient iPSC-CMs. Our Sanger sequencing data revealed that the 5' end of exon 2 remained intact for both patient and control (Figure IV.4A).

To further confirm the monoallelic expression of wild-type *LMNA* allele, we sequenced *LMNA* cDNA at exons 10-11 and the *LMNA* gDNA at the same locus (Figure IV.4B, left panel). At *LMNA* gDNA exon 10, we have previously described a single nucleotide polymorphism (SNP) that occurred exclusively in patient samples and was in *cis* with the mutant allele [16]. Both alleles were expressed at gDNA level, and as such if both wild-type and mutant alleles were expressed, we would observe two peaks in the Sanger chromatogram at locus rs4641. However, if only the wild-type allele was transcribed only one peak should be observed at the same location when sequenced. Our results showed that at the specified region, only one peak was present (Figure IV.4B, right panel), signifying the monoallelic transcription of the wild-type *LMNA* allele in patient iPSC-CMs.

Next, to assess the effect of the splice site mutation at the protein level and to investigate whether the mutant allele is translated, Western Blot was performed on protein lysate collected from two patient and two control iPSC-CMs at day 16 of differentiation. Our data showed that there was a reduction in the amount of full length Lamin A/C protein in patient iPSC-CMs, compared to control iPSC-CMs (Figures IV.4C, IV.4D). In addition, WB

analysis did not detect the predicted mutant Lamin A/C protein further demonstrating that the mutant *LMNA* allele was not translated.

4.3.4. Differential gene expression analysis revealed delayed activation of cardiogenic transcription factors in patient iPSC-CMs

To further elucidate on the molecular mechanisms of *LMNA* splice-site mutation, we conducted scRNA-seq experiments on one patient (P1) and one control (C1) iPSC-CMs on significant time points of the differentiation process (Figure IV.5B). In total, we performed scRNA-seq on 100,094 cells across two biological samples (one control and one patient), with an average read depth of 42,063 reads per cell and 3,949 genes detected per cell (Supplementary Data, Table IV.S3).

The heart development process was initiated by the formation of the primitive streak, which in turn give rise to the mesoderm and endoderm lineages of the three germ layers. Among genes that signified the transition of undifferentiated cells (*POU5F1+*) to differentiated cells of the primitive streak was Brachyury (*TBXT*). Next, the expression of *MESP1* was induced in these cells, signifying their commitment to enter the cardiac mesoderm stage [44]. These cardiac mesoderm cells in turn will give rise to cardiac progenitor cells (CPCs) by upregulating the expression of *ISL1* and *NKX2-5* [45, 46].

Later during differentiation, these CPCs gave rise to the first heart field progenitor cells (FHF), expressing genes such as *HAND1* and *NKX2-5*, and second heart field (SHF) progenitor cells expressing genes such as *HAND2*, *NKX2-5*, and *TBX1*. FHF cells contribute to the formation the cardiac crescent, heart tube and the left ventricle of the heart [47], while the SHF cells have been shown to give rise to the outflow tract, right ventricle, and

the left and right atriums [48]. Using these genes and developmental timeline as our guide, we sought to uncover whether the canonical differentiation processes were disrupted or unaffected by the novel *LMNA* splice-site mutation.

Dimensionality reduction and cell clustering allowed us to classify the cells based on their gene expression profiles and how it changes during the differentiation process (Figure IV.5 B,C). We observed the expression of pluripotency gene Oct4 (*POU5F1*) on day 0 (d0), and genes that marked the presence of mesoderm cells such as *MESP1* on day 2 (d2). On day 4 (d4), the presence of *HAND1*, marker genes for cardiac commitment and differentiation, became prevalent and starting from day 9 (d9) and onwards to day 16 (d16) and 19 (d19) of differentiation we detected the expression of the sarcomeric protein Troponin T (*TNNT2*).

Next, we performed differential gene expression testing to identify genes that are significantly differentially expressed between C1 and P1 iPSC-CMs during each time points of the differentiation (Figure IV.6B,C). At day 0, we found that there was no difference in the expression of pluripotency genes Oct4 (*POU5F1*) and *SOX2* (Figure IV.6B, day 0). At day 2, we managed to identify cell subpopulations with gene expression associated with the formation of mesendoderm cells. These cells expressed genes and transcription factors necessary proper mesendoderm differentiation such as *MIXL1, TBXT*, and *MESP1.* However, the expression of these genes is significantly lowered in P1 iPSC-CMs compared to C1 iPSC-CMs (Figure IV.6B, day 2).

At day 4, we found genes such as *HAND1*, a marker gene for cells of the first heart field, *TMEM88*, a Wnt/β-catenin pathway suppressor known to be a regulator of cardiovascular progenitor cell specification as well as *PDGFRA,* a platelet derived growth

factor gene marking progenitor cells with dual potency of generating cardiac and skeletal myocytes and *KDR*, a cardiac progenitor cell surface marker to be upregulated in C1 iPSC-CMs, compared to P1 iPSC-CMs, indicating C1 iPSC-CMs progressed more readily from mesoderm formation to cardiac specification, than P1 iPSC-CMs (Figure IV.6B, day 4). Interestingly, we discovered that *MESP1*, the gene signifying cardiac mesoderm commitment, was upregulated in P1 iPSC-CMs at day 4, and *HAND1* expression in P1 iPSC-CMs becomes upregulated as the differentiation process continued (Figure IV.5E, middle panel). These observations suggested a delay in P1 iPSC-CMs in activating the genes necessary for cardiac mesoderm specification and cardiac differentiation.

Next, from day 9 to 19 we found a lower expression of *NKX2-5*, a cardiogenic transcription factor, in P1 iPSC-CMs (Figure IV.6B, day 9), while on days 16 and 19, P1 iPSC-CMs have persistently lower expression of Troponin T (*TNNT2*) (Figure IV.6B Day 16, Day 19). Additionally, the expression of this crucial sarcomere protein was downregulated in P1 iPSC-CMs as the cells progressed through the differentiation process (Figure IV.6C, right panel).

4.3.5. Lamin A/C haploinsufficiency is the primary molecular mechanism of the novel Lamin A/C splice-site mutation

Time course differentiation experiment enabled us to trace the expression of certain genes of interest, in particular the nuclear lamina protein genes *LMNA*, *LMNB1* and *LMNB2*. We performed *LMNA*, *LMNB1* and *LMNB2* differential gene expression testing on C1 and P1 iPSC-CMs starting from day 0 to day 19 of differentiation (Figure IV.7A). Here we found several interesting patterns of expression of the nuclear lamina genes. Starting with day 0,

we found that all nuclear lamina genes were expressed in both C1 and P1 iPSCs. These results were in line with previous studies showing Lamin A/C to be lowly expressed, yet detectable, in undifferentiated cells [26, 49-51]. Interestingly, we found a higher expression of Lamin B1 (*LMNB1*) in C1 (p-val = 1.55E-111), while P1 cells expressed higher Lamin A/C (*LMNA,* p-value = 2.02E-162) and Lamin B2 (*LMNB2*, p-value = 2.19E-11). Previous studies conducted in mouse embryonic stem cells (mESCs) showed that higher *LMNA* expression was associated with reduced reprogramming efficiency and lowered differentiation capabilities [50]. However, we have previously observed that the expression levels of pluripotency genes such as *POU5F1* and *SOX2* were not significantly different between C1 and P1 iPSCs, indicating no significant difference in stemness and pluripotency (Figure IV.6B, Day 0).

Next at day 2, we showed significant differences in Lamin A/C, Lamin B1 and Lamin B2 expression, with C1 iPSC-CMs having significantly higher expression of all nuclear lamina genes than P1 iPSC-CMs (Figure IV.7B). The trend observed at day 2 was the opposite as that observed in day 0. For P1 iPSC-CMs, Lamin A/C, Lamin B1 and Lamin B2 expression seemed to be downregulated as the cells entered the differentiation process, while for C1 cells the expression of nuclear lamina proteins were increasing. On day 4, we found Lamin A/C to be differentially expressed with C1 iPSC-CMs expressing significantly more *LMNA* compared to P1 iPSC-CMs (p-value = 3.44E-57). The same expression pattern can be observed at day nine and onwards to days sixteen and nineteen of differentiation for the expression of Lamin A/C (p-value < 0). On the other hand, the differences in Lamin B1 and Lamin B2 expression levels from day nine to nineteen of differentiation here was not statistically significant (p-value > 0.05).

LMNA gene expression level in P1 iPSC-CMs never reached that of C1 iPSC-CMs, indicating that delayed expression was unlikely to be the molecular mechanism of the mutation. Furthermore, combined with our molecular and protein data showing monoallelic expression of wild-type *LMNA* allele and Lamin A/C haploinsufficiency, we concluded that Lamin A/C haploinsufficiency to be the primary molecular mechanism of the novel Lamin A/C splice-site mutation.

4.3.6. scRNA-seq revealed cell subpopulation specific-Lamin A/C haploinsufficiency

One of the hallmarks of laminopathy is tissue-specificity. Laminopathies manifested primarily in mesoderm-derived tissues such as cardiac and skeletal muscles or adipose tissues. Our novel *LMNA* splice-site mutation had been found to only manifest symptoms in the heart, as patients bearing this mutation suffered only from cardiac diseases [16]. We sought to determine whether the Lamin A/C differential expression was restricted only to the mesoderm lineage or whether cells that differentiated to the ectoderm or endoderm lineages were also affected. By performing differential gene expression testing as described previously on ectoderm cells (*PAX6*+ cells) [52] and endoderm cells (*SOX17*+ cells) [53], we found that *LMNA* was not significantly differentially expressed in these lineages (p-value > 0.05), consistent with the tissue specificity observed in our patients (Figure IV.7C, upper panel).

We also expanded our differential gene expression analysis to other mesoderm-derived tissues such as mesenchymal stem cells (*ENG+*) [54], skeletal muscle cells (*MEF2C+*) [55] and smooth muscle cells (*TAGLN+*) [56]. In these lineages, we found Lamin A/C to be significantly differentially expressed (p-value < 0.05, Figure IV.7C, bottom panel).

We also investigated whether hematopoietic stem cells (*HHEX+* cells) [57], another cell type derived from the mesoderm lineage, exhibited Lamin A/C differential expression. Here we found that there was no significant difference in Lamin A/C gene expression in cells destined to form the circulatory system (p-value > 0.05). Our results are consistent with laminopathy phenotypes being observed in mesoderm-derived tissues, except the circulatory system, and highlighted how our patient-specific disease model managed to capture the full extent of the novel Lamin A/C splice-site mutation phenotype.

4.3.7. Pathway analysis revealed signaling pathways involved in impaired differentiation of patient cells

We performed pathway analysis using Ingenuity Pathway Analysis to elucidate signaling pathways and biological processes that were affected by the Lamin mutation. We leveraged the capability of scRNA-seq to identify specific cell subpopulation within a sample and focused our analysis on those cell subpopulation involved in cardiogenesis to mimic the differentiation trajectory of cells as they progressed from iPSCs (d0) to form the primitive streak and cardiac mesoderm cells (d2 and d4), then commitment to cardiac progenitor cells, which give rise to heart field cells (d4) and later fetal (embryonic) cardiomyocytes (d9). Using a list of differentially expressed genes (DEGs) from these cell subpopulations at the corresponding days, we determined the predicted activation or inhibition of signaling pathways in P1 cells, compared to C1, as well as biological process predicted to be affected by the mutation.

On day 0, when both P1 and C1 cells were pluripotent, we found oxidative phosphorylation to be activated in P1 cells. The activation of oxidative phosphorylation

was surprising to observe, as pluripotent cells conventionally prefer to utilize glycolysis for energy production. Conversely, in the primitive streak, cardiac mesoderm at days 2 and 4, cardiac progenitor and heart field cells, oxidative phosphorylation seemed to be inhibited, though it seemed to be activated once more in embryonic cardiomyocytes (Figure IV.8A). Additionally, EIF2 signaling pathway, crucial for protein synthesis, had similar activation/inhibition pattern with oxidative phosphorylation.

Next, as our focus was to determine any pathways that might play a role in disrupting P1 cells' capability for proper differentiation, we focus our analysis on pathways that were activated or inhibited during days 2 to 4 of differentiation. First, we found that the PTEN signaling pathway, crucial in regulating cell growth and promotion of apoptosis [58], was predicted to be activated during this differentiation time frame (Figure IV.8A). Additionally, we found HIPPO signaling pathway to be activated exclusively in the primitive streak population. This pathway has previously been found to inhibit cell proliferation, promote apoptosis, regulate fates of stem and progenitor cells, as well as limiting cell size [59].

Here, we also see a signaling pathway termed "Factors promoting cardiogenesis in vertebrates" to be inhibited (Figure IV.8A). These factors include BMP, FGF, Wnt agonists and Wnt antagonists growth factors that we previously found to be significantly downregulated in P1 cells. We also found the pathway regulating the promotion of epithelial to mesenchymal transition, necessary for the formation of outflow tract regions of the heart, to be inhibited in P1 cells on days 2 and 4. Furthermore, we found that the BMP signaling pathway, widely known as an important cardiogenic signaling pathway [60, 61], was inhibited in the primitive streak, cardiac mesoderm, cardiac progenitor and heart

field populations (Figure IV.8B), but activated in embryonic cardiac population, in contrast to the normal activation/inhibition pattern observed in normal cardiac differentiation process. From these observations, we might predict that the inhibition of BMP signaling pathway in P1 cells led to the lower number of primitive streak cells available to generate cardiac mesoderm cells necessary to give rise to cardiomyocytes.

Next, we wanted to elucidate signaling pathways that could contribute to the manifestation of laminopathy due to Lamin A/C haploinsufficiency. For that, we focused our analysis on the embryonic cardiomyocyte (d9) population. Here, we saw signaling pathways involved in DNA damage repair and cell death, such as the nucleotide excision repair (NER) pathway, Death receptor signaling pathway and Senescence pathway to be activated. Additionally, we discovered that the cardiac hypertrophy signaling pathway, crucial for increasing cardiomyocyte size during growth and development or in response to pathological conditions, was activated. Among these activated signaling pathways, we found Lamin A/C (*LMNA*) to be involved in the Death receptor signaling pathway (Figure IV.7C). The downregulation of *LMNA* found in our dataset is predicted to result in membrane blebbing and cell shrinkage, which eventually led to apoptosis.

Next we seek to determine the biological processes affected by the splice-site Lamin A/C mutation. Here we see that on day 2, terms associated with cell and organism deaths, such as “Organismal death” and “Morbidity” to be activated (z-score > 2), while terms associated with cell differentiation such as “Cardiogenesis”, “Development of Body Axis”, and “Mesoderm Development” to be inhibited (z-score < -2) (Figure IV.8D). IPA also enabled us to predict diseases that could manifest based on the pattern of gene expression in our dataset (Figure IV.8E). Here, based on the gene expression patterns on day 2 and day

4, the occurrence of "congenital heart disease" and "atrial/ventricular septal defect" was predicted to increase. We also saw a predicted occurrence of "cardiomyocyte apoptosis", "cell death of heart cells", and "apoptosis of heart cells". Next, on day 9 we see that left ventricular dysfunction was predicted to occur in P1, consistent with one of the symptoms we observed in our patient.

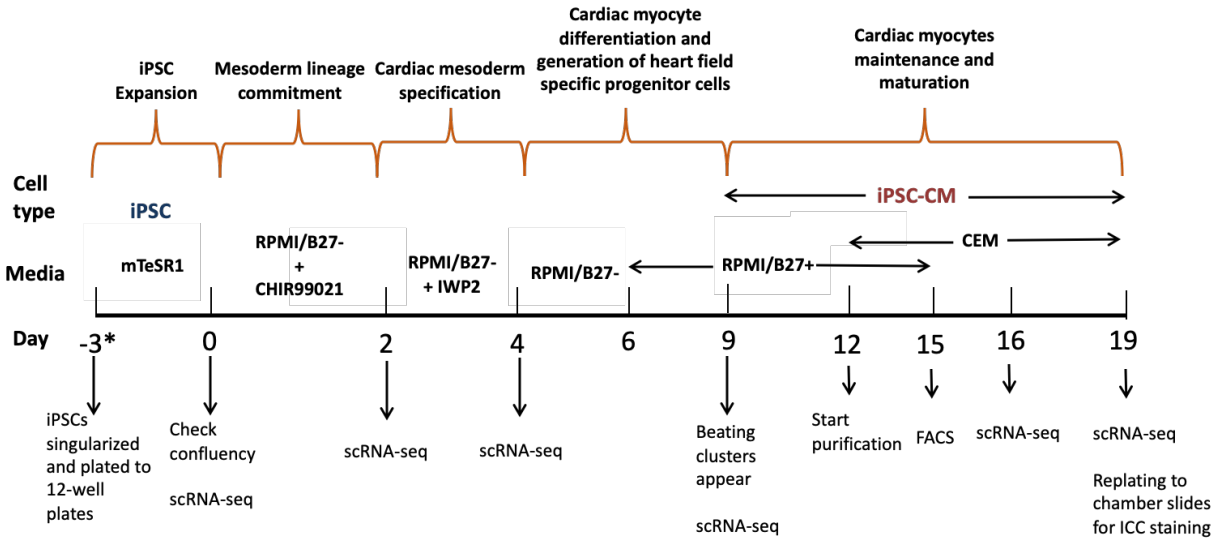

Figure IV.1: Generation of iPSC-derived cardiomyocytes (iPSC-CMs) by Wnt signaling modulation. iPSC lines were seeded at their optimal seeding density to 12-well plates coated with Matrigel. Seventy-two hours later, or when 95% confluency was achieved cardiomyocyte differentiation was initiated by changing iPSC maintenance media with RPMI 1640 supplemented with B-27 supplement without insulin and CHIR99201, a GSK3β inhibitor, to activate the Wnt signaling pathway. Forty-eight hours later, Wnt activation was inhibited by IWP2 addition to initiate cardiac mesoderm specification. Periodic media changes were conducted until days 8 to 10 of differentiation when beating clusters could be observed. On day 12, lactate purification to eliminate non-cardiomyocyte cells was conducted until day 19 when cells are replated to a new 12-well plate and 4-well chamber slides for immunocytochemistry staining. Flow cytometry to quantify Troponin T expression was performed at day 15 on non-lactate purified iPSC-CMs. Additionally, we harvested single cell suspensions at the indicated time points.

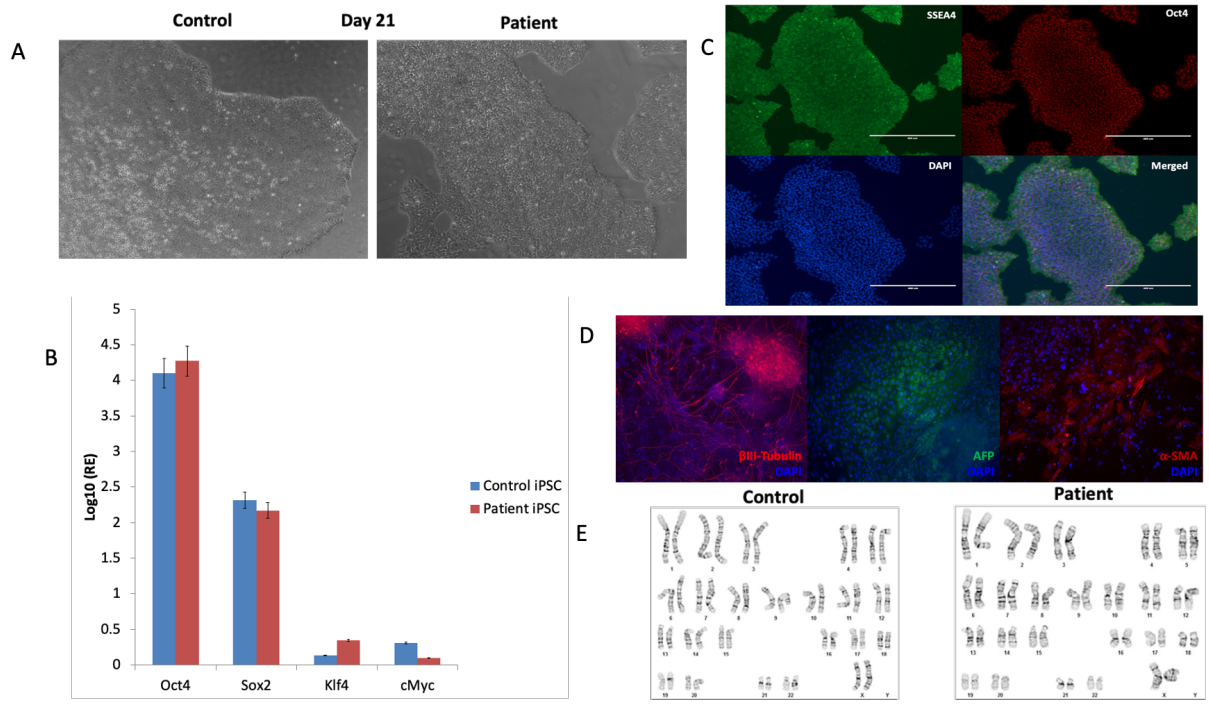

Figure IV.2: Generation and characterization of patient-specific induced pluripotent stem cells (iPSCs). (A) Dermal fibroblast from patient and commercially obtained line were transduced with Sendai virus carrying the Yamanaka factors. Emerging colonies were manually picked and replated on Matrigel. There was no morphological difference between patient and control iPSC. Images taken at 4x magnification. (B) Real-time PCR assay on patient-iPSC line clones (Control iPSC C1 clone 5, and P1 iPSC clone 1) at p15 measuring expression levels of endogenous pluripotency genes. There was no significant difference in the relative expression level of pluripotent genes between patient and control. N = 2, $p > 0.05$, Error bars ± S.E.M. (C) Representative images of immunocytochemistry staining for pluripotent stem cell markers. Scale bar = 400 μm. (D) Representative images of differentiated cells positive for beta-tubulin (ectoderm), alpha-fetoprotein (endoderm) and alpha smooth muscle actin (mesoderm). Nuclei stained with DAPI. Images taken at 10x magnification. (E) Karyograms from patient and control iPSCs indicate normal karyotype (46, XX).

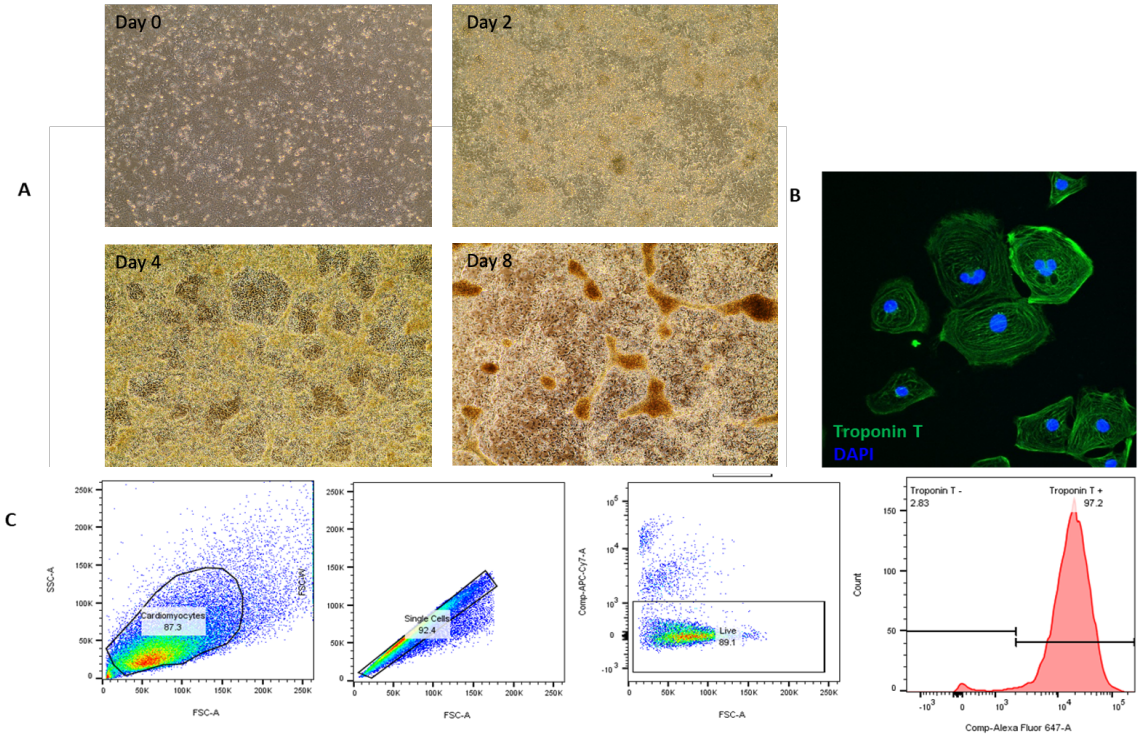

Figure IV.3: Generation and characterization of iPSC-derived cardiomyocytes. **(**A) Brightfield images of C1 clone 14 iPSC-CMs during differentiation traced from day 0, 2, 4 and 8 of differentiation. Images taken at 10X magnification. (B) Immunocytochemistry staining performed on P1 clone 1 iPSC-CMs for cardiac-specific cell marker Troponin T (green) and DAPI (blue). Image was taken at 40X magnification (C) Representative dot plots from flow cytometry. Gating strategy excluded doublets and dead cells.

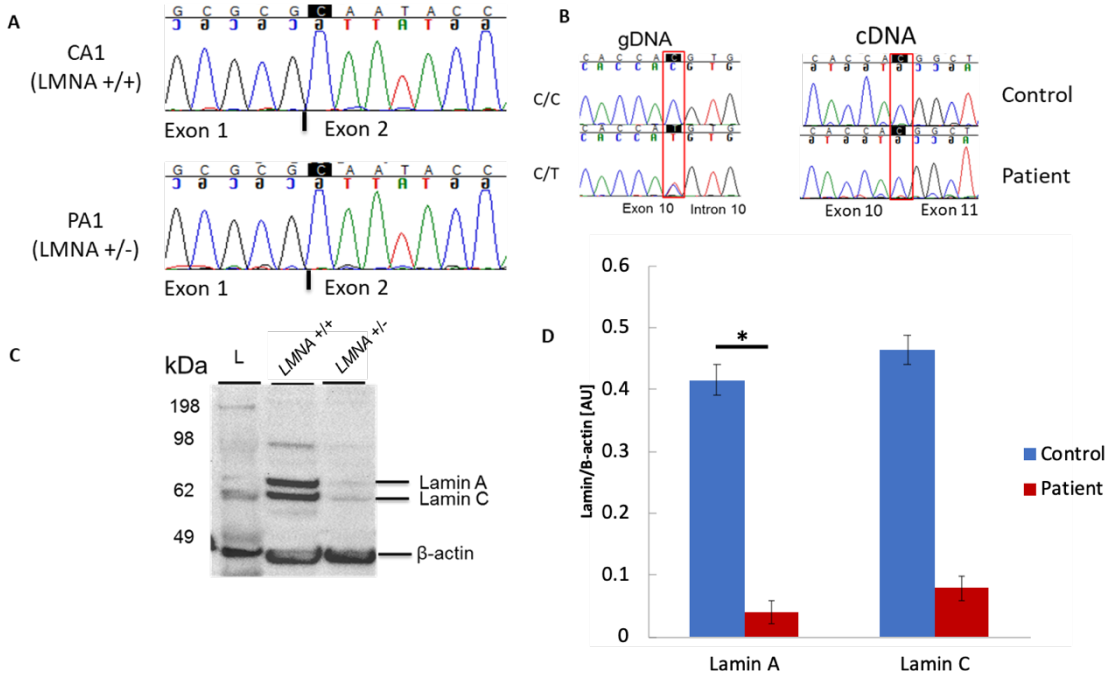

Figure IV.4: Molecular and protein studies revealed monoallelic expression of WT *LMNA* allele and Lamin A/C haploinsufficiency (A) Sanger sequencing chromatogram of *LMNA* exons 1-4 shows intact exon 2. (B) Sanger sequencing performed at exon 10-11 confirms monoallelic expression of wild-type LMNA allele. All chromatograms shown are from C1 clone 14 iPSC-CMs and P1 clone 1 iPSC-CMs (C) Western blot for Lamin A/C protein from C1 clone 14, D3 clone 14 , P1 clone 1 and PA2 clone 13. β-actin was used as loading control. (D) Relative quantification of Lamin A/C bands relative to β-Actin (N = 2, * : $p < 0.05$, error bar = SEM).

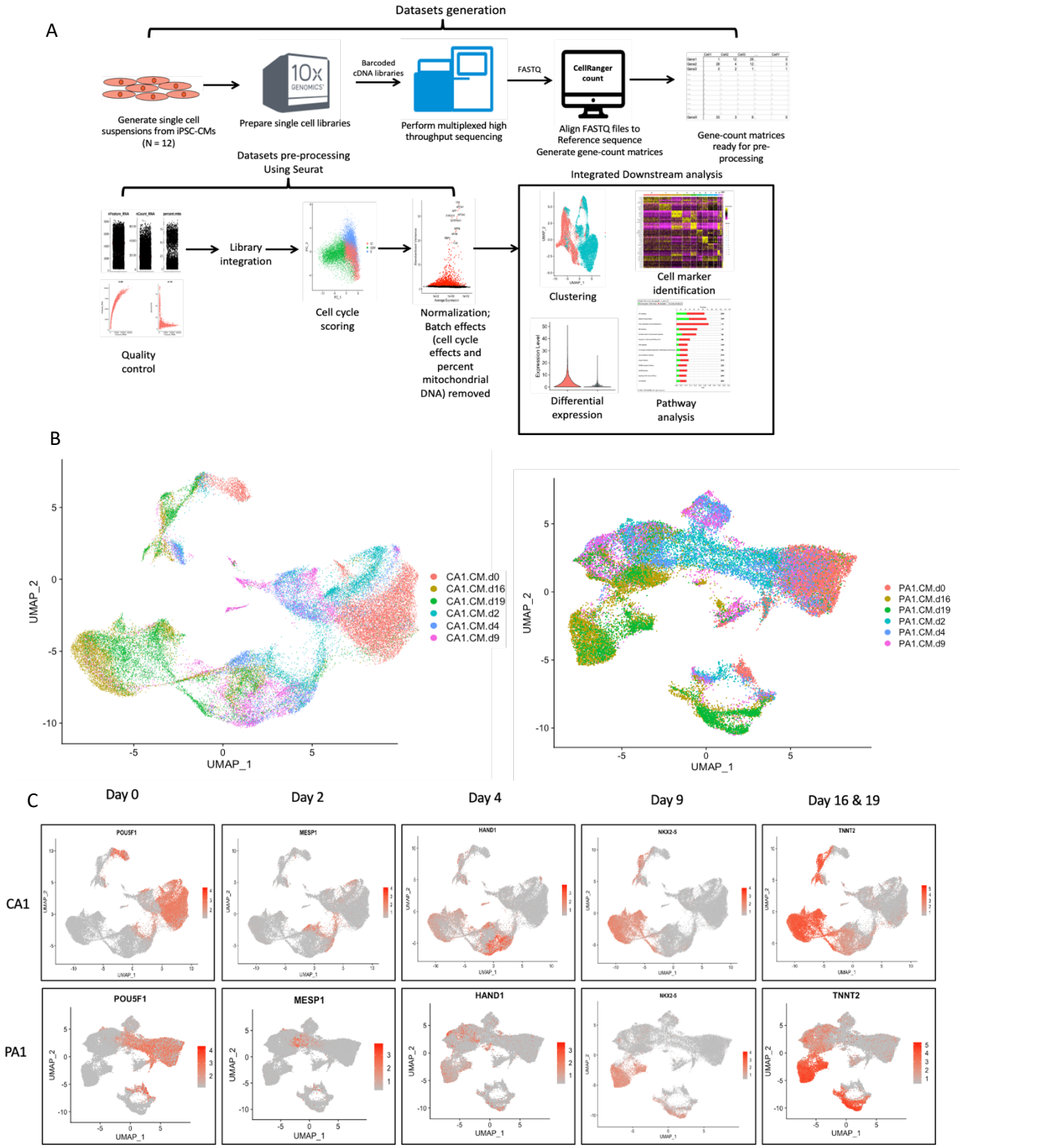

Figure IV.5: Single cell RNA-sequencing studies of cardiomyocyte differentiation (A) Schematic of scRNA-seq workflow showing procedures performed to generate gene-count matrices used as raw data in the gene expression study, the raw data pre-processing steps include quality control to exclude dead cells and cells with low gene expression (nFeature_RNA < 200), library integration, cell cycle scoring and normalization to remove batch effects prior to conducting downstream analysis. (B) UMAP plots showing control (C1 clone 14, left panel) and patient cells (P1 clone 1, right panel) as it transitioned from pluripotent cells (d0), mesendoderm cells (d2), cardiac mesoderm (d4) to immature beating cardiomyocytes (d9) to committed cardiomyocytes (d16 and d19). (C) Cells from both C1 and P1 expressed the appropriate transcription factors and at the appropriate time during differentiation.

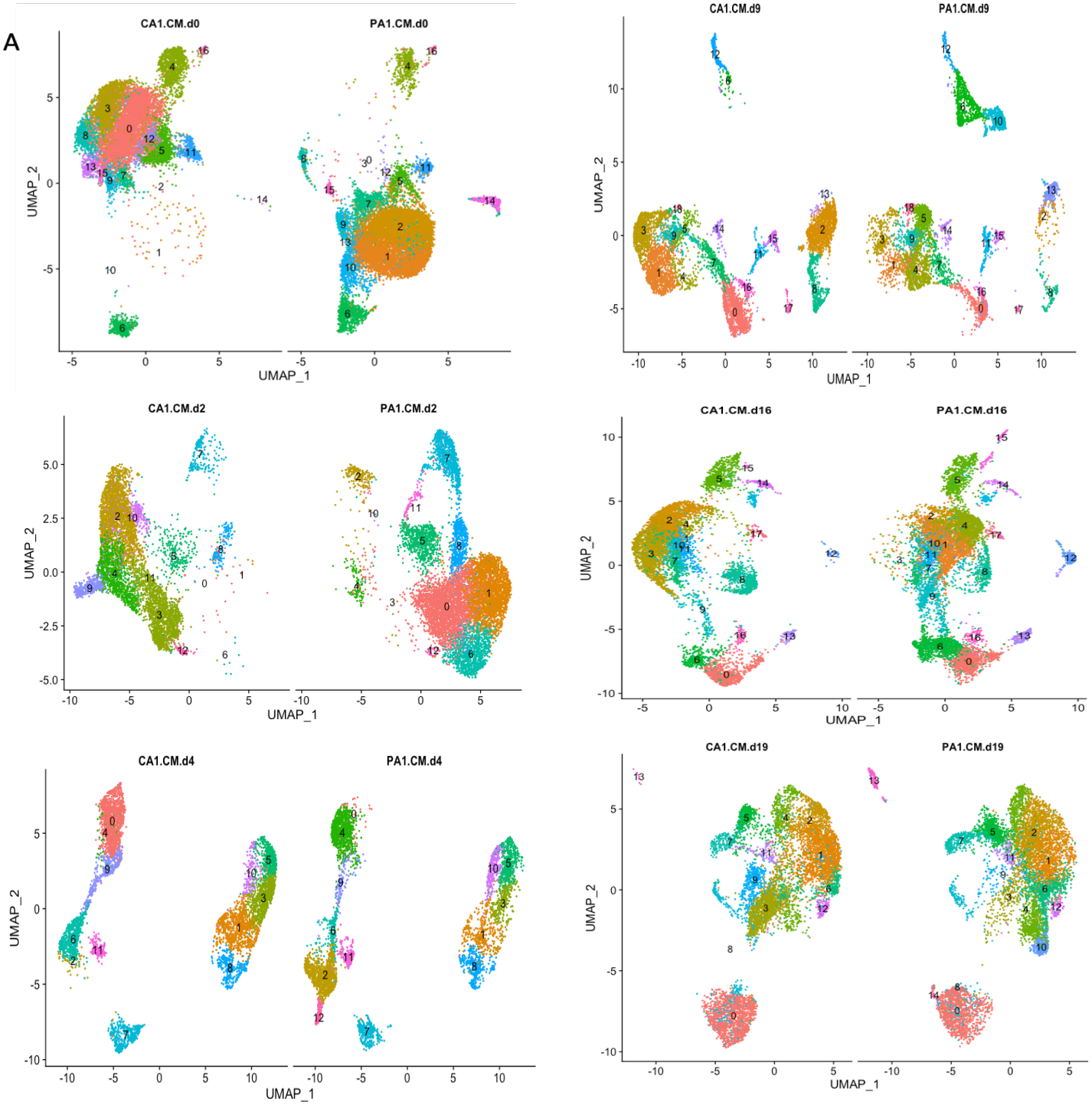
A
CA1.CM.d0
PA1.CM.d0
CA1.CM.d9
PA1.CM.d9
CA1.CM.d2
PA1.CM.d2
CA1.CM.d16
PA1.CM.d16
CA1.CM.d4
PA1.CM.d4
CA1.CM.d19
PA1.CM.d19
UMAP_1
UMAP_2

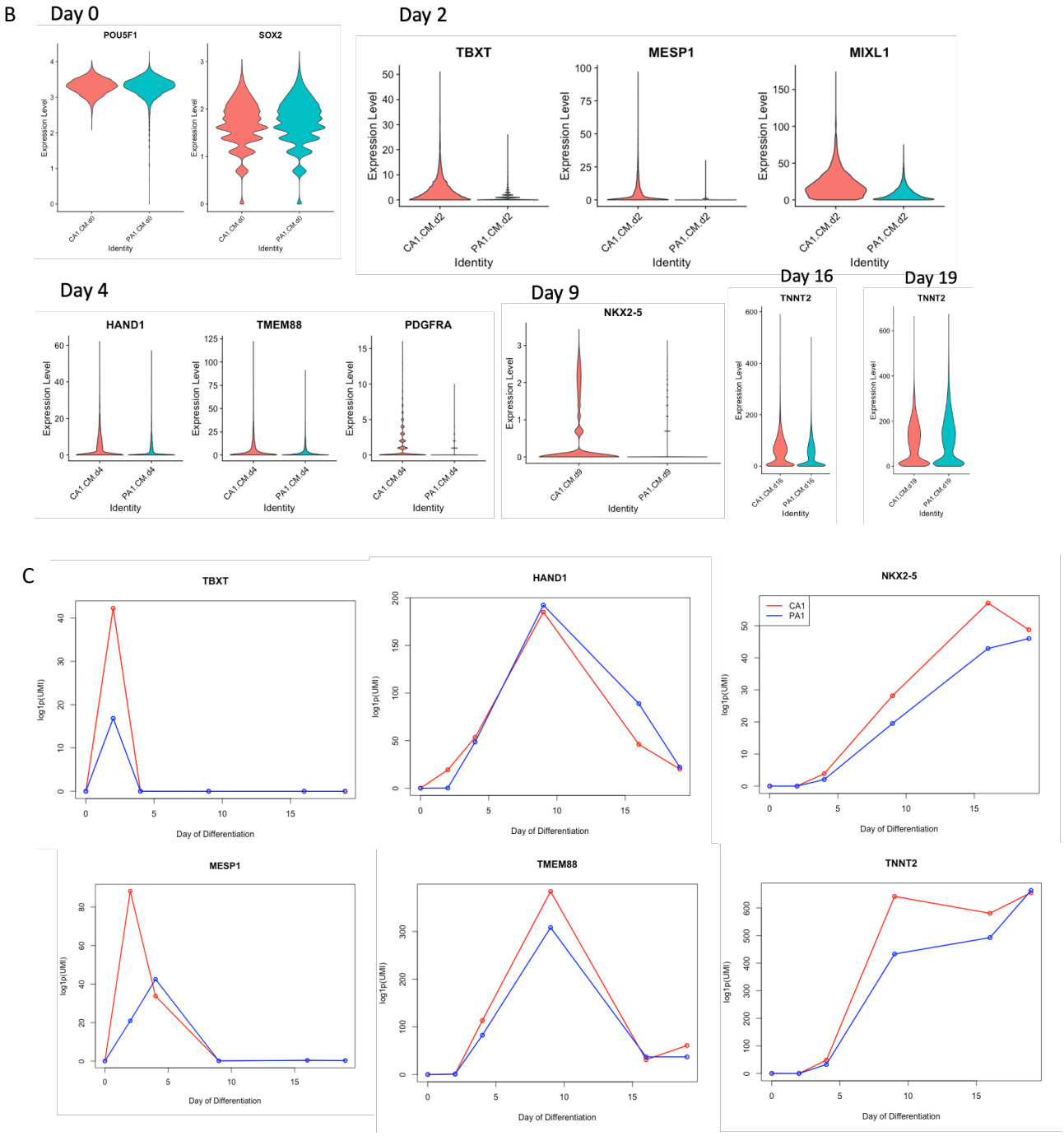

Figure IV.6: Single cell RNA-sequencing of cardiomyocyte differentiation showed lower expression of cardiogenic transcription factors (A) Dimensionality reduction and cell clustering analysis for all timepoints included in the study (B) Violin plots showing expression levels of pluripotency genes (*POU5F1, SOX2*), mesendoderm (*TBXT, MIXL1*), cardiac mesoderm (*MESP1*), primary heart field cells (*HAND1*), signaling regulator integral to cardiac differentiation (*TMEM88*), cell surface markers (*PDGFRA*), cardiogenic transcription factor (*NKX2-5*), and sarcomeric protein (*TNNT2*). (C) Line graphs showing proper temporal expression of mesendoderm transcription factors for C1 and P1 cells. Yet, P1 cells seem to have lower expression of mesendoderm transcription factors and delayed expression of *MESP1*, a cardiac mesoderm commitment marker.

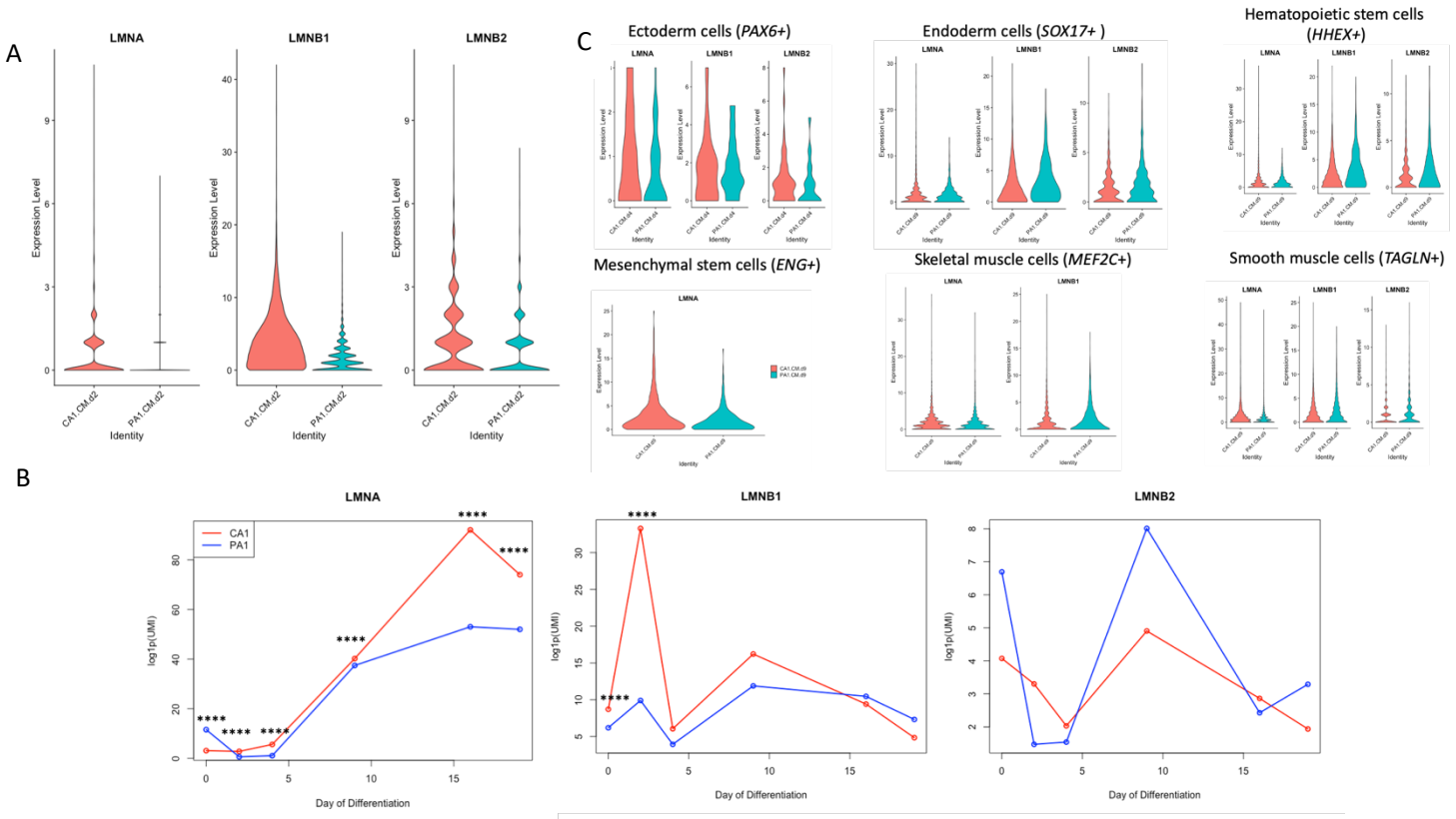

Figure IV.7: Lamin A/C haploinsufficiency is the primary molecular mechanism of the novel Lamin A/C splice-site mutation. (A) Representative violin plots showing differential expression of all nuclear lamina genes: Lamin A/C (*LMNA*), Lamin B1 (*LMNB1*) and Lamin B2 (*LMNB2*). (B) Nuclear lamins genes expression changed during differentiation process. Lamin A/C (*LMNA*) expression started with being higher in P1 cells at day 0. However, as differentiation progressed the level of *LMNA* gene expression stayed low compared to C1 cells. On the other hand, the differences in Lamin B1 and Lamin B2 expression levels were not statistically significant at later time points of the differentiation. Combined with molecular and protein data showing monoallelic expression of wild-type *LMNA* allele and Lamin A/C haploinsufficiency, Lamin A/C haploinsufficiency seems to be the primary molecular mechanism of the novel Lamin A/C splice-site mutation. (C) scRNA-seq revealed cell subpopulation specific-Lamin A/C haploinsufficiency. Differential gene expression testing on ectoderm cells (*PAX6*+ cells), endoderm cells (*SOX17*+ cells) and hematopoietic cells (*HHEX+* cells) found that *LMNA* was not significantly differentially expressed in these lineages (p-value > 0.05). On the other hand, in other mesoderm-derived tissues such as mesenchymal stem cells (*ENG+*), smooth muscle cells (*MEF2C+*) and skeletal muscle cells (*TAGLN+), LMNA* gene expression levels were significantly different (*ENG+* p-value = 0.03; *MEF2C+* p-value = 0.01; *TAGLN+* p-value: 6.90E-54).

A

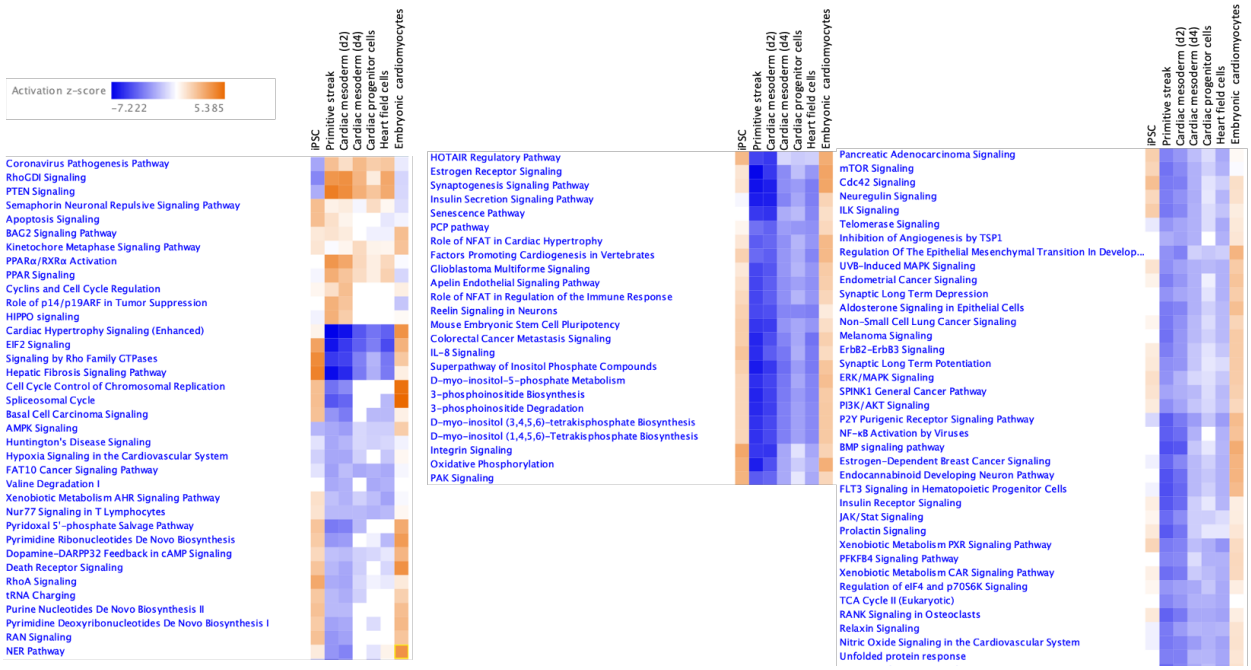
Activation z-score
-7.222
5.385
iPSC
Primitive streak
Cardiac mesoderm (d2)
Cardiac mesoderm (d4)
Cardiac progenitor cells
Heart field cells
Embryonic cardiomyocytes
Coronavirus Pathogenesis Pathway
RhoGDI Signaling
PTEN Signaling
Semaphorin Neuronal Repulsive Signaling Pathway
Apoptosis Signaling
BAG2 Signaling Pathway
Kinetochore Metaphase Signaling Pathway
PPARα/RXRα Activation
PPAR Signaling
Cyclins and Cell Cycle Regulation
Role of p14/p19ARF in Tumor Suppression
HIPPO signaling
Cardiac Hypertrophy Signaling (Enhanced)
EIF2 Signaling
Signaling by Rho Family GTPases
Hepatic Fibrosis Signaling Pathway
Cell Cycle Control of Chromosomal Replication
Spliceosomal Cycle
Basal Cell Carcinoma Signaling
AMPK Signaling
Huntington's Disease Signaling
Hypoxia Signaling in the Cardiovascular System
FAT10 Cancer Signaling Pathway
Valine Degradation I
Xenobiotic Metabolism AHR Signaling Pathway
Nur77 Signaling in T Lymphocytes
Pyridoxal 5'-phosphate Salvage Pathway
Pyrimidine Ribonucleotides De Novo Biosynthesis
Dopamine-DARPP32 Feedback in cAMP Signaling
Death Receptor Signaling
RhoA Signaling
tRNA Charging
Purine Nucleotides De Novo Biosynthesis II
Pyrimidine Deoxyribonucleotides De Novo Biosynthesis I
RAN Signaling
NER Pathway
HOTAIR Regulatory Pathway
Estrogen Receptor Signaling
Synaptogenesis Signaling Pathway
Insulin Secretion Signaling Pathway
Senescence Pathway
PCP pathway
Role of NFAT in Cardiac Hypertrophy
Factors Promoting Cardiogenesis in Vertebrates
Glioblastoma Multiforme Signaling
Apelin Endothelial Signaling Pathway
Role of NFAT in Regulation of the Immune Response
Reelin Signaling in Neurons
Mouse Embryonic Stem Cell Pluripotency
Colorectal Cancer Metastasis Signaling
IL-8 Signaling
Superpathway of Inositol Phosphate Compounds
D-myo-inositol-5-phosphate Metabolism
3-phosphoinositide Biosynthesis
3-phosphoinositide Degradation
D-myo-inositol (3,4,5,6)-tetrakisphosphate Biosynthesis
D-myo-inositol (1,4,5,6)-Tetrakisphosphate Biosynthesis
Integrin Signaling
Oxidative Phosphorylation
PAK Signaling
Pancreatic Adenocarcinoma Signaling
mTOR Signaling
Cdc42 Signaling
Neuregulin Signaling
ILK Signaling
Telomerase Signaling
Inhibition of Angiogenesis by TSP1
Regulation Of The Epithelial Mesenchymal Transition In Develop...
UVB-Induced MAPK Signaling
Endometrial Cancer Signaling
Synaptic Long Term Depression
Aldosterone Signaling in Epithelial Cells
Non-Small Cell Lung Cancer Signaling
Melanoma Signaling
ErbB2-ErbB3 Signaling
Synaptic Long Term Potentiation
ERK/MAPK Signaling
SPINK1 General Cancer Pathway
PI3K/AKT Signaling
P2Y Purigenic Receptor Signaling Pathway
NF-κB Activation by Viruses
BMP signaling pathway
Estrogen-Dependent Breast Cancer Signaling
Endocannabinoid Developing Neuron Pathway
FLT3 Signaling in Hematopoietic Progenitor Cells
Insulin Receptor Signaling
JAK/Stat Signaling
Prolactin Signaling
Xenobiotic Metabolism PXR Signaling Pathway
PFKFB4 Signaling Pathway
Xenobiotic Metabolism CAR Signaling Pathway
Regulation of eIF4 and p70S6K Signaling
TCA Cycle II (Eukaryotic)
RANK Signaling in Osteoclasts
Relaxin Signaling
Nitric Oxide Signaling in the Cardiovascular System
Unfolded protein response

B

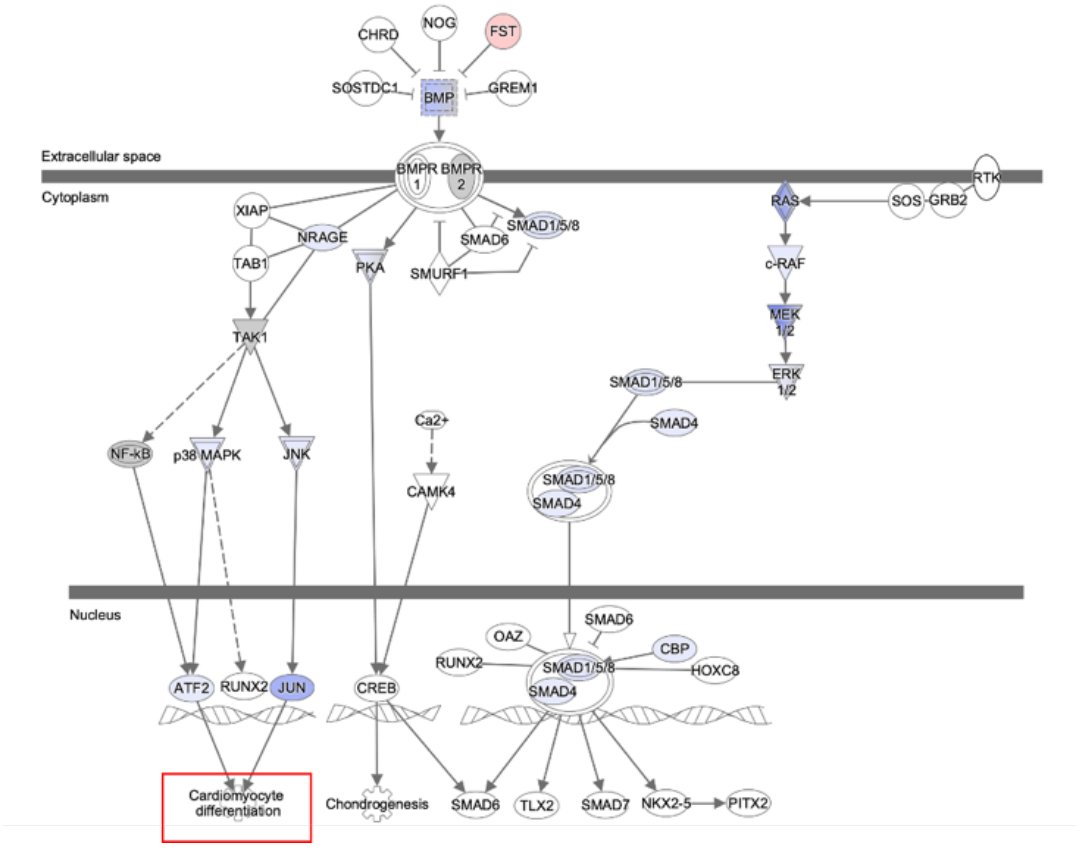
NOG
CHRD
FST
SOSTDC1
BMP
GREM1
Extracellular space
Cytoplasm
BMPR 1
BMPR 2
RTK
XIAP
NRAGE
SMAD1/5/8
SMAD6
TAB1
PKA
SMURF1
RAS
SOS
GRB2
c-RAF
MEK 1/2
ERK 1/2
TAK1
SMAD1/5/8
SMAD4
Ca2+
NF-kB
p38 MAPK
JNK
CAMK4
SMAD1/5/8
SMAD4
Nucleus
SMAD6
OAZ
CBP
RUNX2
SMAD1/5/8
HOXC8
SMAD4
ATF2
RUNX2
JUN
CREB
Cardiomyocyte differentiation
Chondrogenesis
SMAD6
TLX2
SMAD7
NKX2-5
PITX2

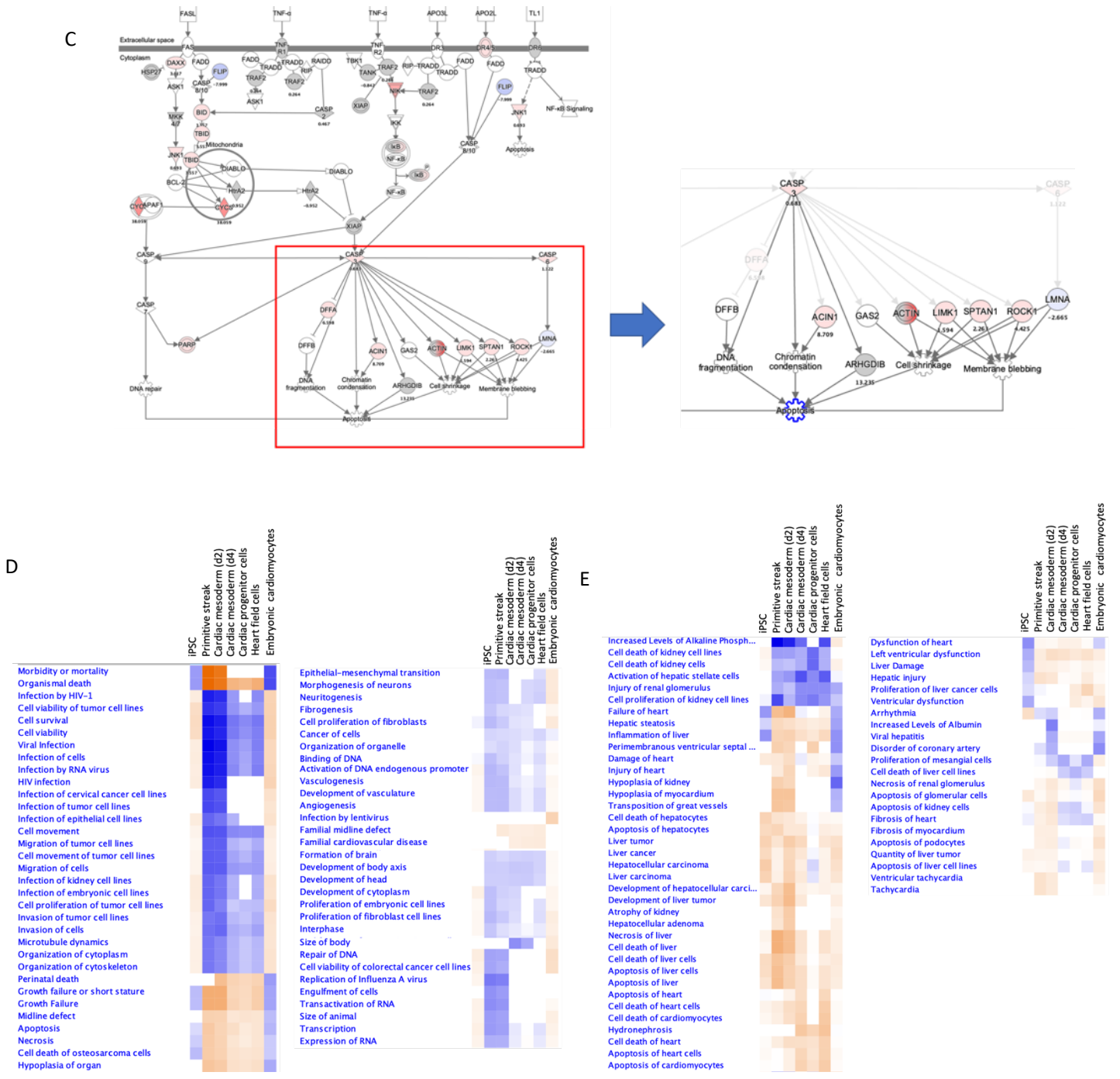

Figure IV.8: Ingenuity Pathway Analysis revealed significant signaling pathways and biological processes that are affected during the cardiac differentiation process. (A) Heatmap showing signaling pathways activated and inhibited in P1 iPSC-CMs, compared to C1 iPSC-CMs, as it progressed through the differentiation process. (B) Inhibition of BMP signaling pathway, not Wnt/β-catenin pathway, caused impaired cardiac differentiation in P1 iPSCs. (C) Lamin A/C haploinsufficiency may contribute to the pathology of laminopathy by activating the Death Receptor Signaling pathway, resulting in cell shrinkage and membrane blebbing, which leads to apoptosis. (D) Heatmap showing biological functions that are predicted to be activated and inhibited in P1 iPSC-CMs. Terms such as "Organismal death" and "Morbidity" are predicted to be activated during the early stages of differentiation, while processes associated with differentiation such as "Epithelial-mesenchymal transition", "Development of body axis" and "Neuritogenesis" was predicted to be inhibited. (E) Heatmap showing diseases predicted to arise on individual days of differentiation. Terms associated with cardiac diseases, such as "Congenital heart disease", "atrial or ventricular septal defect", and "ventricular septal defect" are predicted to be activated on day 2. Additionally, terms associated with cardiac cell survival such as "apoptosis of heart cells" and "apoptosis of cardiomyocytes" and "cell death of cardiomyocytes" are activated on day 4. On day 9, left ventricular dysfunction is also predicted to be activated in patient cells. Orange square, z-score > 2, activation predicted; blue square, z-score < -2, inhibition predicted.

4.4. Discussions

Here we reported the generation of a patient-specific iPSCs using fibroblasts collected from individuals bearing the novel *LMNA* splice-site mutation (*LMNA* c.357-2A>G) and related family controls without *LMNA* mutation and subsequent studies to establish Lamin-associated dilated cardiomyopathy disease model to enable *in-vitro* studies to elucidate on the molecular mechanisms of the mutation. Despite bearing the *LMNA* mutation, we found that there was no significant difference in expression levels of pluripotency genes expressed by patient iPSC-CMs, as shown using qPCR and scRNA-seq. Our findings are consistent with previous studies conducted on mouse embryonic stem cells (mESCs) bearing a heterozygous *Lmna* mutation ($Lmna^{+/-}$) that caused Lamin A/C haploinsufficiency. The authors showed that Lamin A/C haploinsufficiency had no effect on the pluripotency [26]. However, they did note a propensity for the mutant mESCs to differentiate towards the endoderm lineage and a downregulated potential to differentiate towards the myogenic lineage upon induction of embryoid body formation. At present, we cannot conclusively claim whether or not our iPSC lines are biased towards differentiating to certain germ layer lineages as we have not conducted any directed differentiation studies. The extent of our differentiation study was to induce iPSCs to form embryoid bodies, spontaneously differentiate them and stained the cells with antibodies for cell surface marker or transcription factor specific for each of three lineages generated. We found that all of the iPSC lines used in this study able to generate cells representing the ectoderm, endoderm and mesoderm lineages (Figure IV.2D, Supplemental Figure IV.S1). As we only seek to establish and confirm pluripotency of the reprogrammed cell lines, these qualitative studies were sufficient for us.

By modulating the activity of the canonical Wnt/β-catenin pathway in iPSCs using GSK3β inhibitor (CHIR99021) to activate the pathway and Wnt-ligand inhibitor (IWP2) to suppress the Wnt signaling pathway activity, we generated control and patient specific iPSC-CMs from the aforementioned iPSC lines. This method had been widely used by various groups and has consistently been shown to be highly effective in producing cardiomyocytes, based on quantification of Troponin T expressing cells (up to 98%) [36]. Our differentiation studies showed a range of differentiation efficiencies for our cell lines from 18 to 84%, lower compared to previously published differentiation efficiencies using the same protocol [36, 62, 63]. The age range at the time of biopsy for our iPSC lines were 38 to 70 years old.

When we compared the averages of differentiation efficiencies between control iPSCs with patient iPSCs, we found that there was no statistically significant difference (Student's t-test, $p > 0.05$), suggesting that there was no correlation between *LMNA* mutation and differentiation efficiencies. Based on our observations, younger lines tended to have a higher differentiation efficiency compared to older lines, which suggested age as the determinant of our group's iPSC functionality (Table IV.2). Still, we need to keep in mind that our observations here were gleaned from studying six iPSC lines and that the focus of our studies was to generate iPSC-CMs, not to determine factors that influenced differentiation efficiencies. Since other studies have shown that iPSCs generated from cells of varying donor sources, from embryonic to adult, have comparable differentiation efficiencies [64, 65] further studies still need to be conducted to definitively assert that donor age affect differentiation efficiency.

Despite the variance in differentiation efficiencies, we achieved the goal to generate iPSC-CMs to perform disease modeling of Lamin-associated dilated cardiomyopathy *in-vitro*. iPSC-CMs characterization studies showed that our cells formed beating syncytium *in-vitro* and expressed Troponin T based on flow cytometry quantification and immunocytochemistry studies (Figure IV.3B, C). Using the iPSC-CMs generated we performed molecular, protein and single cell RNA-sequencing studies to ascertain the molecular mechanism of the novel *LMNA* splice-site mutation and how it contributed to the disease pathology. We extracted RNA from iPSC-CMs and perform Sanger sequencing on the *LMNA* gene at exons 1-4 and 10-11 to determine the dominant transcript transcribed in our disease model and whether exon skipping, one of the predicted molecular mechanisms of the mutation, occurred. Previously we predicted that exon 2 would be excised out during mRNA processing due to the location of the mutation at the 3' splice site acceptor of intron 1 [16]. Additionally, we predicted that patient iPSC-CMs would have impaired nonsense mediated decay process, which leads to imperfect clearing of the mutant transcript that potentially could impair cellular functions leading to the disease [66]. Our sequencing results at *LMNA* exons 1-4 revealed that only the wild type *LMNA* transcript was present in both control and patient iPSC-CMs. When combined with sequencing results obtained from *LMNA* exons 10-11, we did not observe the predicted mutant *LMNA* transcript in patient iPSC-CMs which suggested monoallelic transcription of *LMNA* gene in patient iPSC-CMs. This observation suggested that only the wild-type *LMNA* allele was expressed in both patients as well as control iPSC-CMs. Combined with western blot studies performed on iPSC-CMs showing significantly lower Lamin A/C protein level in patient iPSC-CMs, we can conclude that the novel Lamin A/C splice-site mutation lead to the monoallelic expression

of *LMNA* transcripts, which in turn caused lower amount of Lamin A/C protein to be translated.

In our differentiation time-course study, we also observe a consistently lower expression of the *LMNA* gene in patient iPSC-CMs, once the cells started to differentiate. Until the last timepoint of the differentiation time-course, *LMNA* expression in patient iPSC-CMs was still significantly lower compared to control iPSC-CMs. Combined with our molecular and protein studies, these observations indicated that delayed *LMNA* expression seemed unlikely to be the molecular mechanisms of the mutation. Our results were consistent with previous iPSC based Lamin-associated cardiac disease modeling studies showing Lamin A/C haploinsufficiency as the primary molecular mechanism of the Lamin A/C mutation [18, 21, 67, 68]. Taken together with results from molecular studies, these observations suggested that Lamin A/C haploinsufficiency is the primary molecular mechanism of Lamin A/C splice site mutation.

The lower amount of Lamin A/C protein available to maintain normal cellular function leads to many dysfunctions related to dilated cardiomyopathy. Among the many dysfunctions that have been documented were nuclear blebbing [69-71], increased cell death [72], and abnormal gene expression [6, 73]. Our pathway analysis showed that pathways associated with apoptosis, senescence and DNA damage are predicted to be activated in patients, consistent with previous findings [74-76]. Coincidentally, we also see the cardiac hypertrophy signaling pathway to be activated in patients at day 9. This pathway is crucial in enlarging cardiomyocyte size and can be activated in response to stress or in response to growth factors to increase cardiomyocyte size to its functional size [77]. Potentially, the increased apoptotic rate and DNA damage sustained by the patient

cells led to lower number of cardiomyocytes available for a functional heart. The lower number of cardiomyocytes triggered the hypertrophic signaling pathway to enlarge the cell size, compensating for the low cell number and eventually giving rise to dilated cardiomyopathy.

Here, we focused our studies on how Lamin A/C mutation affect cellular differentiation in our disease model. By focusing on the early time points (days 0-9), we sought to elucidate the differences on the signaling pathways and biological processes and discover which pathways would contribute to the impaired differentiation we observed. We observed the activation of the oxidative phosphorylation pathway in our patient pluripotent stem cell population in contrast with previous studies showing that pluripotent stem cells preferentially utilize glycolysis for energy production [78-80]. As differentiation progressed, oxidative phosphorylation was shown to be inhibited in our differentiating patient cell samples, only becoming reactivated as the cells transitioned to become embryonic cardiomyocytes on day 9.

The transition from glycolysis to oxidative phosphorylation has been used as one of the hallmarks of cell differentiation, and it has been shown that cells that are incapable of changing its metabolic profile have impaired differentiation capability [81] and experienced a higher degree of cell death [79]. Notably, it has previously been shown that impaired mitochondrial electron transport chain activity in mouse ESCs results in attenuation of heart cell development [82]. Accordingly, Lamin A/C depletion in mesenchymal stem cells have previously been shown to cause accumulation of reactive oxygen species (ROS) and mitochondrial dysfunction, leading to increased oxidative stress and apoptosis [83].

Next, we also discover that the tumor suppressor PTEN signaling pathway, known to inhibit cell proliferation and division [84] was activated in the primitive streak, cardiac mesoderm, cardiac progenitor and heart field cell subpopulations. PTEN signaling pathway has been reported previously to induce apoptosis and cell cycle arrest [85, 86], suggesting that in these cardiogenic cell subpopulations there was a higher degree of cell death and cell cycle arrest in these population. Additionally, overexpression of *PTEN* has been shown to inhibit nuclear accumulation of β-catenin, necessary for transcriptional activation of Wnt-target genes via the TCF/LEF complex [87], some of which are genes involved in mesoderm/mesendoderm formation such as Brachyury (*TBXT*) [88, 89]. The activation of PTEN signaling pathway may have suppressed the activation of Wnt/β-catenin pathway, which led to the lower expression of Wnt target genes that were involved in cardiomyocyte differentiation, increased apoptosis and cell cycle arrest.

Other than the Wnt signaling pathway, the bone morphogenetic protein (BMP) pathway also play a role in heart development. The BMP pathway activation is necessary during the early time points of cardiac development to generate the proper and necessary cardiac progenitor cells, however its activity needs to be suppressed/downregulated for proper heart formation later on as the cardiac progenitors differentiate to cardiomyocytes [61, 90]. Here, we observed the predicted inhibition of BMP signaling pathway in the primitive streak, cardiac mesoderm, cardiac progenitor and heart field cells and the apparent activation of this pathway in the embryonic cardiomyocytes. The activity pattern we observed in our dataset is in contrast to previously established BMP signaling activity patterns necessary for proper heart formation. However, our results are in line with a previously published differentiation study conducted in Lamin-deficient myoblasts

showing downregulation of BMP pathway and an upregulation of the BMP pathway inhibitor *SMAD6,* resulting in premature myoblast differentiation [10]. With the activation of the PTEN signaling pathway resulting in Wnt signaling downregulation, we believe a combination of these factors resulted in the dysregulation of early gene expression in Lamin A/C mutant cells which leads to slower cardiomyocyte differentiation in patient compared to normal controls.

4.5. Conclusions

We are aware of the limitations of our studies as presented here. Additional scRNA-seq study using additional biological replicates need to be conducted to replicate the results observed here. Additionally, molecular studies to validate the predicted activation/inhibition of the significant signaling pathway activities from the pathway analysis also need to be conducted. In the future, we plan to perform electrophysiological assays to determine any phenotypic differences that manifested as a result of the dysregulation of gene expression elucidated here. And finally, our efforts in studying this disease need to include attempts to ameliorate the disease, either through gene editing or pharmacological intervention. All of these proposed experiments will provide the complete and most comprehensive story on how genomic mutations give rise to cardiac diseases and what is the best approach to treat and ameliorate these diseases.

4.6. References

1. Dechat, T., K. Gesson, and R. Foisner, *Lamina-independent lamins in the nuclear interior serve important functions.* Cold Spring Harb Symp Quant Biol, 2010. **75**: p. 533-43.
2. Dechat, T., et al., *Nuclear lamins.* Cold Spring Harb Perspect Biol, 2010. **2**(11): p. a000547.
3. Taniura, H., C. Glass, and L. Gerace, *A chromatin binding site in the tail domain of nuclear lamins that interacts with core histones.* J Cell Biol, 1995. **131**(1): p. 33-44.
4. Moir, R.D., et al., *Disruption of nuclear lamin organization blocks the elongation phase of DNA replication.* J Cell Biol, 2000. **149**(6): p. 1179-92.
5. Pajerowski, J.D., et al., *Physical plasticity of the nucleus in stem cell differentiation.* Proc Natl Acad Sci U S A, 2007. **104**(40): p. 15619-24.
6. Muchir, A., et al., *Activation of MAPK pathways links LMNA mutations to cardiomyopathy in Emery-Dreifuss muscular dystrophy.* J Clin Invest, 2007. **117**(5): p. 1282-93.
7. Muchir, A., et al., *Activation of MAPK in hearts of EMD null mice: similarities between mouse models of X-linked and autosomal dominant Emery Dreifuss muscular dystrophy.* Hum Mol Genet, 2007. **16**(15): p. 1884-95.
8. Liao, C.Y., et al., *Rapamycin Reverses Metabolic Deficits in Lamin A/C-Deficient Mice.* Cell Rep, 2016. **17**(10): p. 2542-2552.
9. Le Dour, C., et al., *Decreased WNT/beta-catenin signalling contributes to the pathogenesis of dilated cardiomyopathy caused by mutations in the lamin a/C gene.* Hum Mol Genet, 2017. **26**(2): p. 333-343.
10. Janin, A., et al., *SMAD6 overexpression leads to accelerated myogenic differentiation of LMNA mutated cells.* Sci Rep, 2018. **8**(1): p. 5618.
11. Lammerding, J., et al., *Lamin A/C deficiency causes defective nuclear mechanics and mechanotransduction.* J Clin Invest, 2004. **113**(3): p. 370-8.
12. Lu, X., et al., *Requirement for lamin B receptor and its regulation by importin {beta} and phosphorylation in nuclear envelope assembly during mitotic exit.* J Biol Chem, 2010. **285**(43): p. 33281-93.
13. Broers, J.L. and F.C. Ramaekers, *The role of the nuclear lamina in cancer and apoptosis.* Adv Exp Med Biol, 2014. **773**: p. 27-48.
14. Brayson, D. and C.M. Shanahan, *Current insights into LMNA cardiomyopathies: Existing models and missing LINCs.* Nucleus, 2017. **8**(1): p. 17-33.
15. Perovanovic, J., et al., *Laminopathies disrupt epigenomic developmental programs and cell fate.* Sci Transl Med, 2016. **8**(335): p. 335ra58.
16. Zaragoza, M.V., et al., *Exome Sequencing Identifies a Novel LMNA Splice-Site Mutation and Multigenic Heterozygosity of Potential Modifiers in a Family with Sick Sinus Syndrome, Dilated Cardiomyopathy, and Sudden Cardiac Death.* PLoS One, 2016. **11**(5): p. e0155421.
17. Takahashi, K., et al., *Induction of pluripotent stem cells from adult human fibroblasts by defined factors.* Cell, 2007. **131**(5): p. 861-72.
18. Siu, C.W., et al., *Modeling of lamin A/C mutation premature cardiac aging using patient-specific induced pluripotent stem cells.* Aging (Albany NY), 2012. **4**(11): p. 803-822.
19. Carvajal-Vergara, X., et al., *Patient-specific induced pluripotent stem-cell-derived models of LEOPARD syndrome.* Nature, 2010. **465**(7299): p. 808-12.
20. Sun, N., et al., *Patient-specific induced pluripotent stem cells as a model for familial dilated cardiomyopathy.* Sci Transl Med, 2012. **4**(130): p. 130ra47.
21. Ho, J.C., et al., *Generation of induced pluripotent stem cell lines from 3 distinct laminopathies bearing heterogeneous mutations in lamin A/C.* Aging (Albany NY), 2011. **3**(4): p. 380-90.
22. Hescheler, J., et al., *Embryonic stem cells: a model to study structural and functional properties in cardiomyogenesis.* Cardiovasc Res, 1997. **36**(2): p. 149-62.
23. Wobus, A.M., et al., *Embryonic stem cells as a model to study cardiac, skeletal muscle, and vascular smooth muscle cell differentiation.* Methods Mol Biol, 2002. **185**: p. 127-56.
24. Kee, K., et al., *Bone morphogenetic proteins induce germ cell differentiation from human embryonic stem cells.* Stem Cells Dev, 2006. **15**(6): p. 831-7.

25. Xu, X., V.L. Browning, and J.S. Odorico, *Activin, BMP and FGF pathways cooperate to promote endoderm and pancreatic lineage cell differentiation from human embryonic stem cells.* Mech Dev, 2011. **128**(7-10): p. 412-27.
26. Sehgal, P., et al., *Lamin A/C haploinsufficiency modulates the differentiation potential of mouse embryonic stem cells.* PLoS One, 2013. **8**(2): p. e57891.
27. Frock, R.L., et al., *Lamin A/C and emerin are critical for skeletal muscle satellite cell differentiation.* Genes Dev, 2006. **20**(4): p. 486-500.
28. Bermeo, S., et al., *Lamin A/C Acts as an Essential Factor in Mesenchymal Stem Cell Differentiation Through the Regulation of the Dynamics of the Wnt/beta-Catenin Pathway.* J Cell Biochem, 2015. **116**(10): p. 2344-53.
29. Patel, A.P., et al., *Single-cell RNA-seq highlights intratumoral heterogeneity in primary glioblastoma.* Science, 2014. **344**(6190): p. 1396-401.
30. Nguyen, Q.H., et al., *Single-cell RNA-seq of human induced pluripotent stem cells reveals cellular heterogeneity and cell state transitions between subpopulations.* Genome Res, 2018. **28**(7): p. 1053-1066.
31. Plasschaert, L.W., et al., *A single-cell atlas of the airway epithelium reveals the CFTR-rich pulmonary ionocyte.* Nature, 2018. **560**(7718): p. 377-381.
32. Churko, J.M., et al., *Defining human cardiac transcription factor hierarchies using integrated single-cell heterogeneity analysis.* Nat Commun, 2018. **9**(1): p. 4906.
33. Friedman, C.E., et al., *Single-Cell Transcriptomic Analysis of Cardiac Differentiation from Human PSCs Reveals HOPX-Dependent Cardiomyocyte Maturation.* Cell Stem Cell, 2018. **23**(4): p. 586-598 e8.
34. Ruan, H., et al., *Single-cell reconstruction of differentiation trajectory reveals a critical role of ETS1 in human cardiac lineage commitment.* BMC Biol, 2019. **17**(1): p. 89.
35. Lian, X., et al., *Directed cardiomyocyte differentiation from human pluripotent stem cells by modulating Wnt/beta-catenin signaling under fully defined conditions.* Nat Protoc, 2013. **8**(1): p. 162-75.
36. Lian, X., et al., *Robust cardiomyocyte differentiation from human pluripotent stem cells via temporal modulation of canonical Wnt signaling.* Proc Natl Acad Sci U S A, 2012. **109**(27): p. E1848-57.
37. Takahashi, K., et al., *Human induced pluripotent stem cells on autologous feeders.* PLoS One, 2009. **4**(12): p. e8067.
38. Bhattacharya, S., et al., *High efficiency differentiation of human pluripotent stem cells to cardiomyocytes and characterization by flow cytometry.* J Vis Exp, 2014(91): p. 52010.
39. Tohyama, S., et al., *Distinct metabolic flow enables large-scale purification of mouse and human pluripotent stem cell-derived cardiomyocytes.* Cell Stem Cell, 2013. **12**(1): p. 127-37.
40. Zheng, G.X., et al., *Massively parallel digital transcriptional profiling of single cells.* Nat Commun, 2017. **8**: p. 14049.
41. Zhang, X., et al., *Comparative Analysis of Droplet-Based Ultra-High-Throughput Single-Cell RNA-Seq Systems.* Mol Cell, 2019. **73**(1): p. 130-142 e5.
42. Hafemeister, C. and R. Satija, *Normalization and variance stabilization of single-cell RNA-seq data using regularized negative binomial regression.* Genome Biol, 2019. **20**(1): p. 296.
43. Stuart, T., et al., *Comprehensive Integration of Single-Cell Data.* Cell, 2019. **177**(7): p. 1888-1902 e21.
44. Lindsley, R.C., et al., *Mesp1 coordinately regulates cardiovascular fate restriction and epithelial-mesenchymal transition in differentiating ESCs.* Cell Stem Cell, 2008. **3**(1): p. 55-68.
45. Cai, C.L., et al., *Isl1 identifies a cardiac progenitor population that proliferates prior to differentiation and contributes a majority of cells to the heart.* Dev Cell, 2003. **5**(6): p. 877-89.
46. Liu, Y. and R.J. Schwartz, *Transient Mesp1 expression: a driver of cardiac cell fate determination.* Transcription, 2013. **4**(3): p. 92-6.
47. Barreto, S., et al., *Cardiac Progenitor Cells from Stem Cells: Learning from Genetics and Biomaterials.* Cells, 2019. **8**(12).
48. Dyer, L.A. and M.L. Kirby, *The role of secondary heart field in cardiac development.* Dev Biol, 2009. **336**(2): p. 137-44.
49. Constantinescu, D., et al., *Lamin A/C expression is a marker of mouse and human embryonic stem cell differentiation.* Stem Cells, 2006. **24**(1): p. 177-85.
50. Zuo, B., et al., *Influences of lamin A levels on induction of pluripotent stem cells.* Biol Open, 2012. **1**(11): p. 1118-27.

51. Eckersley-Maslin, M.A., et al., *Lamin A/C is expressed in pluripotent mouse embryonic stem cells.* Nucleus, 2013. **4**(1): p. 53-60.
52. Zhang, X., et al., *Pax6 is a human neuroectoderm cell fate determinant.* Cell Stem Cell, 2010. **7**(1): p. 90-100.
53. Wang, P., et al., *Targeting SOX17 in human embryonic stem cells creates unique strategies for isolating and analyzing developing endoderm.* Cell Stem Cell, 2011. **8**(3): p. 335-46.
54. Maleki, M., et al., *Comparison of mesenchymal stem cell markers in multiple human adult stem cells.* Int J Stem Cells, 2014. **7**(2): p. 118-26.
55. Gossett, L.A., et al., *A new myocyte-specific enhancer-binding factor that recognizes a conserved element associated with multiple muscle-specific genes.* Mol Cell Biol, 1989. **9**(11): p. 5022-33.
56. Camoretti-Mercado, B., et al., *Expression and cytogenetic localization of the human SM22 gene (TAGLN).* Genomics, 1998. **49**(3): p. 452-7.
57. Bedford, F.K., et al., *HEX: a novel homeobox gene expressed during haematopoiesis and conserved between mouse and human.* Nucleic Acids Res, 1993. **21**(5): p. 1245-9.
58. Chen, C.Y., et al., *PTEN: Tumor Suppressor and Metabolic Regulator.* Front Endocrinol (Lausanne), 2018. **9**: p. 338.
59. Ramos, A. and F.D. Camargo, *The Hippo signaling pathway and stem cell biology.* Trends Cell Biol, 2012. **22**(7): p. 339-46.
60. Wang, J., et al., *Bmp signaling regulates myocardial differentiation from cardiac progenitors through a MicroRNA-mediated mechanism.* Dev Cell, 2010. **19**(6): p. 903-12.
61. de Pater, E., et al., *Bmp signaling exerts opposite effects on cardiac differentiation.* Circ Res, 2012. **110**(4): p. 578-87.
62. Burridge, P.W., A. Holmstrom, and J.C. Wu, *Chemically Defined Culture and Cardiomyocyte Differentiation of Human Pluripotent Stem Cells.* Curr Protoc Hum Genet, 2015. **87**: p. 21 3 1-21 3 15.
63. Wu, H., et al., *Modelling diastolic dysfunction in induced pluripotent stem cell-derived cardiomyocytes from hypertrophic cardiomyopathy patients.* Eur Heart J, 2019. **40**(45): p. 3685-3695.
64. Prigione, A., et al., *Human induced pluripotent stem cells harbor homoplasmic and heteroplasmic mitochondrial DNA mutations while maintaining human embryonic stem cell-like metabolic reprogramming.* Stem Cells, 2011. **29**(9): p. 1338-48.
65. Wen, Y., et al., *Reprogramming of fibroblasts from older women with pelvic floor disorders alters cellular behavior associated with donor age.* Stem Cells Transl Med, 2013. **2**(2): p. 118-28.
66. Parks, S.B., et al., *Lamin A/C mutation analysis in a cohort of 324 unrelated patients with idiopathic or familial dilated cardiomyopathy.* Am Heart J, 2008. **156**(1): p. 161-9.
67. Wolf, C.M., et al., *Lamin A/C haploinsufficiency causes dilated cardiomyopathy and apoptosis-triggered cardiac conduction system disease.* J Mol Cell Cardiol, 2008. **44**(2): p. 293-303.
68. Mozzetta, C. and F.S. Tedesco, *Challenging the "chromatin hypothesis" of cardiac laminopathies with LMNA mutant iPS cells.* J Cell Biol, 2019. **218**(9): p. 2826-2828.
69. Raharjo, W.H., et al., *Nuclear envelope defects associated with LMNA mutations cause dilated cardiomyopathy and Emery-Dreifuss muscular dystrophy.* J Cell Sci, 2001. **114**(Pt 24): p. 4447-57.
70. Goldman, R.D., et al., *Accumulation of mutant lamin A causes progressive changes in nuclear architecture in Hutchinson-Gilford progeria syndrome.* Proc Natl Acad Sci U S A, 2004. **101**(24): p. 8963-8.
71. Stephens, A.D., et al., *Chromatin histone modifications and rigidity affect nuclear morphology independent of lamins.* Mol Biol Cell, 2018. **29**(2): p. 220-233.
72. Shah, P., K. Wolf, and J. Lammerding, *Bursting the Bubble - Nuclear Envelope Rupture as a Path to Genomic Instability?* Trends Cell Biol, 2017. **27**(8): p. 546-555.
73. Muchir, A., et al., *Abnormal p38alpha mitogen-activated protein kinase signaling in dilated cardiomyopathy caused by lamin A/C gene mutation.* Hum Mol Genet, 2012. **21**(19): p. 4325-33.
74. Sen-Chowdhry, S. and W.J. McKenna, *Sudden death from genetic and acquired cardiomyopathies.* Circulation, 2012. **125**(12): p. 1563-76.
75. Forleo, C., et al., *Clinical and functional characterization of a novel mutation in lamin a/c gene in a multigenerational family with arrhythmogenic cardiac laminopathy.* PLoS One, 2015. **10**(4): p. e0121723.

76. Chen, N.Y., et al., *Fibroblasts lacking nuclear lamins do not have nuclear blebs or protrusions but nevertheless have frequent nuclear membrane ruptures.* Proc Natl Acad Sci U S A, 2018. **115**(40): p. 10100-10105.
77. Quiles, J.M., et al., *Identification of transcriptome signature for myocardial reductive stress.* Redox Biol, 2017. **13**: p. 568-580.
78. Zhang, J., et al., *UCP2 regulates energy metabolism and differentiation potential of human pluripotent stem cells.* EMBO J, 2011. **30**(24): p. 4860-73.
79. Kondoh, H., et al., *A high glycolytic flux supports the proliferative potential of murine embryonic stem cells.* Antioxid Redox Signal, 2007. **9**(3): p. 293-9.
80. Hopkinson, B.M., et al., *Bioenergetic Changes during Differentiation of Human Embryonic Stem Cells along the Hepatic Lineage.* Oxid Med Cell Longev, 2017. **2017**: p. 5080128.
81. Chen, C.T., et al., *Coordinated changes of mitochondrial biogenesis and antioxidant enzymes during osteogenic differentiation of human mesenchymal stem cells.* Stem Cells, 2008. **26**(4): p. 960-8.
82. Spitkovsky, D., et al., *Activity of complex III of the mitochondrial electron transport chain is essential for early heart muscle cell differentiation.* FASEB J, 2004. **18**(11): p. 1300-2.
83. Sieprath, T., et al., *Sustained accumulation of prelamin A and depletion of lamin A/C both cause oxidative stress and mitochondrial dysfunction but induce different cell fates.* Nucleus, 2015. **6**(3): p. 236-46.
84. Dahia, P.L., *PTEN, a unique tumor suppressor gene.* Endocr Relat Cancer, 2000. **7**(2): p. 115-29.
85. Weng, L., J. Brown, and C. Eng, *PTEN induces apoptosis and cell cycle arrest through phosphoinositol-3-kinase/Akt-dependent and -independent pathways.* Hum Mol Genet, 2001. **10**(3): p. 237-42.
86. Weng, L.P., J.L. Brown, and C. Eng, *PTEN coordinates G(1) arrest by down-regulating cyclin D1 via its protein phosphatase activity and up-regulating p27 via its lipid phosphatase activity in a breast cancer model.* Hum Mol Genet, 2001. **10**(6): p. 599-604.
87. Persad, S., et al., *Tumor suppressor PTEN inhibits nuclear accumulation of beta-catenin and T cell/lymphoid enhancer factor 1-mediated transcriptional activation.* J Cell Biol, 2001. **153**(6): p. 1161-74.
88. Vonica, A. and B.M. Gumbiner, *Zygotic Wnt activity is required for Brachyury expression in the early Xenopus laevis embryo.* Dev Biol, 2002. **250**(1): p. 112-27.
89. Gomez, G.A., et al., *WNT/beta-catenin modulates the axial identity of embryonic stem cell-derived human neural crest.* Development, 2019. **146**(16).
90. Klaus, A., et al., *Distinct roles of Wnt/beta-catenin and Bmp signaling during early cardiogenesis.* Proc Natl Acad Sci U S A, 2007. **104**(47): p. 18531-6.

CHAPTER 5

Summarizations, Future Directions and Significance

5.1. Summarizations

My studies, as described here, elaborated on the diversity of molecular mechanisms of two different types of Lamin A/C mutations on various cellular processes, as follows:

First, in Chapter 2, by performing molecular expression studies, I discovered that the novel Lamin A/C missense mutation (*LMNA* c.736C>T), manifested in monoallelic transcription of *LMNA* transcript, as well as significant reduction of Lamin A/C mRNA levels in fibroblasts harvested from affected individuals. Both observations were consistent with of Lamin A/C haploinsufficiency as the primary genetic mechanism of this particular Lamin A/C missense mutation. In this study, I showed that the use of fibroblasts, one of the most common somatic cell types used in molecular expression studies, was sufficient to detect the predicted phenotypes of the mutation.

In Chapter 3, I showed that the novel Lamin A/C splice site mutation (*LMNA* c.357-2A>G) manifested in a distinct manner than the previously studied Lamin A/C missense mutation (*LMNA* c.736C>T). By comparing transcriptomic profiles of three patient samples to three related and unrelated control samples, I seek to investigate the molecular mechanisms of Lamin A/C splice-site mutation and how this mutation might alter genome-wide gene expression patterns along with any changes in signaling pathway activities that could potentially contribute to the pathogenesis of Lamin-associated cardiac diseases. To complement the molecular expression studies, I also performed protein expression studies to I also seek to discover whether there were any compensatory mechanisms by the other nuclear lamina proteins, Lamin B1 and Lamin B2, to maintain proper nuclear structure. Using fibroblasts as the primary platform to perform transcriptomic profiling, molecular and protein expression studies, I found that there was no significant difference in *LMNA*

mRNA levels between patients and control fibroblasts. This finding was underscored by the results of Lamin A/C Western Blot that showed similar protein expression levels between patients and controls. With regards to compensatory mechanisms by Lamins B1 and B2, I also found that the transcript levels of these nuclear lamina proteins were not elevated, signifying compensatory mechanisms did not occur. These assays showed that despite the monoallelic expression of wild-type *LMNA* transcript in patient fibroblasts, one copy of the wild-type allele was sufficient to maintain normal levels of Lamin A/C protein in fibroblasts. These findings also suggest that cardiac tissues are more sensitive to decreases in Lamin A/C protein level.

Next, by performing differentially expressed genes (DEGs) and pathway analysis, I discovered eight significantly differentially expressed genes between patients and controls, chief among them was the downregulation of insulin binding growth factor protein 5 (*IGFBP5*) expression in patient fibroblasts. Along with the other DEGs, pathway analysis implicated the ERK/MAPK signaling pathway in the disease pathology. Here, I postulated that the downregulation of *IGFBP5*, which has been shown to decrease ERK1/2 phosphorylation and ultimately suppressed ERK/MAPK signaling activity, contributed to the maintenance of cellular homeostasis in patient fibroblasts and explained why there were no significant differences between patients and controls fibroblasts.

Finally, in Chapter 4 I showed the utility of induced pluripotent stem cells (iPSCs) in performing disease modeling studies. My previous studies highlighted the importance of using the appropriate cell types to study certain diseases. I have previously shown that while some phenotypic features of Lamin A/C mutations could be observed in unaffected cells such as fibroblasts, others necessitated the generation of the corresponding affected

cell types *in-vitro*. As I did not observe any phenotypic differences in *LMNA* c.357-2A>G mutant fibroblasts, I sought to generate cardiomyocytes bearing the same genotype by first reprogramming these somatic cells to its corresponding induced pluripotent stem cells (iPSCs) using Yamanaka factors, and secondly differentiating the iPSCs to iPSC-derived cardiomyocytes (iPSC-CMs) via Wnt/β-catenin signaling activity modulation. The resulting patient iPSCs showed similar levels of pluripotency as iPSCs generated from control fibroblasts, suggesting that the *LMNA* mutation had no impact on pluripotency. Additionally, through spontaneous embryoid body formation and differentiation, I showed that both patient and control iPSC lines were capable of forming cells in the three primary germ layer lineages, underscoring their pluripotency. Next, the cardiomyocyte differentiation protocol successfully yielded iPSC-CMs that formed beating syncytium *in-vitro* and expressed Troponin T, as quantified by flow cytometry and visualized by immunofluorescence imaging.

I repeated the same *LMNA* molecular and protein expression studies on patient and control iPSC-CMs to determine the primary mechanisms of Lamin A/C splice-site mutation and found iPSC-CMs had monoallelic expression of *LMNA* transcript, in the same manner as their corresponding fibroblasts did. However, iPSC-CMs have a marked reduction in Lamin A/C protein expression, with Lamin A being more significantly reduced in patient iPSC-CMs compared to control iPSC-CMs. While Lamin C protein expression was reduced in patient iPSC-CMs, it was not statistically significantly reduced. The results of the expression studies were consistent with Lamin A/C haploinsufficiency being the primary molecular mechanisms of the Lamin A/C splice-site mutation. Next, I intended to elucidate on what cellular processes were affected by the Lamin A/C splice-site mutation. Since Lamin A/C

has been documented to influence cell fate and differentiation trajectory, I decided to examine how Lamin A/C haploinsufficiency potentially affect cell differentiation and how this led to the cardiac dysfunctions observed in patients. By performing time-course scRNA-seq study on iPSC-CMs, I showed that there was a lag in activation of mesoderm and mesendoderm genes which led to the lower expression of cardiogenic transcription factors and important sarcomeric proteins in patient iPSC-CMs. I also showed that during the time course of differentiation, *LMNA* expression levels in patient iPSC-CMs remained significantly lower than control iPSC-CMs and never reached similar expression levels even at the last observed timepoint of the differentiation study. Finally, by examining *LMNA* gene expression in different cell subpopulations identified by scRNA-seq, I found that significant reduction of *LMNA* expression only occurred in cells that were derived from the mesoderm lineage, with the exception of cells destined to give rise to the circulatory system.

Furthermore, by performing pathway analysis of DEGs at days 0, 2, 4, and 9 from cells that represented the path from pluripotency to embryonic cardiomyocyte, I uncovered signaling pathways and biological processes that were implicated in the differentiation lag of patient iPSC-CMs. First, I showed that patient iPSCs have a unique metabolic profile that utilized oxidative phosphorylation instead of glycolysis for energy production. On days 2 and 4, I identified two primary signaling pathways implicated in the delayed cardiac differentiation: PTEN signaling pathway and BMP signaling pathway. I predicted that the activation of PTEN signaling, which has been shown to prevent beta-catenin accumulation, thus suppressing Wnt signaling pathway activity, led to the lower expression of Wnt target genes, chief among them were Brachyury (*TBXT*), *MIXL1* and *EOMES*. In addition to PTEN signaling pathway, I also observed the apparent inhibition of BMP signaling pathway as one

of the contributing factors in the differentiation lag of patient iPSC-CMs. Finally, I showed the involvement of Lamin A/C haploinsufficiency in the activation of Death Receptor signaling pathway, which was predicted to result in membrane blebbing and cell death.

5.2. Future Directions

Validation of proposed molecular mechanisms

In chapter 4, I showed that patient iPSC-CMs differentiated at a slower pace than control iPSC-CMs. This was accompanied by a change in energy production pathways (glycolysis compared to oxidative phosphorylation), inhibition of cardiogenic signaling pathway and the apparent activation of signaling pathways associated with apoptosis and DNA damage repair. The results reported here offered new insight to the various cellular processes affected by the novel Lamin A/C splice-site mutation. Further validation of the activation and inhibition of these pathways need to be performed *in-vitro* to further solidify the information discovered through bioinformatics analysis. The approaches I described here should be considered as high priority experiments as they will validate the bioinformatic findings and strengthen the proposed hypothesis. Approaches that could be used include quantification of gene expression levels using quantitative real time PCR or protein studies using Western Blot to measure expression of genes and proteins associated with the pathways identified in this study.

Tissue-specificity of Lamin A/C haploinsufficiency was described here, with Lamin A/C haploinsufficiency only occurring in cells of the mesoderm lineages with the exception of cells destined to give rise to the hematopoietic lineage. Directed differentiation of iPSCs to give rise to cells in the ectoderm, endoderm and mesoderm lineages can be performed

using a wide array of published differentiation protocols [1] or commercial protocols, then Lamin A/C immunoblotting will be performed to validate Lamin A/C haploinsufficiency in all three germlines.

Additionally, since I found potential increase in susceptibility to apoptosis and DNA damage in P1 iPSC-CMs, studies to detect DNA fragmentation and double stranded breaks using TUNEL assay should be conducted [2]. This would ensure that the increase in DNA damage and cell death predicted by pathway analysis was not an artifact of the sequencing process, as dead cells were not filtered out or excluded prior to libraries generation. Finally, nuclear architecture morphology studies should be conducted to assess the effects of Lamin A/C haploinsufficiency on nuclear membrane architecture [3].

Tissue specificity and epigenetic dysregulation

Laminopathies remained a curious group of diseases, primarily because of its peculiar tissue-specific manifestation. While I have provided evidence showing how Lamin A/C haploinsufficiency manifested in affected cells, further studies still need to be conducted to determine what factors play a role in limiting the occurrence of these defects in mesoderm-derived cell types. That is: why did Lamin A/C haploinsufficiency only occur in iPSC-CMs, as opposed to fibroblasts *and* iPSC-CMs, even though both cells expressed the mutation? This inexplicable phenomenon remained an unsolved question in the field, and more in-depth studies would need to be conducted.

Perhaps the answers lie in the epigenome of the cells. Lamin A/C has been shown previously to form genomic regions termed Lamina-associated domains (LADs) which were highly compacted chromatin marked with modifications that signified suppression of

gene expression (heterochromatin). This may be one way that Lamin A/C regulates gene expression, in addition to sequestration of transcription factors. Since Lamin A/C haploinsufficiency has previously been shown to cause diminished LADs size and aberrant gene expression, these observations suggested that the epigenome might play a role in the manifestation of laminopathies [4]. When one considered that the epigenome of a cell differed based on cell type [5], comparing the epigenomes of different cell types bearing *LMNA* mutations might provide insight as to how *LMNA* mutations inflicted cell-type specific disturbances. Approaches that could be taken included chromatin immunoprecipitation followed by high throughput sequencing (ChIP-seq) which would enable genome-wide mapping of Lamin A/C binding partners [6]. Alternative or additional approaches to consider included assay for transposase-accessible chromatin using sequencing (ATAC-seq) which enabled evaluation of chromatin architecture and how the presence of *LMNA* mutation perturbed its formation [7]. Uncovering new and novel information on this frontier would aid tremendously in the development of new therapeutics for laminopathies and lamin-associated cardiac diseases.

Mitochondrial dysfunction of patient iPSCs

Mitochondrial dysfunction has been shown to occur in several laminopathies, chief among them Hutchinson-Gilford Progeria Syndrome (HGPS) and lamin-associated cardiac dysfunctions [8]. Furthermore, the mitochondrion has been implicated in maintenance of pluripotency in iPSCs, regulation of cell fate and reprogramming efficiency [9, 10]. Elucidating how Lamin A/C mutation affected the mitochondria could pave the way in providing novel solutions and therapeutic targets to ameliorate laminopathies. Further,

assessing the differences in metabolic profile between C1 and P1 iPSCs would provide better insight to the distinctions between iPSCs generated from somatic cells bearing *LMNA* mutation and its normal counterpart. Hypothesis to be tested include *LMNA* mutation prevented complete reprogramming of somatic cells, thus *LMNA* mutant iPSCs retained the metabolic profile of its somatic cell counterparts and iPSCs bearing *LMNA* mutation were initially partially differentiated (less pluripotent) compared to control iPSCs.

Functional studies of iPSC-derived cardiomyocytes

Finally, the generation of iPSC-based disease modeling has enabled the study of multitude of diseases that otherwise would remain understudied due to limitations, both biological and ethical, inherent to the cell types needed for thorough *in-vitro* investigations. By generating patient-specific iPSC-CMs, functional studies examining multiple cardiac functionalities, such as cardiomyocyte contractile strength, beat rate and conductivity, should be pursued to further elucidate the effects of Lamin A/C mutation on cardiac functionality. Furthermore, iPSC-based disease modeling has been used to perform high throughput drug screening to discover which drug would be the best choice to treat diseases in rapid fashion [11]. This approach would complement the cardiac functionality studies and offer great insight to treatment and therapeutic approaches that could be applied to Lamin-associated cardiac disease.

CRISPR/Cas9-mediated genome editing to create isogenic control cell lines

Pharmaceutical intervention has been the primary approach to cure diseases. However, with advancements gained in the field of gene editing it was now possible to get

to the root cause of many diseases caused by genetic mutations [12, 13]. I will use CRISPR/Cas9-mediated gene editing to correct the *LMNA* mutation in three patient iPSC lines. Then, I will differentiate the gene edited cell lines to cardiomyocytes using standard differentiation protocol. Previously, I designed CRISPR RNAs (crRNAs) that will efficiently target the *LMNA* gene at c.357-2A>G, incorporating these considerations: 1) the protospacer adjacent motif (PAM) sequence needs to be near the edit site, 2) the double strand break by Cas9 nuclease needs to be within 10 bases of the edit site and 3) the crRNA needs to have low off-target effects [14]. Benchling provided on-target and off-target scores for the crRNA chosen. A high "on target" score indicates higher on target activity by Cas9 nuclease [15], while "off-target score" is an inverse probability of how likely the gRNA will bind to other areas on the genome [16]. Using Benchling's algorithm, I generated five crRNAs to target LMNA gene at the 3' end of intron 1 and the 5' end of exon 2 (Table V.1).

Three out of five candidate guide RNAs (gRNAs) that generated double stranded break (DSB) nearest to the target site were synthesized and used for pilot electroporation trial using HEK293FT cells. Using optimized protocol determined in pilot study using HPRT1 gRNA, I transfected three candidate LMNA gRNAs: LMNA1, LMNA2 and LMNA3 (Table V.1) to HEK293FT cells and harvested the genomic DNA after 48 hours to perform genomic cleavage detection (GCD) assay. To detect and amplify the modified genomic region, I used previously designed primer pairs [17]. Figure V.1 showed that in HEK293FT cells LMNA2 has the highest cleavage efficiency compared to LMNA1 and 3. Based on this result, LMNA2 should be the gRNA used for gene editing experiments.

Performing gene editing on our patient iPSC lines to see whether the phenotypes associated with the mutation, such as monoallelic *LMNA* mRNA, Lamin A/C

haploinsufficiency and slower rate of cardiomyocyte differentiation, were ameliorated would be useful to advance our understanding of how genetic mutations give rise to diseases.

Table V.1. List of candidate guide RNA (gRNA) to be used for splice-site mutation editing.

gRNA name	crRNA sequence (5' to 3')	PAM site	On-target score	Off-target score	DSB distance from target site
LMNA1	GGTATTGCTAAAGAAGAGAG	GGG	70.6	48.8	9 nt
LMNA2	CTTCTTTAGCAATACCAAGA	AGG	58.9	57.1	9 nt
LMNA3	TTGGTATTGCTAAAGAAGAG	AGG	62.0	49.3	7 nt
LMNA4	TTTAGCAATACCAAGAAGGA	GGG	65.4	52.1	13 nt
LMNA5	CTTTAGCAATACCAAGAAGG	AGG	64.1	53.9	14 nt

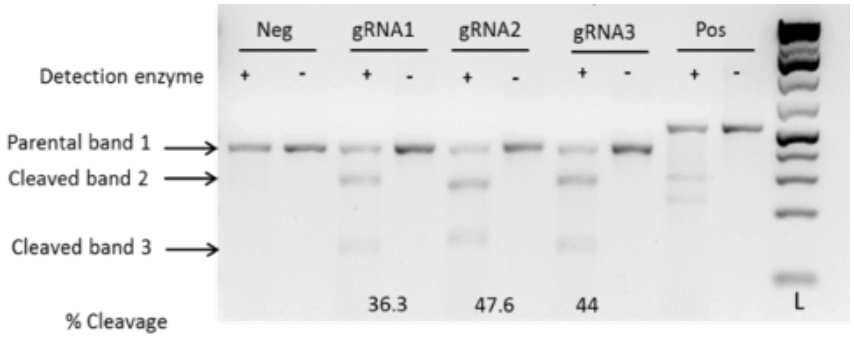

Figure V.1: *LMNA* gRNAs validation. HEK293 FT cells were electroporated using Neon transfection system with TrueCut Cas9 nuclease and three different gRNAs targeting the *LMNA* gene. Negative and positive control samples for gene modification were also prepared.

5.3. Significance

Here, I described the development of cardiomyocytes from human iPSCs that closely mimic the *in-vivo* conditions we seek to replicate. These cardiomyocytes formed beating syncytium, expressed Troponin T *in-vitro* and enabled us to elucidate the molecular mechanisms of Lamin A/C splice-site mutation. Similar to previous *LMNA* iPSC-based disease modeling studies, my study showed that Lamin A/C haploinsufficiency was the primary molecular mechanism of the novel *LMNA* splice-site mutation. In contrast to previous studies, I successfully showed that Lamin A/C haploinsufficiency was restricted to

mesoderm derived cells, underscoring the suitability of the *in-vitro* model developed here to study *LMNA*-associated cardiac diseases and other laminopathies. Furthermore, here I proposed suggestions as to how the novel Lamin A/C splice-site mutation affect expression of genes involved in cardiomyocyte differentiation and how it potentially impacted the cardiac differentiation process.

Here, we used single cell RNA sequencing (scRNA-seq) to further study how this mutation affected various cellular processes. By using this approach, I managed to uncover significant molecular phenotypic differences between diseased and non-diseased cells and showed the tissue specificity of Lamin A/C haploinsufficiency. scRNA-seq also elucidated the heterogeneity of cells produced by our differentiation process, providing a more comprehensive view of cardiomyocyte development *in-vitro*. Furthermore, we provided additional data to facilitate development of future studies for the treatment of laminopathies.

5.4. References

1. Hildebrandt, M.R., et al., *Precision Health Resource of Control iPSC Lines for Versatile Multilineage Differentiation.* Stem Cell Reports, 2019. **13**(6): p. 1126-1141.
2. Darzynkiewicz, Z., D. Galkowski, and H. Zhao, *Analysis of apoptosis by cytometry using TUNEL assay.* Methods, 2008. **44**(3): p. 250-4.
3. Core, J.Q., et al., *Age of heart disease presentation and dysmorphic nuclei in patients with LMNA mutations.* PLoS One, 2017. **12**(11): p. e0188256.
4. Perovanovic, J., et al., *Laminopathies disrupt epigenomic developmental programs and cell fate.* Sci Transl Med, 2016. **8**(335): p. 335ra58.
5. Bernstein, B.E., A. Meissner, and E.S. Lander, *The mammalian epigenome.* Cell, 2007. **128**(4): p. 669-81.
6. Cheedipudi, S.M., et al., *Genomic Reorganization of Lamin-Associated Domains in Cardiac Myocytes Is Associated With Differential Gene Expression and DNA Methylation in Human Dilated Cardiomyopathy.* Circ Res, 2019. **124**(8): p. 1198-1213.
7. Buenrostro, J.D., et al., *Transposition of native chromatin for fast and sensitive epigenomic profiling of open chromatin, DNA-binding proteins and nucleosome position.* Nat Methods, 2013. **10**(12): p. 1213-8.
8. Rivera-Torres, J., et al., *Identification of mitochondrial dysfunction in Hutchinson-Gilford progeria syndrome through use of stable isotope labeling with amino acids in cell culture.* J Proteomics, 2013. **91**: p. 466-77.
9. Folmes, C.D., et al., *Somatic oxidative bioenergetics transitions into pluripotency-dependent glycolysis to facilitate nuclear reprogramming.* Cell Metab, 2011. **14**(2): p. 264-71.
10. Prowse, A.B., et al., *Analysis of mitochondrial function and localisation during human embryonic stem cell differentiation in vitro.* PLoS One, 2012. **7**(12): p. e52214.
11. Ebert, A.D., P. Liang, and J.C. Wu, *Induced pluripotent stem cells as a disease modeling and drug screening platform.* J Cardiovasc Pharmacol, 2012. **60**(4): p. 408-16.
12. Sano, S., et al., *CRISPR-Mediated Gene Editing to Assess the Roles of Tet2 and Dnmt3a in Clonal Hematopoiesis and Cardiovascular Disease.* Circ Res, 2018. **123**(3): p. 335-341.
13. Moretti, A., et al., *Somatic gene editing ameliorates skeletal and cardiac muscle failure in pig and human models of Duchenne muscular dystrophy.* Nat Med, 2020. **26**(2): p. 207-214.
14. Kwart, D., et al., *Precise and efficient scarless genome editing in stem cells using CORRECT.* Nat Protoc, 2017. **12**(2): p. 329-354.
15. Hsu, P.D., et al., *DNA targeting specificity of RNA-guided Cas9 nucleases.* Nat Biotechnol, 2013. **31**(9): p. 827-32.
16. Doench, J.G., et al., *Optimized sgRNA design to maximize activity and minimize off-target effects of CRISPR-Cas9.* Nat Biotechnol, 2016. **34**(2): p. 184-191.
17. Zaragoza, M.V., et al., *Exome Sequencing Identifies a Novel LMNA Splice-Site Mutation and Multigenic Heterozygosity of Potential Modifiers in a Family with Sick Sinus Syndrome, Dilated Cardiomyopathy, and Sudden Cardiac Death.* PLoS One, 2016. **11**(5): p. e0155421.

Supplementary Data

Table II.S1. Main clinical features of the study family.

ID [a]	Sex	Age (y)	Cardiac History (Age at Diagnosis)[b]	Dupuytren's Disease (Px Age)	Ledderhose Disease (Px Age)	Other Significant Medical and Social History
I-1	M	d.59	Unknown	Unknown	Unknown	Unknown
I-2	F	d.51	Sudden death (51)	Unknown	Unknown	Unknown
I-3	M	d.80	Unknown	Unknown	Unknown	Unknown
I-4	F	d.75	Unknown	Unknown	Unknown	Unknown
II-1	M	d.neonate	Unknown	Unknown	Unknown	Unknown
II-2	F	d.52	Sudden death (52)	Unknown	Unknown	Unknown
II-3	M	d.74	Unknown	Unknown	Unknown	Unknown
II-4	F	d.16	Unknown	Unknown	Unknown	Unknown
II-5	M	d.53	Sudden death (53)	Unknown	Unknown	Unknown
II-6	F	d.87	Unknown	Unknown	Unknown	Unknown
II-7	M	d.68	Irregular heart beat (40s), pacemaker (64), HF (66), cardiac arrest (68)	Unknown	Unknown	Unknown
II-8	F	d.79	None	Yes (40s), Surgery x1 (60)	Unknown	Emphysema, lung cancer (79), alcoholism, tobacco use
II-9	M	d.unknown	Unknown	Unknown	Unknown	Unknown
III-1	M	d.58	CAD, MI (31, 58)	No	Unknown	None
III-2	F	d.74	AF, DCM, HF, ICD (68), ASD-repair (73), VT (72), pulmonary HTN (73)	Yes (50s), Surgery x1 (60)	No	Myelodysplastic syndrome, chronic renal insufficiency
III-3	M	d.76	None	No	No	Brain tumor (76)
III-4	F	75	AFL (61), bradycardia, pacemaker (66), ICD (73), normal echo (73)	Yes (40s)	Yes (40s)	None
III-5	M	d.57	Irregular heart beat (50s), enlarged heart (55), sudden death, HF (57)	Yes (20s), Surgery x4	No	Alcohol binge drinking
III-6	F	80	Unknown	Unknown	Unknown	Unknown
IV-1	F	60	None, normal echo, holter studies (56)	No	No	None
IV-2	F	58	Syncope, SSS, pacemaker (45), AF, NSVT, AV block, DCM, ICD (55)	Yes (50)	Yes (55)	Hyperlipidemia
IV-3	F	55	Syncope x3 (50, 52, 53), bradycardia (50), normal echo (53)	No	Yes (51)	None, normal CK (50)
IV-4	F	49	Dyspnea, bradycardia, palpitations, mild DCM (42), PVCs, NSVT (47)	No	Plantar nodule?	None
IV-5	F	47	None, normal echo, EKG (37)	No	No	Hypothyroidism

[a]Individuals with cardiac disease (arrhythmia, ventricular dysfunction, sudden death) with or without Dupuytren's Disease are highlighted in yellow (n=10). The maternal grandmother with Dupuytren's Disease and no cardiac disease is highlighted in green.
[b]Clinical features for an additional family member was removed after consent to publish was declined.
Abbreviations: y, years old; Px, presentation; d., died; HF, heart failure; CAD, coronary artery disease; MI, myocardial infarction; AF, atrial fibrillation; DCM, dilated cardiomyopathy; ICD, implantable cardiac defibrillator; ASD, atrial septal defect; VT, ventricular tachycardia; HTN, hypertension; AFL, atrial flutter; SSS, sick sinus syndrome; NSVT, nonsustained ventricular tachycardia; PVC, premature ventricular contraction; CK, creatine kinase

Table II.S2. Exome Sequencing Studies of Four Family Members: Sequencing-Mapping & Variant Calling-Filtering

	Family Member				All Four Family Members: Average/Sample
	III-4	IV-3	Patient 3	IV-1	
Hand/Feet Phenotype	DD & LD	LD only	DD only	Unaffected	
Sequencing-Mapping					
Raw data (bp)	7,907,552,128	8,967,512,187	7,055,268,986	8,411,863,057	8,085,549,090
Reads-total	104,800,788	118,853,834	93,507,716	111,492,986	107,163,831
Reads mapped	104,136,200	118,129,101	92,924,198	110,810,461	106,499,990
% Reads mapped	99.4%	99.4%	99.4%	99.4%	99.4%
Mean coverage depth	78X	88X	72X	85X	81X
Mean coverage ≥ 30X	85.7%	87.5%	83.2%	86.7%	85.8%
Bases: % ≥ Q30	90.4%	90.5%	90.0%	90.6%	90.4%
Bases: Mean Quality Score	32.62	32.64	32.55	32.67	32.62
Variant Calling-Filtering					
Total unique variants	20,144	20,445	20,576	20,500	20,416
Heterozygous variants	12,555	12,894	13,093	12,955	12,874

HET/Non-synonymous variants	6,327	6,445	6,614	6,564	6,488
HET/NS/Highly-conserved variants	1,677	1,681	1,815	1,761	1,734

Abbreviations: DD, Dupuytren's Disease; LD, Ledderhose Disease; Q, Quality Score; HET, heterozygous; NS, non-synonymous

Table II.S3.Exome Sequencing Studies of Four Family Members: Candidate Variants by Allele Frequency (n=98). Novel or rare (allele frequency <1%) variants considered as high-priority candidates are highlighted in yellow. The USF3 variant was excluded since it is an inframe-deletion of one codon and the clinical significance of the variant is likely benign (ClinVar variant # 218482).

Gene	Position (hg38)	DNA variant	Protein change	dbSNP (rs)	ExAC Frequency
ASTE1	Chr3:131025077	c.230T>C	p.Val77Ala	novel	no data
FZD2	Chr17:44558223	c.535A>C	p.Thr179Pro	novel	no data
FSD1	Chr19:4311959	c.608G>A	p.Arg203Gln	novel	no data
LMNA	Chr1:156134901	c.736C>T	p.Gln246Ter	267607587	no data
USF3	Chr3:113657264-113657266	c.4416_4418delGCA	p.Gln1478del	10606566	no data
OR51A7	Chr11:4908132	c.763A>G	p.Ile255Val	144609747	0.0040
SYPL2	Chr1:109476793	c.272A>T	p.Tyr91Phe	79613472	0.0086
CARD14	Chr17:80202245	c.2044C>T	p.Arg682Trp	117918077	0.0110
COL24A1	Chr1:86126053	c.283G>A	p.Val95Met	74097691	0.0127
OSGEPL1	Chr2:189755490	c.292G>A	p.Ala98Thr	75321854	0.0416
PEX11G	Chr19:7477282	c.436C>T	p.Leu146Phe	11668511	0.0488
OR10T2	Chr1:158398602	c.865G>A	p.Val289Ile	61818748	0.0504
MUC6	Chr11:1021268	c.3536A>G	p.Asn1179Ser	113451874	0.0524
DOCK6	Chr19:11214289	c.4324G>A	p.Ala1442Thr	34243815	0.0681
FAM221A	Chr7:23698272	c.544A>G	p.Ser182Gly	35928055	0.0791
COX4I1	Chr16:85801212	c.7G>A	p.Ala3Thr	11557187	0.0906
OR52L1	Chr11:5986542	c.389C>T	p.Ser130Leu	61750896	0.0965
RERGL	Chr12:18081322	c.484A>G	p.Met162Val	941048	0.0987
CAMTA1	Chr1:7737443	c.3531C>G	p.Asn1177Lys	41278952	0.1167
KANK3	Chr19:8325009-8325011	c.2022_2024delGGA	p.Glu674del	111905975	0.1298
OR52J3	Chr11:5047067	c.542G>A	p.Cys181Tyr	58664826	0.1303
NLRP14	Chr11:7038750	c.164G>A	p.Arg55Gln	61063081	0.1500
TLN2	Chr15:62819540	c.6796T>C	p.Phe2266Leu	3816988	0.1640
COL24A1	Chr1:86046853	c.1922G>A	p.Arg641His	60891279	0.1703
BAIAP2	Chr17:81115790	c.1556A>G	p.Gln519Arg	4969391	0.1823
RBMXL2	Chr11:7089317	c.197C>T	p.Ala66Val	11041170	0.2020
ACAN	Chr15:88872016	c.7005C>G	p.Asp2335Glu	3817428	0.2023
C5orf49	Chr5:7835442	c.204G>C	p.Gln68His	6883562	0.2134
SSC4D	Chr7:76400378	c.383G>A	p.Arg128His	4728712	0.2209
MATN4	Chr20:45297933	c.1564G>A	p.Gly522Ser	2227275	0.2300
PTCRA	Chr6:42923284	c.316G>A	p.Val106Ile	9471966	0.2383
PTPRG	Chr3:62203515	c.1720G>A	p.Gly574Ser	2292245	0.2385
OR13C9	Chr9:104617614	c.591C>A	p.Phe197Leu	10761054	0.2444
QRFPR	Chr4:121329579	c.1031T>C	p.Leu344Ser	2302310	0.2485

SPTA1	Chr1:158627717	c.5572C>G	p.Leu1858Val	3737515	0.2567
NRAP	Chr10:113633160	c.1556A>T	p.Asn519Ile	2270182	0.2638
GLMP	Chr1:156294149	c.667A>G	p.Ile223Val	10908495	0.2688
C21orf58	Chr21:46302071-46302072	c.578_579insCCA	p.His193_Ala194insHis	71318063	0.2852
HDGF	Chr1:156743766	c.650C>T	p.Pro217Leu	4399146	0.2854
KRT40	Chr17:40983118	c.458C>T	p.Thr153Met	9908304	0.2925
APOB	Chr2:21008652	c.8216C>T	p.Pro2739Leu	676210	0.2928
KRT40	Chr17:40983969	c.305G>A	p.Ser102Asn	1510068	0.2934
MED12L	Chr3:151372636	c.3629G>A	p.Arg1210Gln	3732765	0.3060
ST5	Chr11:8730093	c.1197C>G	p.Asp399Glu	3812762	0.3119
CALU	Chr7:128754552	c.245C>T	p.Ala82Val	2307040	0.3138
BRC1	Chr17:43092418	c.3113A>G	p.Glu1038Gly	16941	0.3429
MYO19	Chr17:36498436	c.2587C>T	p.Leu863Phe	2306590	0.3462
SMG6	Chr17:2188471	c.190G>A	p.Ala64Thr	903160	0.3491
CSPG4	Chr15:75677729	c.5108G>A	p.Arg1703His	8023621	0.3496
ETV1	Chr7:13939184	c.298A>G	p.Ser100Gly	9639168	0.3500
NRAP	Chr10:113590838	c.4696C>T	p.Arg1566Cys	188543474582927,	0.3535
RHPN2	Chr19:32999660	c.1151A>G	p.Gln384Arg	201801079	0.3653
RHBG	Chr1:156377340	c.20G>A	p.Gly7Asp	2245623	0.3740
NAALADL2	Chr3:175096948	c.232G>A	p.Gly68Ser	9823911	0.3835
INO80D	Chr2:206046504	c.1073C>T	p.Ala358Val	2909111	0.3865
KRT72	Chr12:52592403	c.791A>G	p.Tyr264Cys	12833456	0.3870
DST	Chr6:56618003	c.6031G>C	p.Val2011Leu	6459166	0.3887
OR2G3	Chr1:247606450	c.865A>G	p.Ile289Val	61730407	0.3979
KRTAP4-8	Chr17:41098083-41098084	c.1_2insA	p.Met1Asnfs	201764113	0.4025
BRC1	Chr17:43092919	c.2612C>T	p.Pro871Leu	799917	0.4100
WDR72	Chr15:53710894	c.917C>T	p.Pro306Leu	551225	0.4113
EFCAB6	Chr22:43687562	c.1051A>G	p.Thr351Ala	5764214	0.4235
MROH8	Chr20:37155091	c.1076A>G	p.Lys359Arg	1615246	0.4285
THSD7A	Chr7:11469934	c.2313C>G	p.Asp771Glu	2285744	0.4303
NBR1	Chr17:43209941	c.2768A>G	p.His923Arg	8482	0.4349
ATP13A5	Chr3:193276754	c.3392T>C	p.Val1131Ala	2271791	0.4362
MGAM	Chr7:142065775	c.4714A>T	p.Met1572Leu	4507684	0.4367
TMEM241	Chr18:23373756	c.28C>T	p.Leu10Phe	8099409	0.4377
TNC	Chr9:115084301	c.2039A>G	p.Gln680Arg	1061494	0.4408
HS6ST1	Chr2:128318303	c.261C>A	p.Asp87Glu	200979099	0.4625
LETMD1	Chr12:51049161	c.250G>A	p.Val84Ile	12379	0.4645
MROH8	Chr20:37112391	c.2777A>G	p.Gln926Arg	1744760	0.4781
PSPC1	Chr13:19703273	c.1474A>G	p.Met492Val	3852596	0.4797
RFX8	Chr2:101402446	c.1235T>C	p.Met412Thr	2175968	0.4965
WDR4	Chr21:42873634	c.213G>C	p.Lys71Asn	2248490	0.4968

ANKRD35	Chr1:145872788	c.1711C>G	p.Gln571Glu	11579366	0.5068
RB1CC1	Chr8:52674146	c.701T>C	p.Met234Thr	17337252	0.5110
MALRD1	Chr10:19331510	c.3829A>G	p.Ile1277Va	7100403	0.5211
HELQ	Chr4:83453327	c.916G>A	p.Val306Ile	1494961	0.5623
PCMTD1	Chr8:51820490	c.707A>T	p.Asn236Ile	12335014	0.5638
TNS2	Chr12:53049172	c.29G>C	p.Arg10Thr	12369033	0.5647
RGS9BP	Chr19:32676549	c.286G>T	p.Ala96Ser	259290	0.5674
TMEM185B	Chr2:120222852	c.125C>G	p.Ala42Gly	11550347	0.5829
LRP4	Chr11:46877220	c.3256A>G	p.Ile1086Val	6485702	0.5849
ABCA6	Chr17:69085689	c.3965A>G	p.Asn1322Ser	2302134	0.5867
RCBTB1	Chr13:49567209	c.71C>T	p.Ala24Val	4942848	0.6165
MRPL30	Chr2:99195607	c.388G>A	p.Ala130Thr	1044575	0.6366
PAPPA	Chr9:116344602	c.3671C>A	p.Ser1224Tyr	7020782	0.6687
C9orf129	Chr9:93335465	c.274G>A	p.Gly92Ser	3122944	0.7128
WDR91	Chr7:135204389	c.770C>T	p.Pro257Leu	292592	0.7135
GEN1	Chr2:17761508	c.274T>A	p.Ser92Thr	1812152	0.7138
EPB41L4A	Chr5:112184043	c.1595A>G	p.Asn532Ser	1560058	0.7349
ADGRE2	Chr19:14751618	c.1668G>C	p.Leu556Phe	2524383	0.7371
KRT74	Chr12:52571389	c.813A>C	p.Glu271Asp	670741	0.7449
OBSL1	Chr2:219556695	c.4095G>C	p.Glu1365Asp	1983210	0.7461
OR56B1	Chr11:5736832	c.316T>C	p.Cys106Arg	7397032	0.8171
ZZEF1	Chr17:4142807	c.89T>C	p.Val30Ala	1454121	0.8454
BRDT	Chr1:91962938	c.184C>A	p.Gln62Lys	10783071	0.8763

Table III.S1: Sequencing statistics

Group	SampleID	Total Number of Reads (left+right)	Overall read mapping rate	Concordant Pair Alignment Rate
Unrelated controls	RNA1_U1	116,415,950	88.6%	83.6%
	RNA2_U2	119,163,654	90.8%	86.2%
	RNA3_U3	127,339,996	92.4%	88.1%
Controls	RNA4_C1	119,696,150	88.9%	84.0%
	RNA5_C2	123,096,068	89.4%	84.7%
	RNA6_C3	112,137,798	89.1%	84.4%
Patients	RNA7_P1	159,013,354	88.8%	84.0%
	RNA8_P2	142,759,722	91.9%	87.3%
	RNA9_P3	140,901,146	91.4%	87.1%

Table III.S2: qPCR Primer sequences

Gene name (Symbol)	**Primer sequence (5'→ 3')**
Lamin A (*LMNA*)	CTC CAC ATC TGC CTT AAA AC GCT AGC CTC TAT AAA AGC AC
Lamin C (*LMNC*)	AGA ACA TCT ACA GTG AGG AG CAG AAT AAG TCT TCT CCA GC
Lamin B1 (*LMNB1*)	GCG TGC GTG TCT ATG CTA AG TCA TGC GGC TTT CCA TCA GT
Lamin B2 (*LMNB2*)	TTT TCC ACC AAC AGG GGG AC ACG TTC TGG CAG TTC GCT TA
Insulin Growth Factor binding protein 5 (*IGFBP5*)	GCC CTC CAC CTC TCT CTA CA TCA CGG GAG TCT CTC TCG AT
Housekeeping gene: Beta actin (*ACTB*)	GAC GAC ATG GAG AAA ATC TG ATG ATC TGG GTC ATC TTC TC

Table III.S3: RNA-seq expression values for *LMNA*, *LMNC* and *IGFBP5*

Sample	**LMNA_NM_170707**	**LMNC_NM_005572**	***LMNA* to *LMNC* ratio**	**IGFBP5_NM_000599**
All Unrelated Controls	124.946	300.189	0.416	152.317
U1	122.652	322.642	0.380	26.8803
U2	136.26	343.83	0.396	57.5047
U3	115.927	234.096	0.495	372.565
All Controls	116.521	280.476	0.415	125.739
C1	127.337	317.053	0.402	65.8477
C2	112.905	273.745	0.412	127.077
C3	109.32	250.63	0.436	184.293
All Patients	67.6258	172.028	0.393	17.7081
P1	69.795	196.989	0.354	9.63751
P2	72.2225	171.963	0.420	5.8749
P3	60.8598	147.132	0.414	37.6119

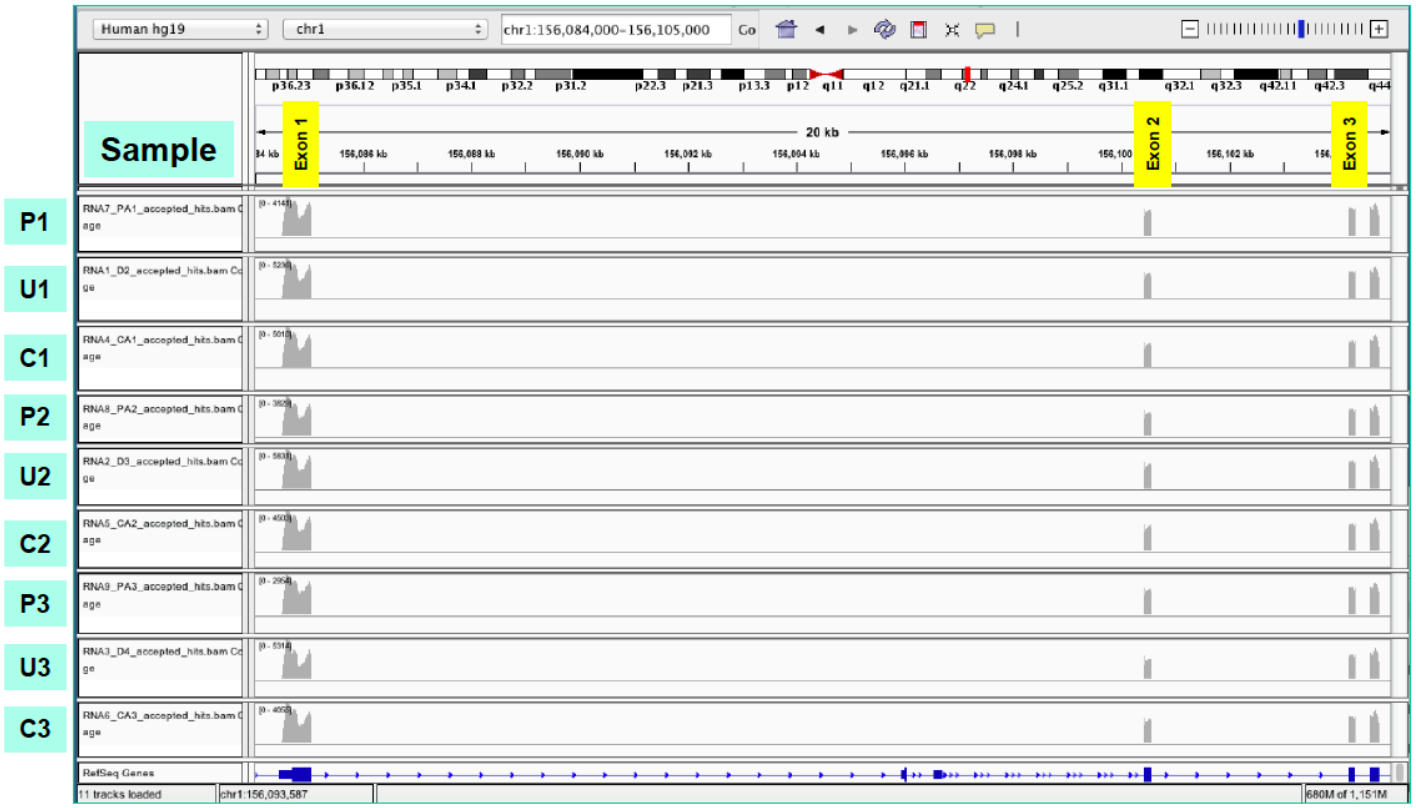

Figure III.S1: Integrative Genomics Viewer (IGV) screenshots showing expression of *LMNA* transcripts at Exons 1, 2 and 3 for all samples. There was a peak at each exon, indicating similar read coverage across all *LMNA* exons for all samples.

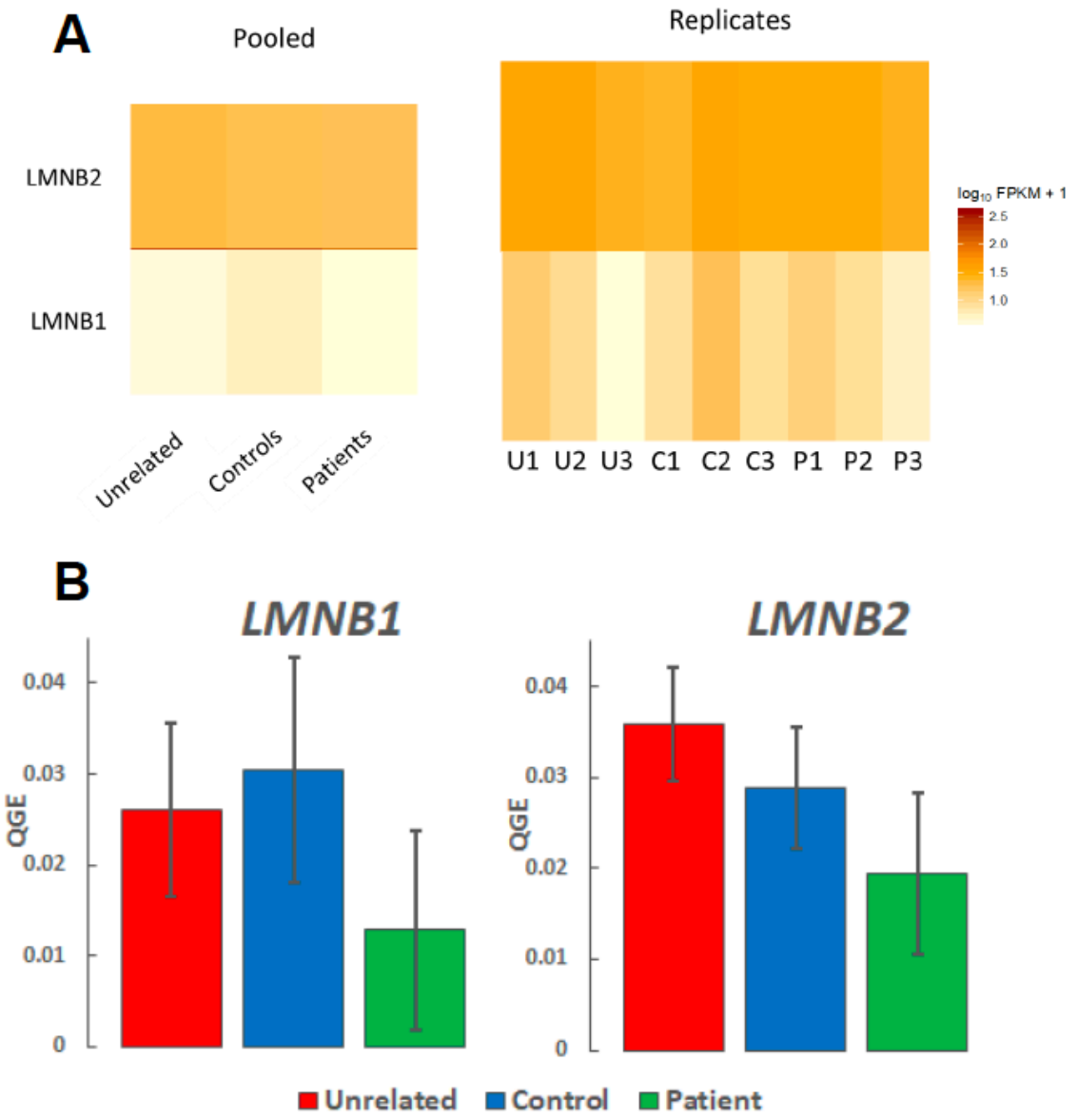

Figure III.S2. Lamin B1 and Lamin B2 heatmap and qPCR validation**.** (A) Heatmap showing Lamin B1 (*LMNB1*) and Lamin B2 (*LMNB2*) expression across all samples as pooled (left panel) and with replicates shown (right panel). There was no significant difference in the expression of *LMNB1* and *LMNB2* across all samples (FDR-adjusted p-value ≥ 0.05). (B) RNA-seq validation of Lamin B1 and Lamin B2 transcript levels by quantitative PCR (qPCR). qPCR was performed on cDNA generated from unrelated control, control and patient

fibroblasts to measure Lamin B1 and Lamin B2 transcript levels. There were no statistically significant differences in transcript levels (average QGE +/-standard error of the mean (SEM)) between groups for Lamin B1 [$F(2,6)= 0.70$, $p=0.53$] and for Lamin B2 [$F(2,6)= 1.29$, $p=0.34$]. Statistical analysis was performed using One-way ANOVA followed by Tukey post hoc test.

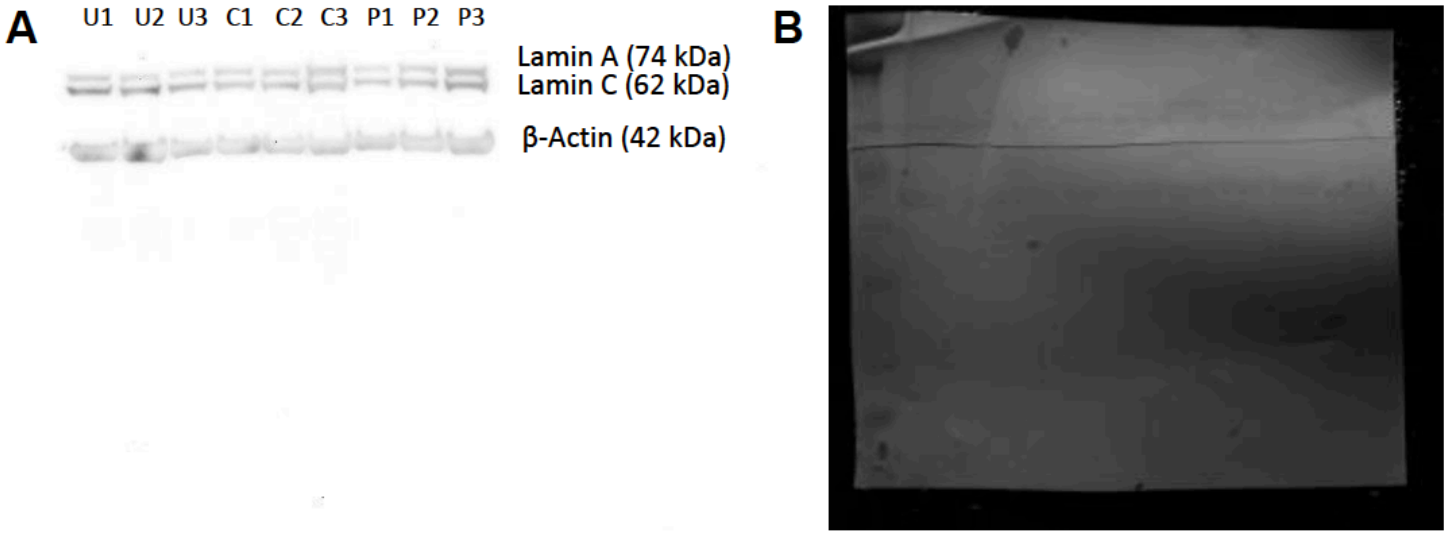

Figure III.S3. Original Lamin A/C Western Blot. (A) Fibroblasts from three unrelated (U1-U3), three control (C1-C3) and three patient (P1-P3) samples were seeded and grown to confluency, then total protein lysates were extracted for Western blot. Immunoblotting were conducted using N-terminus Lamin A/C antibody and β-Actin as loading control. (B) Membrane image under white light illumination.

Table IV.S1: Summary of differentiation optimization results for control lines

iPS Cell line	Clone	Optimal seeding density in 12-wp (cells/well)	Differentiation efficiency (% cTNT+ cells)
Control A1	14	275,000	67.4
Control A3	6	275,000	60
Donor 3	14	150,000	71.9

Table IV.S2: Summary of differentiation optimization results for patient lines

iPS Cell line	Clone	Optimal seeding density in 12-wp (cells/well)	Differentiation efficiency (%cTNT+ cells)
Patient A1	1	150,000	85
Patient A2	13	225,000	55
Patient A3	4	275,000	18

Table IV.S3: scRNA-seq libraries statistics

Sample	Estimated Cell number	Mean reads per cell	Mean genes detected per cell	% Reads mapped confidently to genome
CA1 d0	13,471	39,451	4,410	93.1
CA1 d2	6,360	44,140	4,396	94.2
CA1 d4	5,570	36,259	3,698	93.3
CA1 d9	7,306	47,307	3,908	93.6
CA1 d16	9,822	46,790	4,068	92.9
CA1 d19	12,601	41,416	3,550	93.9
PA1 d0	14,080	40,657	4,482	93
PA1 d2	9,938	33,542	3,555	93.9
PA1 d4	4,962	32,913	3,526	93.4
PA1 d9	5,585	54,878	4,161	93.4
PA1 d16	10,836	43,074	4,040	92.9
PA1 d19	13,034	44,325	3,588	93.6

Table IV.S4: List of antibodies used in the study

Name	Clonality	Host Species	Isotype	Application	Concentration	Dilution	Company	Catalog Number	Notes
Anti-Lamin A + C	monoclonal	mouse	IgG1	Western Blot	200 ug/ml	1:400	Santa Cruz Biotechnology	sc-376248	
Anti-B-actin	monoclonal	mouse	IgG2b	Western Blot	1 mg/mL	1:1000	Fisher Sci	PIMA515739	
Goat Anti mouse IgG H&L (HRP)	polyclonal	Goat	IgG	Western Blot	2 mg/ml	1:5000	ABCAM INC./Abcam	ab205719	Use for the detection of Lamin A/C and B-Actin
Alexa Fluor® 647 Mouse Anti-Cardiac Troponin T	monoclonal	rabbit	IgG1	Flow cytometry	0.2 mg/ml	1:200	BD Pharmingen	565744	
Anti-Cardiac Troponin T-FITC	monoclonal	human recombinant	Recombinant Human IgG1	Immunocytochemistry	200X	1:200	Miltenyi Biotec Inc./ Miltenyi Biotec	130-106-687	
Anti-Tra-1-60	monoclonal	mouse	IgM	Immunocytochemistry	100 ug	1:100	Thermo Fisher Scientific	A24868	
Anti-SOX2	polyclonal	rat	IgG	Immunocytochemistry	100 ug	1:100	Thermo Fisher Scientific	A24759	
Anti-SSEA4	monoclonal	mouse	IgG3	Immunocytochemistry	0.5 mg/ml	1:100	Thermo Fisher Scientific	A24866	
Anti-OCT4	monoclonal	rabbit	IgG	Immunocytochemistry	0.672 mg/ml	1:100	Thermo Fisher Scientific	A24867	
Anti-Alpha smooth muscle Actin	N/A	mouse	IgG2	Immunocytochemistry	100X	1:100	Thermo Fisher Scientific	A25531	
Anti-beta III tubulin	N/A	rabbit	N/A	Immunocytochemistry	500X	1:500	Thermo Fisher Scientific	A25532	
Anti-Alpha Feto protein	N/A	mouse	IgG1	Immunocytochemistry	500X	1:500	Thermo Fisher Scientific	A25530	
Alexa Fluor® 647 donkey anti-rabbit	N/A	Donkey	N/A	Immunocytochemistry	250X	1:250	Thermo Fisher Scientific	A25537	Use for the detection of beta III Tubulin
Alexa Fluor® 488 goat anti-mouse IgG1	N/A	Goat	IgG1	Immunocytochemistry	250X	1:250	Thermo Fisher Scientific	A25536	Use for the detection of Alpha Feto protein
Alexa Fluor® 594 goat anti-mouse IgG2	N/A	Goat	IgG2	Immunocytochemistry	250X	1:250	Thermo Fisher Scientific	A25534	Use for the detection of Alpha smooth muscle actin
Alexa Fluor® 488 goat anti-mouse IgG3	N/A	Goat	IgG3	Immunocytochemistry	250X	1:250	Thermo Fisher Scientific	A24877	Use for the detection of SSEA4
Alexa Fluor® 594 goat anti-mouse IgM	N/A	Goat	IgM	Immunocytochemistry	250X	1:250	Thermo Fisher Scientific	A24872	Use for the detection of Tra 1-60
Alexa Fluor® 594 donkey anti-rabbit	N/A	Donkey	N/A	Immunocytochemistry	250X	1:250	Thermo Fisher Scientific	A24870	Use for the detection of Oct4
Alexa Fluor® 488 donkey anti-rat	N/A	Donkey	N/A	Immunocytochemistry	250X	1:250	Thermo Fisher Scientific	A24876	Use for the detection of SOX2

Table IV.S5: List of PCR and qPCR Primers used in the study

Gene name (Symbol)	Primer sequence (5'→ 3')	KiCqStart Primer pair number
LMNA_RT_2 (Lamin A/C exon 1-4)	GTG ACT CAG TGT TCG CGG G TCC ACC AGT CGG GTC TCA T	N/A
LMNA_E10 (Lamin A/C exon 10-11)	GCG CTC AGT GAC TGT GGT TG GTG ACC AGA TTG TCC CCG AA	N/A
OCT3/4 (*POU5F1*)	GAC AGG GGG AGG GGA GGA GCT AGG CTT CCC TCC AAC CAG TTG CCC CAA AC	N/A
KLF4 (*KLF4*)	ACG ATC GTG GCC CCG GAA AAG GAC C TGA TTG TAG TGC TTT CTG GCT GGG CTC C	N/A
MYC (*MYC*)	GCG TCC TGG GAA GGG AGA TCC GGA GC TTG AGG GGC ATC GTC GCG GGA GGC TG	N/A
SOX2 (*SOX2*)	GGG AAA TGG GAG GGG TGC AAA AGA GG TTG CGT GAG TGT GGA TGG GAT TGG TG	N/A
Housekeeping gene: N-acetyltransferase 1 (*NAT1*)	TAA GAA AGG GGA TCA TGG AC GGA TGT TAA GGT TCT CAA AGG	Primer pair ID number 3

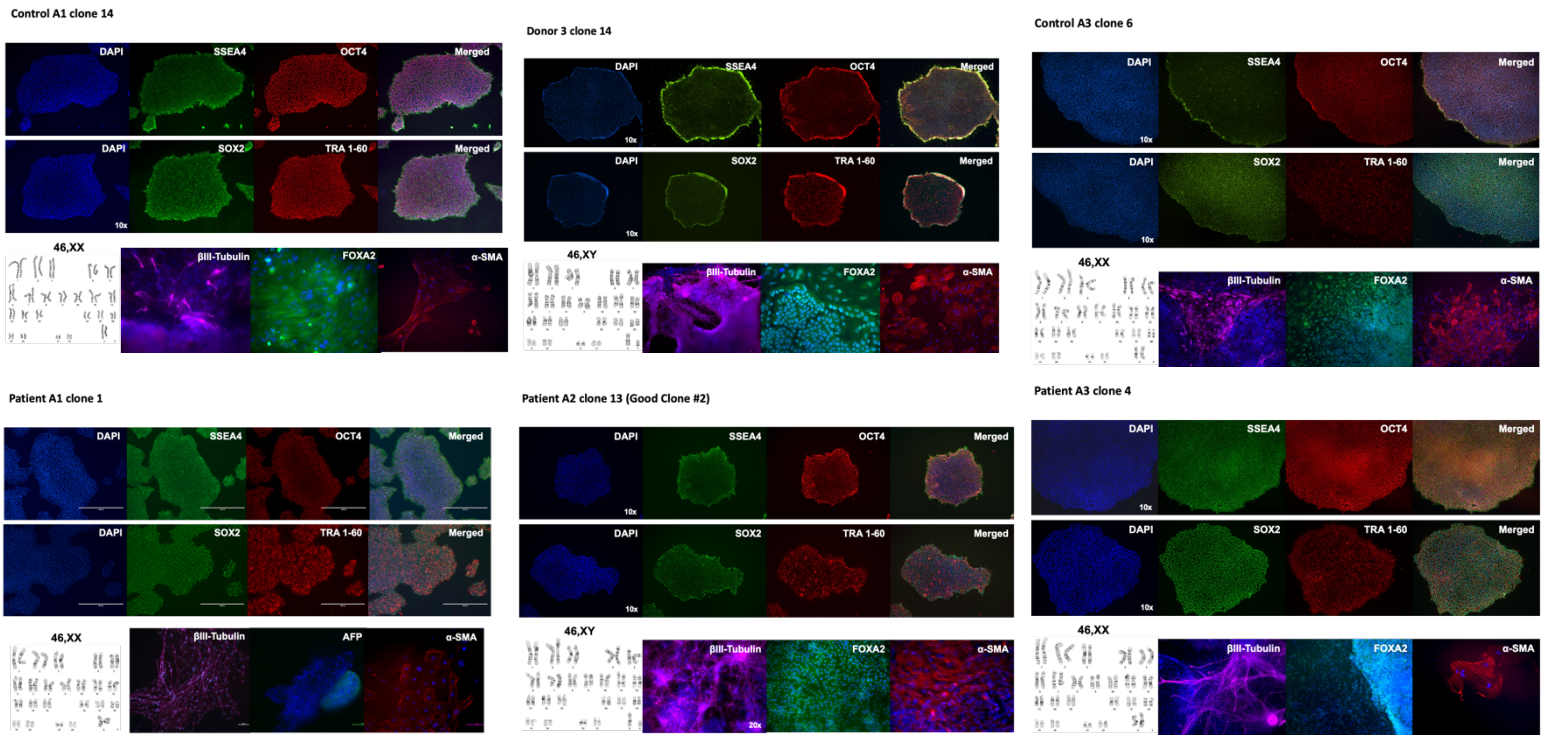

Figure IV.S1: Characterization of iPSC lines used in the study. Pluripotency assessment and karyotyping was performed on 6 iPSC lines by immunocytochemistry staining and immunofluorescence visualization of established pluripotency markers (*SSEA4*, *OCT4*, *SOX2*, and *TRA 1-60*) and three germ layer markers (β-III-tubulin, *FOXA2* and α-smooth muscle actin) to ensure iPSC lines generated from fibroblasts are pluripotent cells. Karyotyping was performed to ensure there was no chromosomal abnormalities associated with the reprogramming process or the *LMNA* mutation.

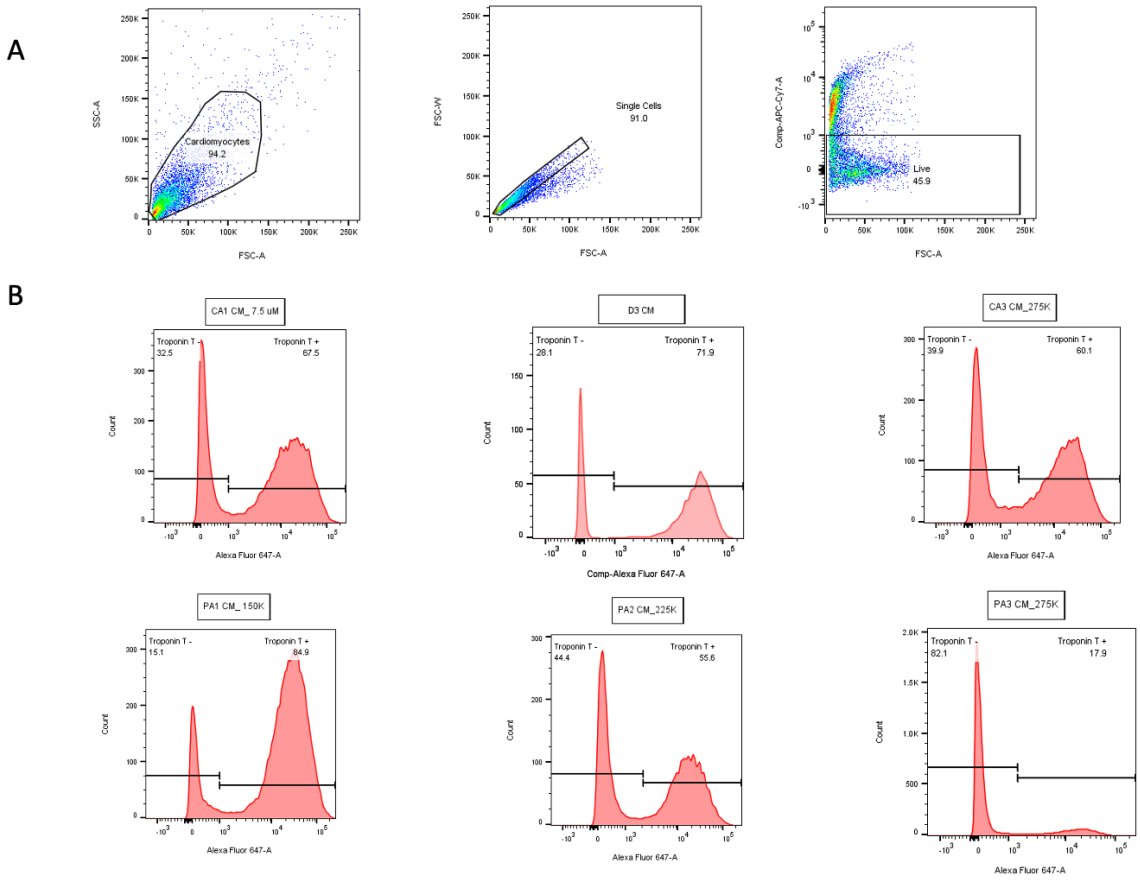

Figure IV.S2: Quantification of Troponin T-expressing cells. Flow cytometry was performed on iPSC-CMs generated from 3 control iPSCs and 3 patient iPSCs. Cells are gated to exclude debris, doublets and dead cells. Only live single cells were used to quantify Troponin T expression.

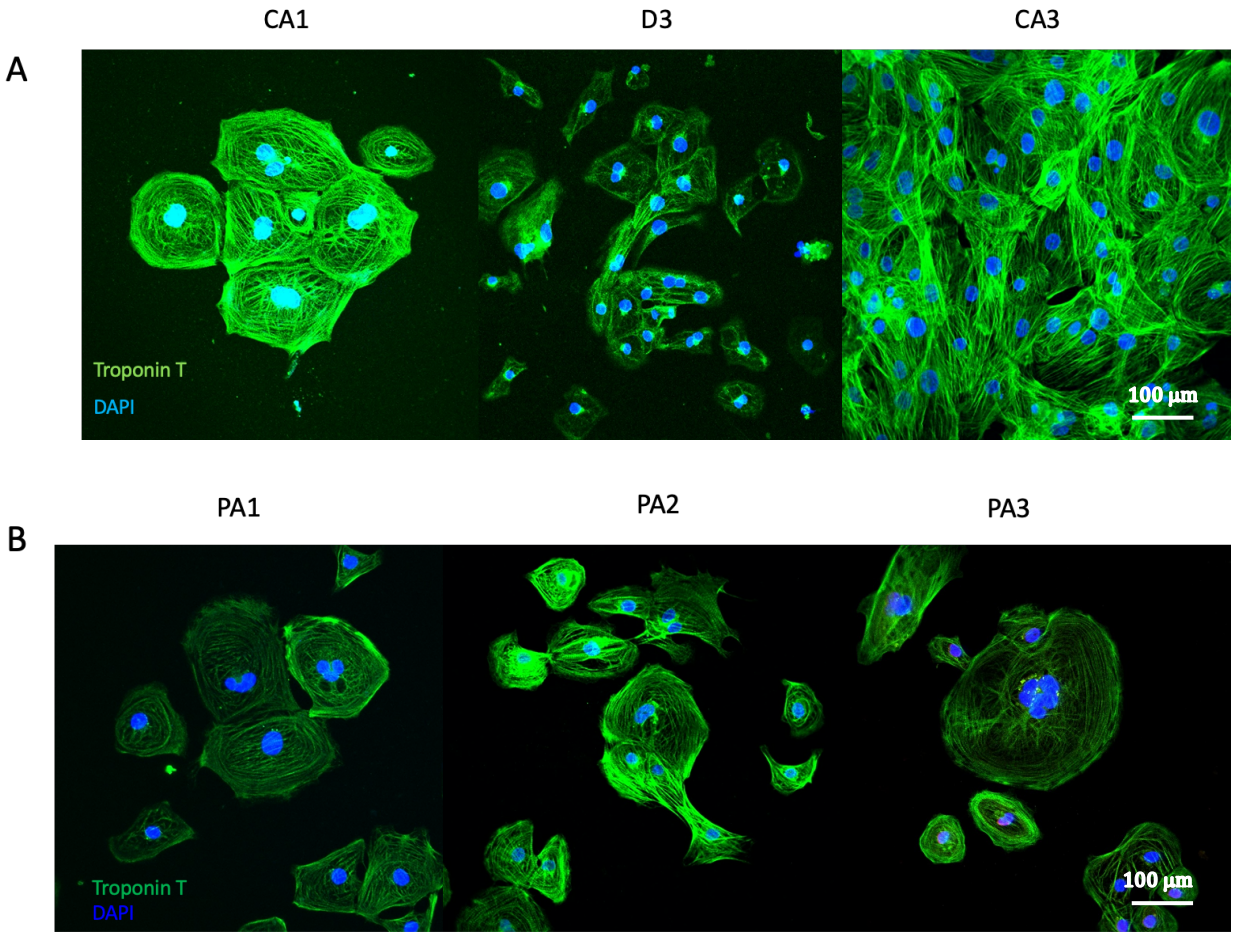

Figure IV.S3: Troponin T staining and visualization by immunocytochemistry and immunofluorescence. iPSC-CMs seeded at low density on chamber slides were fixed and stained with Troponin T antibody and visualized using confocal microscopy. iPSC-CMs generated from C1-3 (A) and P1-3 (B) iPSCs all expressed Troponin T. All images were taken at 40X magnification.

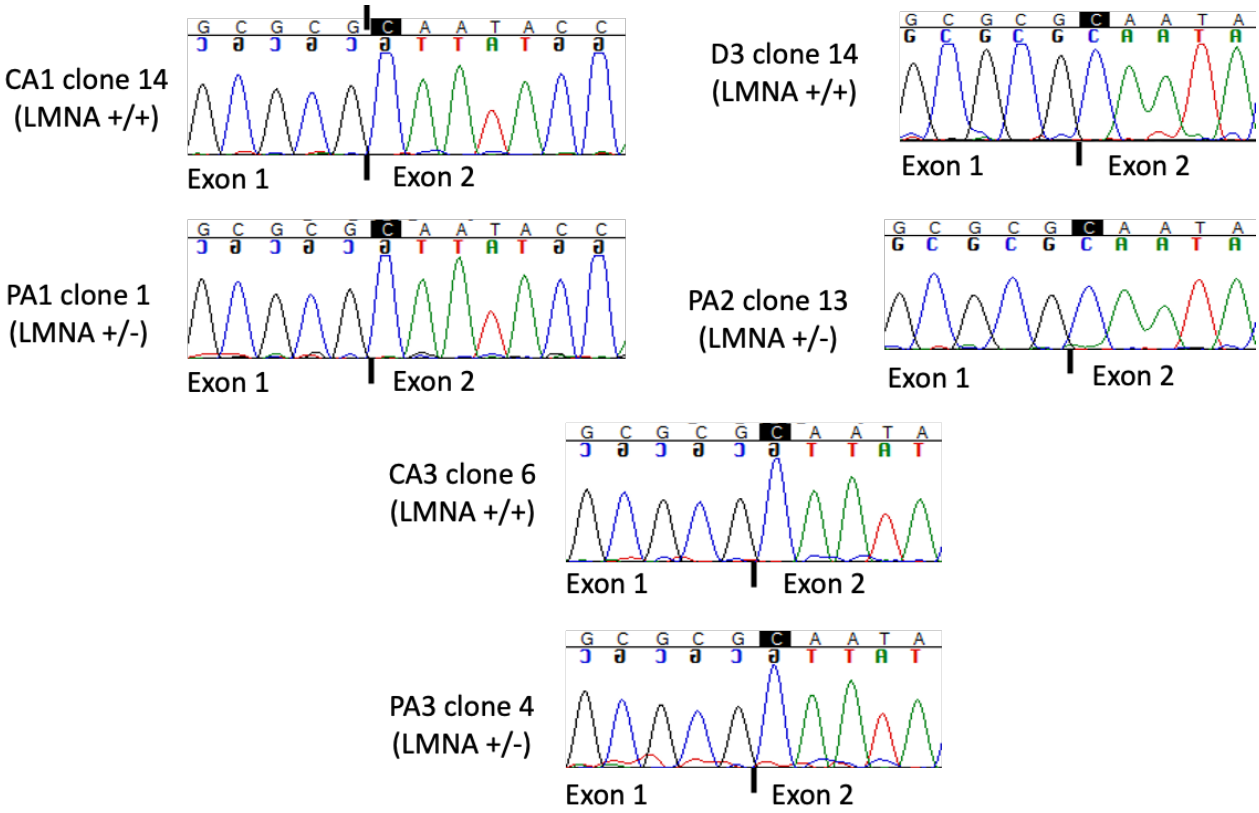

Figure IV.S4: Sanger sequencing chromatograms of *LMNA* cDNA (Exons 1-4). Sequencing chromatograms for 3' end of LMNA exon 1 and 5' end of LMNA exon 2 showing intact exon 1-exon 2 junctions for all samples, suggesting that the predicted exon-skipping due to the *LMNA* splice-site mutation did not occur in patient samples.

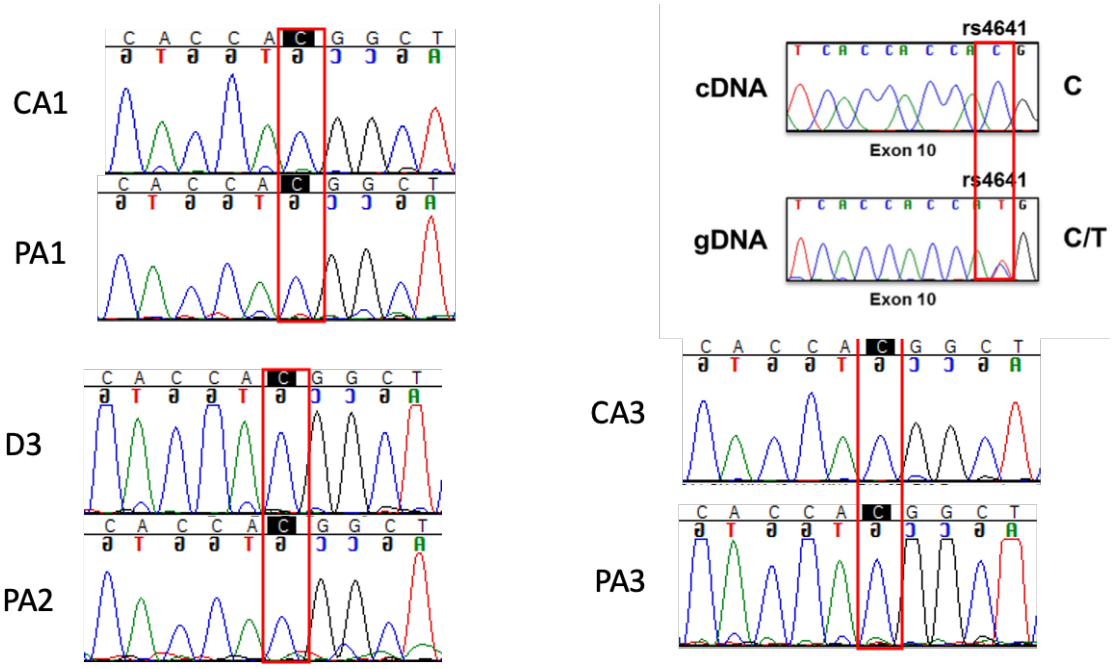

Figure IV.S5: Sanger sequencing chromatograms of *LMNA* cDNA (Exons 10-11). To determine whether both wild-type and mutant *LMNA* allele are expressed in patient cells or monoallelic *LMNA* allele expression is occurring we utilized the presence of a SNP in exon 10 in-cis with the mutant *LMNA* allele appearing exclusively in patient. We found that all patient samples only express the wild-type *LMNA* allele as evidenced by the single peak on the chromatogram at this specific locus (red box).

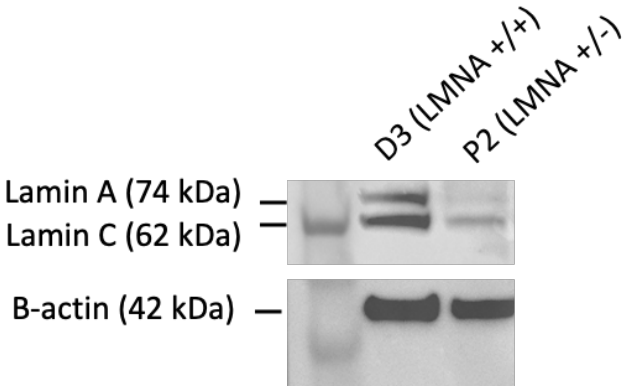

Figure IV.S6: Immunoblot of D3 and P2 iPSC-CMs stained for Lamin A/C and Beta Actin, showing faint Lamin A/C bands for P2 iPSC-CMs indicating lower Lamin A/C protein levels.

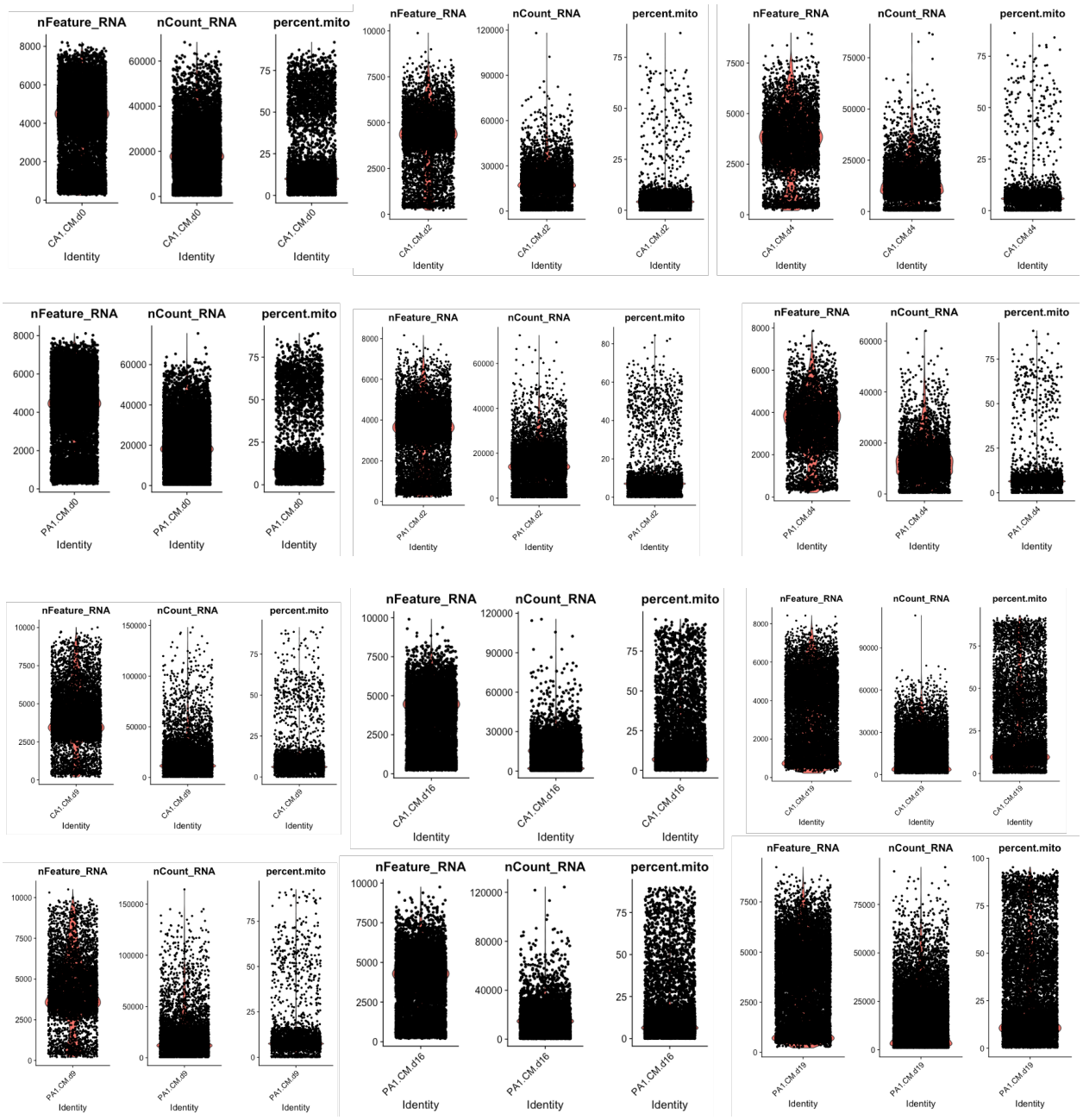

Figure IV.S7: Violin plots showing distribution of unique molecular identifier (UMI) count (nCount_RNA), number of genes captured (nFeature_RNA) and percentage of mitochondrial DNA contamination (percent.mito) for each time points assayed for single cell RNA-sequencing.

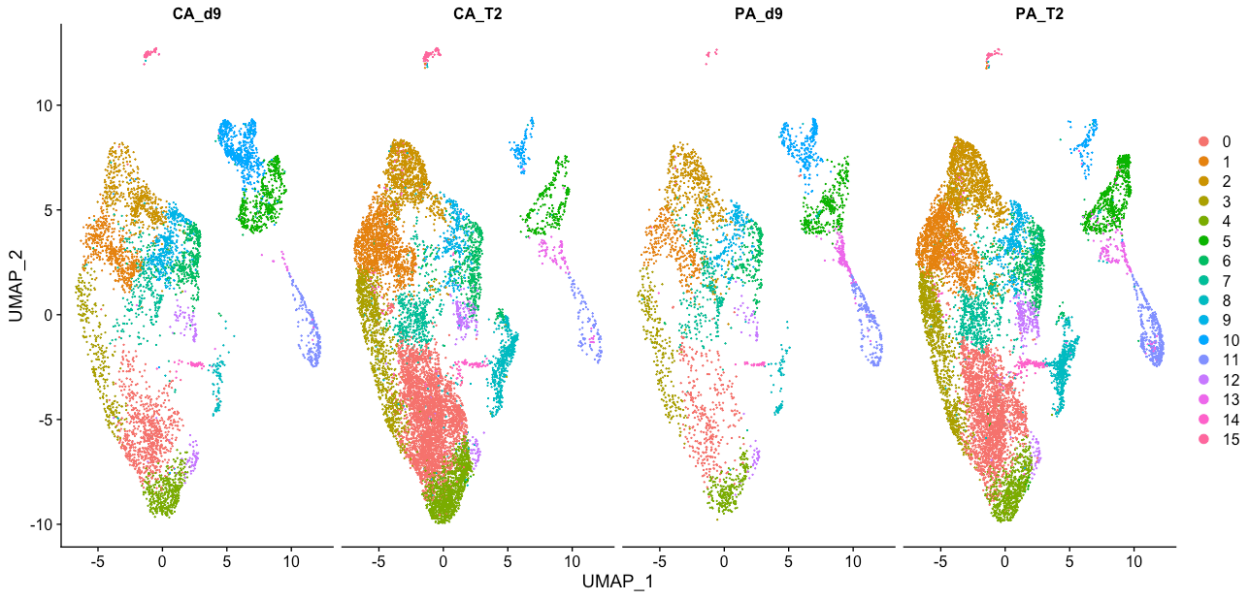

Figure IV.S8: Integrated comparison analysis of overlapping time points between two iPSC-CM differentiation protocols, Wnt signaling modulation (d9) and Gibco PSC Cardiomyocyte Differentiation kit (T2), showed similar gene expression profiles and cell subpopulations between all samples analyzed. The high degree of similarity between cell subtypes suggested that both differentiation protocols were capable of generating the same cell types.

R scripts used to perform dimensionality reduction and cell clustering:

```
library(Seurat)
library(dplyr)
library(Matrix)
library(ggplot2)

PA1_CM_d0.data <- Read10X(data.dir = "/Volumes/Seagate Backup Plus
Drive/scRNA/PA1_iPSC/outs/filtered_feature_bc_matrix/")
PA1_d0 <- CreateSeuratObject(PA1_CM_d0.data, project = "PA1.CM.d0", min.cells = 3,
min.features = 200)

CA1_CM_d0.data <- Read10X(data.dir = "/Volumes/Seagate Backup Plus
Drive/scRNA/CA1_iPSC/outs/filtered_feature_bc_matrix/")
CA1_d0 <- CreateSeuratObject(CA1_CM_d0.data, project = "CA1.CM.d0", min.cells = 3,
min.features = 200)

CA1_d0[["percent.mito"]] <- PercentageFeatureSet(object = CA1_d0, pattern = "^MT-")
PA1_d0[["percent.mito"]] <- PercentageFeatureSet(object = PA1_d0, pattern = "^MT-")
VlnPlot(object = CA1_d0, features = c("nFeature_RNA", "nCount_RNA", "percent.mito"), ncol
= 3)
VlnPlot(object = PA1_d0, features = c("nFeature_RNA", "nCount_RNA", "percent.mito"), ncol
= 3)

plot1 <- FeatureScatter(object = CA1_d0, feature1 = "nCount_RNA", feature2 =
"percent.mito")
plot2 <- FeatureScatter(object = CA1_d0, feature1 = "nCount_RNA", feature2 =
"nFeature_RNA")
CombinePlots(plots = list(plot1,plot2))

plot1 <- FeatureScatter(object = PA1_d0, feature1 = "nCount_RNA", feature2 =
"percent.mito")
plot2 <- FeatureScatter(object = PA1_d0, feature1 = "nCount_RNA", feature2 =
"nFeature_RNA")
CombinePlots(plots = list(plot1,plot2))

CA1_d0 <- subset(x = CA1_d0, subset = nFeature_RNA > 200 & nFeature_RNA < 8000 &
percent.mito < 25)
PA1_d0 <- subset(x = PA1_d0, subset = nFeature_RNA > 200 & nFeature_RNA < 8000 &
percent.mito < 20)

CA1_PA1_d0 <- merge(x = CA1_d0, y = PA1_d0, add.cell.ids = c("CA1_d0", "PA1_d0"), project
= "CA1.PA1.d0")
```

```
CA1_PA1_d0_Split <- SplitObject(CA1_PA1_d0, split.by = "orig.ident")

for(i in 1:length(CA1_PA1_d0_Split)) {
  CA1_PA1_d0_Split[[i]] <- SCTransform(CA1_PA1_d0_Split[[i]], verbose = F)
}

CA1_PA1_d0_features <- SelectIntegrationFeatures(object.list = CA1_PA1_d0_Split)
CA1_PA1_d0_Split <- PrepSCTIntegration(object.list = CA1_PA1_d0_Split, anchor.features =
CA1_PA1_d0_features)
integrate.data <- FindIntegrationAnchors(object.list = CA1_PA1_d0_Split,
normalization.method = "SCT",
                                         anchor.features = CA1_PA1_d0_features)
combine.data <- IntegrateData(anchorset = integrate.data, normalization.method = "SCT")
DefaultAssay(combine.data) <- "integrated"

combine.data <- RunPCA(combine.data, features = VariableFeatures(combine.data),
ndims.print = 1:10, nfeatures.print = 10)
DimHeatmap(combine.data, dims = c(3, 4, 8, 10))

s.genes <- cc.genes$s.genes
g2m.genes <- cc.genes$g2m.genes

combine.data <- CellCycleScoring(combine.data, s.features = s.genes, g2m.features =
g2m.genes, set.ident = T)
head(combine.data[[]])
RidgePlot(combine.data, features = c("CCND1", "TOP2A", "MCM6", "MKI67"), ncol = 2)
combine.data <- RunPCA(combine.data, features = c(s.genes, g2m.genes))
p1 <- DimPlot(combine.data, group.by = "orig.ident")
p2 <- DimPlot(combine.data)
CombinePlots(plots = list(p1,p2))

DimPlot(combine.data, split.by = "orig.ident", label = T, pt.size = 0.25) + NoLegend()
combine.data$CC.Difference <- combine.data$S.Score - combine.data$G2M.Score

combine.data <- SCTransform(combine.data, vars.to.regress = c("percent.mito",
"CC.Difference"))
combine.data <- RunPCA(combine.data,verbose = F)
combine.data <- RunUMAP(combine.data,dims = 1:30)
combine.data <- FindNeighbors(combine.data, dims = 1:30)
combine.data <- FindClusters(combine.data, dims = 1:30)

DimPlot(combine.data, reduction = "umap", split.by = "orig.ident", label = T, pt.size = 0.25)

all.markers <- FindAllMarkers(object = combine.data, only.pos = T, min.pct = 0.25,
logfc.threshold = 0.25)
all.markers %>% group_by(cluster) %>% top_n(n = 5, wt = avg_logFC) -> top5
```

```
DoHeatmap(combine.data, features = top5$gene)
```

R script used to perform differential gene expression analysis:

```
DefaultAssay(combine.data) <- "RNA"
Idents(combine.data) <- "orig.ident"
DE_genes_d0 <- FindMarkers(combine.data, ident.1 = "CA1.CM.d0", ident.2 = "PA1.CM.d0",
verbose = F)
DE_genes_d0$gene <- rownames(DE_genes_d0)
DoHeatmap(combine.data, features = DE_genes$gene)
```